NUCLEATION AND CONDENSATIONAL GROWTH OF AEROSOLS: APPLICATION TO SILICON PRODUCTION

Thesis by

Md. Khairul Alam

In Partial Fulfillment of the Requirements

for the Degree of

Doctor of Philosophy

California Institute of Technology

Pasadena, California

1984

(submitted August 15, 1983)

ACKNOWLEDGEMENTS

I would like to thank my advisor, Professor Richard Flagan for his support and guidance throughout this study. His insights and assistance in development of the experiment were especially valuable. I have also benefitted from my discussions with other faculty members, including Professors Rannie, John Seinfeld, Glen Cass, Rolf Sabersky and James Knowles. Dr. Fred Gelbard of Chevron provided valuable help on a number of occasions.

Andy Pesthy developed some of the concepts which forms the starting point for the theoretical analysis, and his suggestions were helpful and very welcome. My interaction with fellow students have been productive and enjoyable. I would specially like to thank Connie Senior, Pratim Biswas, Joe Leone, Carol Jones, Dale Warren, Ellen Johnson, Susan Larson, Martha Conklin, Jed Waldmen, Mark Cohen and Mark Bassett. Ellen Johnson helped in carrying out some of the experiments. My stay at Caltech was made particularly enjoyable by my officemate Alan Stone, who has been a close friend to me and my family.

I am indebted to Elaine Granger, Sandy Brooks, Melinda Hendrix-Werts and Joan Mathews for their friendly assistance in preparing this and other manuscripts. Also thanks to Theresa Fall and Linda McArdle for help in drafting the figures. The help from Elton Daly, Rich Eastvedt, Joe Fontana and Leonard Montenegro in building the experimental setup is greatly appreciated.

I also take this opportunity to thank my parents, the Dhesi and the Alam families for following and encouraging my progress. And most of all, I appreciate the support and patience of my wife Natasha and the company of our children, Mishima and Sahar Tapan.

This work was supported by the Jet Propulsion Laboratory of the California Institute of Technology and the Department of Energy under the Flat Plate Solar Array Project.

CONTENTS

LIST OF TABLES

LIST OF FIGURES

ABSTRACT

A theoretical analysis of aerosol nucleation and condensational growth is developed. A growing aerosol depletes the surrounding vapor, leading to the development of a spherically symmetric radial distribution of monomer partial pressure. A symmetric radial temperature profile is simultaneously developed due to release of latent heat of condensation. These local perturbations are analyzed to determine the total effect on the nucleation rate. The analysis forms the basis for building an experimental reactor for production of large particles of silicon for semiconductors and photovoltaic cells. The large size of the silicon particles facilitates separation and processing of the product.

CHAPTER 1

INTRODUCTION

This thesis has been organized in two major sections. The initial chapters are devoted to the analysis of simultaneous nucleation and aerosol growth by condensation, and subsequent chapters deal with the application of the theoretical analysis to the development of an aerosol reactor for silicon production.

Nucleation and condensation are phase transitions which play a major role in initiating aerosol formation and growth. Although heterogeneous nuclei are usually present, homogeneous nucleation can be the prevailing mechanism in phase changes. Examples are: combustion generated particles, aerosols condensed in supersonic nozzles (1) and shock tubes, in the formation of ceramics (2), in direct coal combustion (3) and in chemical reactions (4) where involatile products are produced.

The theories of homogeneous nucleation can be divided into two major groups (5), the classical Volmer-Becker-Doering theory (9,10) and the Lothe-Pound formulations (11). Experimental results have indicated that data from a class of vapors agree with the Classical theory (water, ethanol, toluene); data from some others agree with the Lothe-Pound theory (Ammonia, Iron).

The rate of new particle formation by homogeneous nucleation is, in both these formulations, assumed to be unaffected by particles in the gas.

Foreign particles or particles formed by prior nucleation act as sinks for vapor that might otherwise contribute to nucleation. Pesthy, et al. (6) have recently shown that the average nucleation rate is proportional to the product of the initial undisturbed, or intrinsic, nucleation rate and a term which is dependent largely on the volume fraction of aerosol present in the system. The nucleation rate for dibutyl phthalate was predicted to quench gradually, effectively ceasing when the fraction of vapor condensed into aerosol approaches 5 to 9%. Pesthy and coworkers treated the case of the formation and growth of particles in the continuum size range. Although this assumption may not lead to serious discrepancies for condensation of organic vapors like dibutyl phthalate at ambient temperatures, nucleation generated particles often remain in the free molecular or transition size range for long times. Examples include combustion generated soot and ash fume aerosols, and sulfate aerosols formed under dry atmospheric conditions. Even when particle growth into the continuum size range does occur, most of the dynamic processes may take place in the free molecular and transition regimes.

In chapters 2 and 3, an extension of the analysis of Pesthy is developed to explore the interaction between nucleation and particle growth in the free molecular and transition size ranges and an analytical criterion for control of nucleation is obtained.

The theory of simultaneous nucleation and aerosol growth is then applied to the design of an aerosol reactor for the production of silicon for photovoltaic and other semiconductor applications. A common feature of many of the methods for production of high purity silicon is the conversion of metallurgical grade silicon to volatile compounds such as

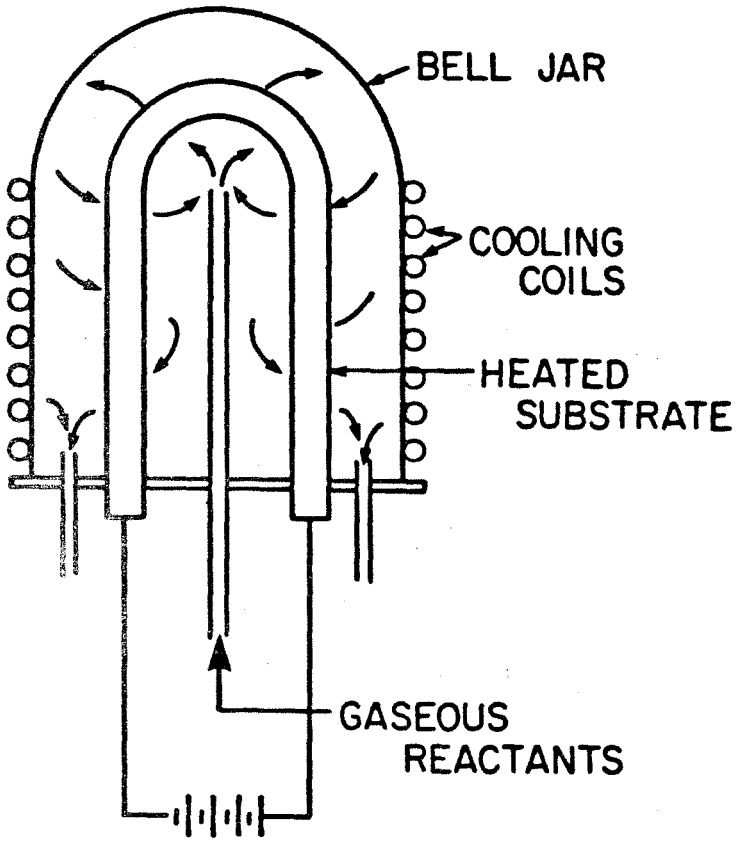

Figure 1. Bell Jar Reactor for production of silicon by Siemens Process.

silicon tetrachloride, di- or tri-chlorosilane, other halo-silanes, or silane. Distillation methods are then used to remove the impurities from these materials. Once the volatile species have been purified, the precursor compounds are reacted to produce solid silicon. The conventional Siemens process for producing silicon involves direct chemical vapor deposition on a heated substrate. The vapor deposition is slow due to mass transfer limitations. The slow deposition and large heat losses make the silicon produced by this method quite expensive. Nevertheless, Siemens-type reactors, like the bell jar reactor shown in Fig. 1, currently account for the vast majority of the silicon produced for semiconductor applications.

Entrained bed or "free space" reactors have been considered as an alternate method for silicon production. The Jet Propulsion Laboratory (7) and Union Carbide (8) have experimented with free-space reactors (Fig. 2) designed to generate a silicon powder by the thermally induced decomposition of silane gas. The pyrolytic decomposition of silane is sufficiently rapid at high temperatures (600 °C to 1000°C) that efficient conversion of silane to condensed phase products can be achieved in a few seconds or less. Much of the effort in the Union Carbide and JPL projects was devoted to growth of product particles sufficiently large so that simple processes like the cyclone illustrated in Fig. 2 can be used to separate the particles from the gases. In spite of these efforts, the silicon powder generated by the JPL and Union Carbide bench scale reactors consisted of particles in the 0.1 to 0.5 micron size range. Such small particles must be separated from the carrier gas by filtration since their terminal settling velocities are below 1mm/sec and their aerodynamic

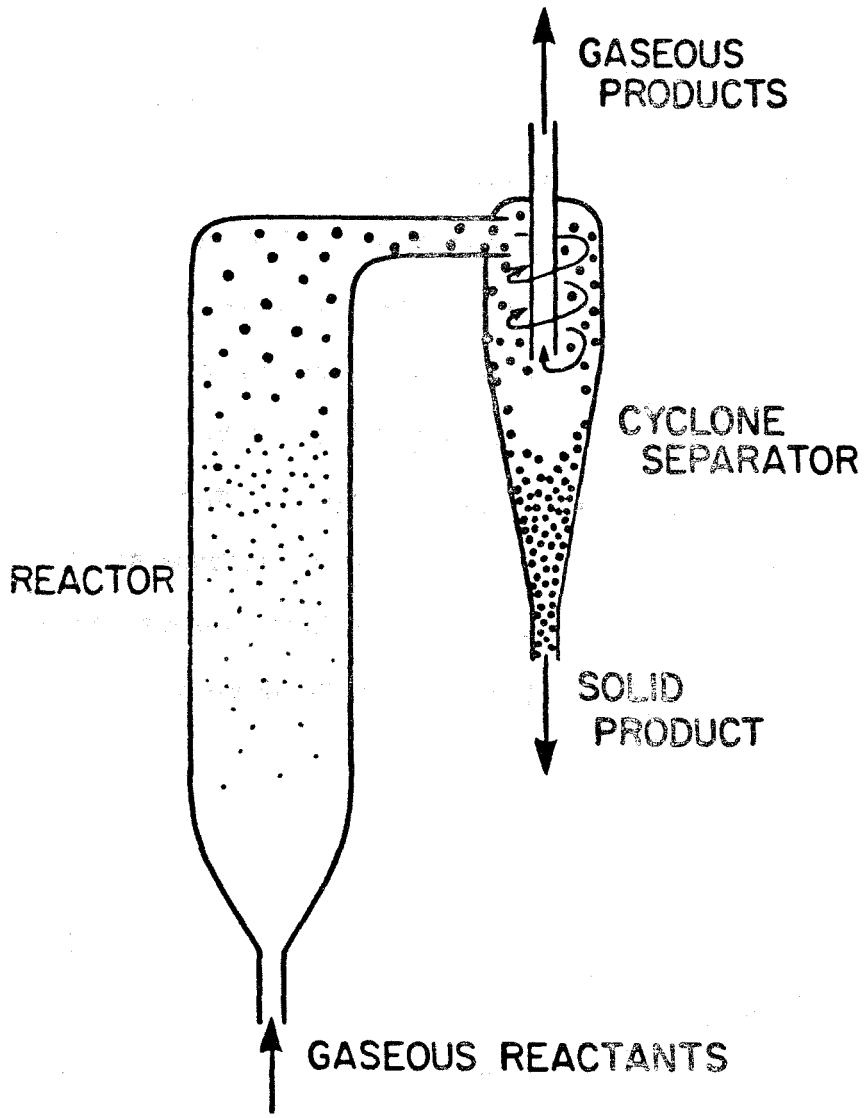

Figure 2. A Free Space Reactor system for production of silicon.

relaxation times are well below 1 msec. This introduces serious problems in particle collection, transport and melting, and greatly increases the risk of contamination. It is therefore, desirable to produce larger particles in a free space reactor.

At the operating conditions of the JPL and Union Carbide Systems, the products condense homogeneously to form a large number of very small particles which then grow by heterogeneous condensation and coagulation. To grow large particles of silicon, it is required that homogeneous nucleation be substantially reduced, while promoting heterogeneous condensation. The analysis developed for control of nucleation indicates how a reactor should be operated to grow large particles by pyrolysis of silane. The design of the aerosol reactor is discussed in Chapter 4. The experimental reactor and experimental results are described in chapter 5. The final chapter (6) is devoted to discussion and conclusions.

References (Chapter 1)

1) P. P. Wegener, Acta Mech, Vol 21, p. 65, (1975).

2) A. I. Bereznoi, "Glass-Ceramics and Photo-Sitalls," Plenum Press, New York, (1970).

3) K. H. Im and P. M. Chung, AIChE Journal, Vol 26, No 4, pp 655-663, (1980).

4) J. L. Katz and M. C. Donahue, J. Colloid and Interface Sci., Vol 85, No 1, pp 267-277, (1982).

5) G. S. Springer, "Adv. In Heat Transfer", T. F. Irvine and J. P. Hartnett, eds., Vol 14, pp 281-346, Academic Press, New York, (1978).

6) A. J. Pesthy, R. C. Flagan and J. H. Seinfeld, J. Colloid and Interface Sci., Vol 82, pp 465-479, (1981).

7) H. Levin, "Pyrolysis of Silane in Free Space," Proceedings of Symposium on Materials and New Processing Technologies for Photovoltaics, Electrochemical Society, (1980).

8) J. R. Lay and S. K. Iya, "Silane Pyrolysis in a Free Space Reactor," Proc. 15th IEEE Photovoltaic Specialists Conference, Florida, May, (1981).

9) M. Volmer, Z. Elektrochem., Vol 35, pp 555-561 (1929).

10) R. Becker and W. Doering, Ann. Phys. (Leipzig), Vol 24, pp 719-752, (1935).

11) J. Lothe and G. M. Pound, J. Chem. Phys., Vol 36, pp 2080-2085, (1962).

CHAPTER 2

SIMULTANEOUS NUCLEATION AND CONDENSATION

2.1 Introduction

The local perturbations on nucleation rates due to an aerosol growing by condensation are due to the changes in the vapor concentration and the temperature profiles around the individual particles. In order to determine the change in nucleation rates, it is necessary to determine the vapor concentration and temperature profiles in the region surrounding a growing particle. The problem is unsteady, but it is possible to find analytical solutions to a quasi-steady-state. The results are then combined with particle growth laws to predict the time evolution of the aerosol produced by the vapor. Stationary nucleation theory is assumed to be applicable to the region in the vicinity of the particles. We shall limit our consideration to dilute systems in which the partial pressure of the condensing vapor is small compared to the total pressure.

2.2 Homogenous Nucleation

In a system containing supersaturated vapor, condensation will occur on free surfaces. At the same time, clusters of vapor molecules will form by collisions between the molecules. Of these, the smaller clusters tend to evaporate while the larger clusters tend to grow, so supersaturated vapor is in a metastable state. This is illustrated in Fig. 3 where the variation of Gibbs free energy ΔG is plotted as function of cluster size g. ΔG first increases with g, reaches a maximum at g^* and then decreases continuously. The maximum is attained due to a balance between the volume

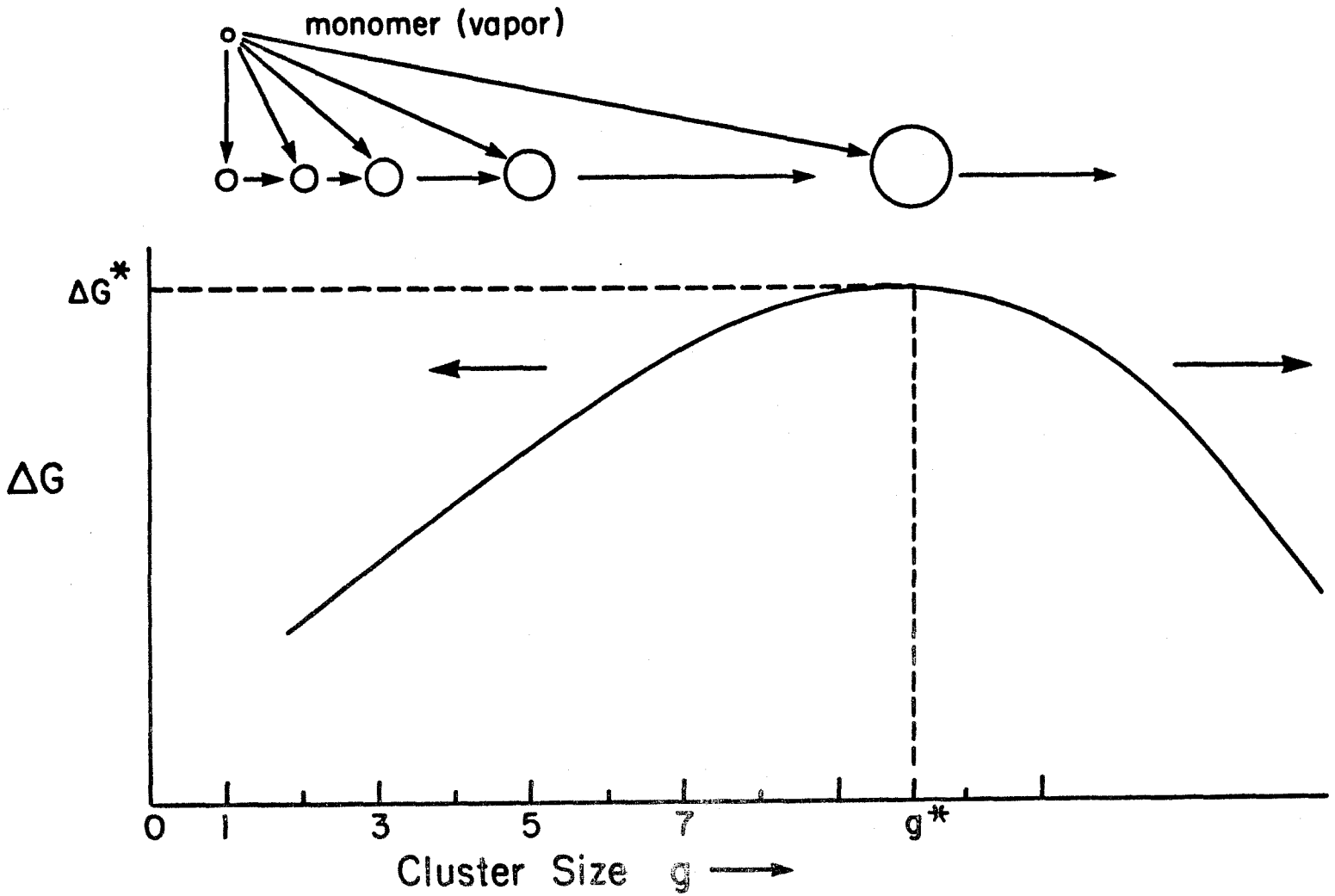

Figure 3. Gibbs free energy for clusters of vapor molecules.

and surface free energies. Once a cluster reaches the critical size g^*, it grows rapidly by condensation. Therefore $\Delta G = \Delta G^*$ is the condition for onset of condensation.

The 'classical' theory for the steady state rate of nucleation has been developed by Frenkel (12), Zeldovich (13), Volmer (14), Becker-Doering (15) and others. In the classical formulation two major assumptions are made: (I) the flat film surface tension is used to describe the surface energy of the vapor clusters, and (II) the clusters are assumed to be at 'rest', undergoing neither translational nor rotational motion. The results of this theory are presented in Table 1(a).

The classical theory was further modified by using statistical mechanics to eliminate the two aforementioned assumptions. These methods have been developed by, among others, Abraham (16), Kuhrt (17) and Lothe and Pound (18). The non-classical formulations are shown in Table 1(b). These formulations predict nucleation rates as much as 10^{12}-10^{18} times higher than the classical theory.

Experimental data indicate that the classical theory results are more accurate than the results of Lothe-Pound theory for some liquids (water, methanol, octane etc.), and for certain other liquids (ammonia, iron) the opposite is true.

2.3 Boundary conditions for condensation

The condensation flux to particles in the continuum size range is easily calculated as a diffusive flux. For particles which are not in the continuum size range, i.e. when the dimensions of the particle are comparable to or less than the mean free path of the condensing vapor

Table 1a. Nucleation rates in classical theory

Frenkel $$J_F = \left[\xi_c \frac{4\pi a^{*2} P_A}{(2\pi m k T)^{1/2}}\right]\left[\frac{a^{1/2} v_m}{2\pi a^{*2} (kT)^{1/2}}\right]\left[\frac{P_A}{kT} \exp\left(-\frac{4\, a^{*2}\sigma}{3kT}\right)\right]$$

Zeldovich $$J_z = J_F$$

Volmer (1929) $$J_v = J_F \frac{8\pi v_m (\sigma/kT)^{3/2}}{(\ell n\, S)^2}$$

Becker-Doering $$J_{BD} = J_F (g^*)^{-2/3}$$

Sundquist-Oriani $$J_{SO} = J_F (2)^{-g^*}$$

Critical radius for nucleation $$a^* = \frac{2\sigma v_m}{kT\, \ell n\, S}$$

Table 1b. Nucleation rates in modified (non-classical) formulations

Lothe-Pound

$$J_{LP} = \left[\xi_c \frac{4\pi a^{*2}_{LP} P_A}{(2\pi mkT)^{1/2}}\right]\left[\frac{\sigma^{1/2} v_m}{2\pi a^{*2}_{LP} (kT)^{1/2}}\right]\left[4.4 \times 10^{-2}\left(\frac{mkT}{v_m}\right)^3 \frac{a^{*12}}{h^6} \exp\left(-\frac{4 a^{*2}_{LP} \sigma}{3kT}\right)\right]$$

Abraham

$$J_A = \left[\xi_c \frac{4\pi a^{*2} P_A}{(2\pi mkT)^{1/2}}\right]\left[\frac{\sigma^{1/2} v_m}{2\pi a^{*2} (kT)^{1/2}}\right]\left[\frac{4.4 \times 10^{-2}\left(\frac{mkT}{v_m}\right)^{3/2} a^{*9/2} \nu}{h^2\left(\frac{64}{15}\right)^{3/2} \pi^5} \exp\left(-\frac{4\pi a^{*2} e}{3kT}\right)\right]$$

Critical radius

$$a^*_{LP} = \frac{2\sigma v_m}{kT \ln S}\left(1 - \frac{3kT}{2\pi\sigma a^{*2}_{LP}}\right)^{\dagger}$$

Critical radius

$$a^* = \frac{2\sigma v_m}{kT \ln S}$$

†Expression is implicit for a^*_{LP}.

molecules, the theory must be modified.

The rate of condensational growth of a spherical particle of radius a is a function of the Knudsen number $K_n = \lambda_A/a$, where λ_A is the mean free path of the condensing vapor. For Kn << 1, the transport processes are well described by the continuum theory. In cases where Kn >> 1, i.e., the free molecular regime, the kinetic theory of gases may be readily applied. For intermediate values of Kn, only approximate descriptions of the transport processes are possible.

Jeans (3) showed that the effective mean free path λ_A in a binary mixture of species A and B is given by

$$\lambda_A = \left\{ \frac{\pi}{kT}\left[P_A\sigma_{AA}^2\sqrt{2} + P_B\sigma_{AB}^2(1+Z)^{1/2}\right] \right\}^{-1}$$

where P_A and P_B are the partial pressures, σ_{AA} is the collision diameter for binary collisions between molecules of A, and σ_{AB} for collisions between molecules of A and B. Z is the ratio of molar weights, i.e., $Z = M_A/M_B$.

In the particular case being considered $P_A << P_B$, i.e., the background gas pressure $P_B \simeq P$, where P is the total pressure. Consequently the expression for λ_A simplifies to

$$\lambda_A = \left\{ \frac{\pi P}{kT}\sigma_{AB}^2(1+Z)^{1/2} \right\}^{-1} \qquad (1)$$

It also follows that

$$\lambda_B = \left\{ \frac{\pi P}{kT}\sigma_{BB}^2\sqrt{2} \right\}^{-1} \qquad (2)$$

From Eq. (1) and (2),

$$\frac{\lambda_B}{\lambda_A} = \frac{\sigma_{AB}^2}{\sigma_{BB}^2}\sqrt{\frac{1+Z}{2}}$$

and since $\sigma_{AB} = (\sigma_{AA}+\sigma_{BB})/2$

$$\frac{\lambda_B}{\lambda_A} = \frac{1}{4}\left(1 + \frac{\sigma_{AA}}{\sigma_{BB}}\right)^2\sqrt{\frac{1+Z}{2}} \qquad (3)$$

It is possible to recast eqn. 3 in terms of the kinematic viscosity ν_B of the species B.

$$\lambda_B = \nu_B\left(\frac{\pi M_B}{2RT}\right)^{1/2} = 2\,\frac{\nu_B}{\overline{V}_B}$$

where $\overline{V}_B = (\frac{8RT}{\pi M_B})^{1/2}$ is the mean velocity of molecules of B. Similarly the mean velocity of molecules of A is given by

$$\overline{V}_A = \left(\frac{8RT}{\pi M_A}\right)^{1/2} \qquad (4)$$

Transport processes at intermediate values of the Knudsen number may be described approximately by the flux matching method (4). This method has been used to compute the rate of growth of particles by condensation and adsorption, and heat transfer between the particle and the surrounding gas. In the flux-matching method, the region surrounding a spherical particle is divided into two parts by a concentric boundary sphere

which is located at a distance ℓ from the particle surface (Fig. 4). Within this boundary sphere the fluxes are described by the kinetic theory results for the free molecular regime. Outside the boundary sphere the fluxes are described using continuum transport theory. The fluxes calculated by the two methods are then matched at the boundary sphere. If the fluxes are matched at the particle surface, i.e., $\ell = 0$, the flux of mass I to the particle surface becomes simply (5)

$$\frac{I}{I_c} = \left(1 + \frac{I_c}{I_{fm}}\right)^{-1} \tag{5}$$

where the subscripts c and fm denote continuum and free molecular fluxes, respectively. The ratio of the free molecular mass flux to the continuum mass flux may be written (5)

$$\frac{I_c}{I_{fm}} = \beta Kn$$

where β is a parameter whose value will be determined in subsequent equations. So Eq. (5) becomes

$$\frac{I}{I_c} = (1 + \beta Kn)^{-1} \tag{6}$$

Similarly the heat flux may be described by

$$\frac{Q}{Q_c} = (1 + \gamma Kn)^{-1}$$

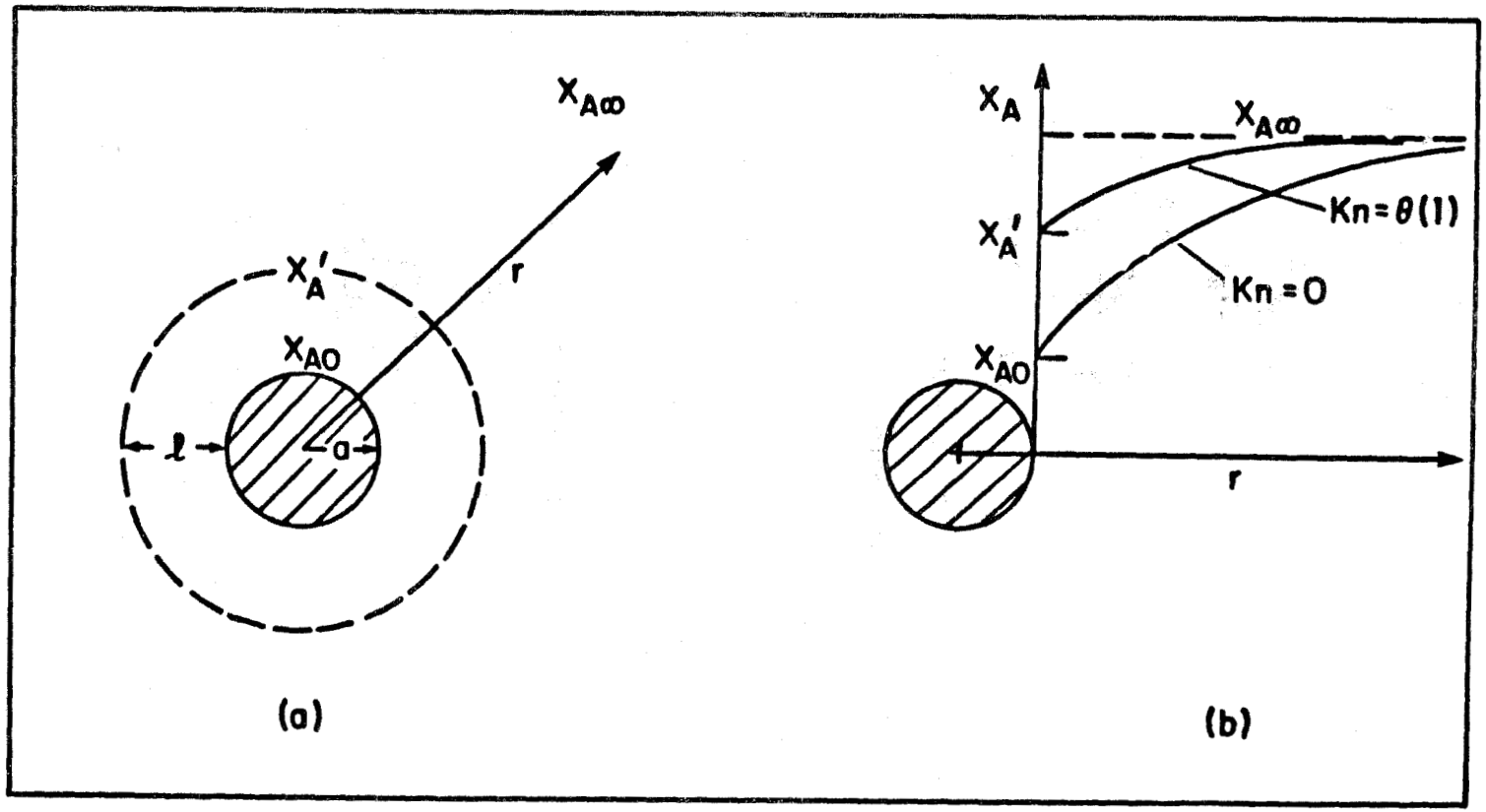

Figure 4. Illustration of the flux matching method

(a) Boundary sphere and vapor concentrations.

(b) Vapor concentration as a function of radial distance.

β and γ relate the continuum transport properties D_{AB} and K_T to the free molecular transport properties given by the kinetic theory of gases (5,6). The relationship is given by

$$\beta = \frac{4D_{AB}}{\lambda_A \bar{V}_A} \tag{7}$$

$$\gamma = \frac{4\ K_T T}{\lambda_A \bar{V}_B P\left(\frac{C_{vB}}{R} + \frac{1}{2}\right)} \tag{8}$$

Fuchs and Sutugin (5) assumed $\beta = 4/3$ in their calculation of condensational growth rates in the transition regime. Davis and Ray (7) have recently shown that this assumption can lead to substantial errors in the mass transfer rates since the dependence of the mass flux on the molecular weight and properties of the condensing species is neglected.

The diffusivity of the binary system (A,B) and the thermal conductivity of the major species B must be known if more precise values of β and γ (Eqs. 7 and 8) are to be used. Using a Leonard-Jones interaction potential, these transport coefficients become (6):

$$D_{AB} = \frac{1.8824 \times 10^{-22}}{P \sigma_{AB}^2\ \Omega_{AB}^{(1,1)}} \sqrt{\frac{T^3}{ZM_B}(1 + Z)} \qquad m^2/sec \tag{9}$$

$$K_T = \frac{8.3264 \times 10^{-22}}{\sigma_{BB}^2\ \Omega_{BB}^{(2,2)}} \left(\frac{4}{15}\frac{C_{vB}}{R} + \frac{3}{5}\right)\sqrt{\frac{T}{M_B}} \qquad W/m°K \tag{10}$$

where the collision integrals $\Omega_{AB}^{(1,1)}$ and $\Omega_{BB}^{(2,2)}$ are functions of the reduced temperatures, $T_{AB} = \frac{kT}{\epsilon_{AB}}$ and $T_{BB} = \frac{kT}{\epsilon_{BB}}$, respectively. ϵ_{AB} and ϵ_{BB} are Leonard-Jones parameters. C_{vB} is the molar specific heat of B. For diatomic gases $C_v = \frac{5}{2}R$. Thus β and γ become

$$\beta = 1.1784 \frac{(1+Z)}{\Omega_{AB}^{(1,1)}} \tag{11}$$

$$\gamma = 7.37\left(\frac{\frac{4}{15}\frac{C_{vB}}{R} + \frac{3}{5}}{\frac{C_{vB}}{R} + \frac{1}{2}}\right) \frac{\left(1 + \sigma_{AA}/\sigma_{BB}\right)^2}{4\,\Omega_{BB}^{(2,2)}} \sqrt{\frac{1+Z}{2}} \tag{12}$$

For a specified binary gas mixture, β and γ are weak functions of temperature. Since the temperature variation in the vicinity of a growing particle is small, we shall assume β and γ are constants in this analysis.

The mass flux predicted using Eqs. (5) and (11) is compared with experimental data of Davis and Ray (7) in Fig. 5. The theoretical formulation of Sitarski-Nowakowski is also shown (8), and corresponds to:

$$\frac{I}{I_{fm}} = \frac{Kn\left\{1 + \frac{3(1+z)^2}{4(3+5z)}\,Kn\right\}}{\left\{\frac{8\Omega_{AB}^{(1,1)}}{3\pi(1+z)} + \left[\frac{1+2z}{\pi(3+5z)} + \frac{1}{2}\right]Kn + \frac{9(1+z)^2}{8(3+5z)}\,Kn^2\right\}} \tag{13}$$

The Fuchs-Sutugin formulation is the expresssion:

$$\frac{I}{I_{fm}} = \frac{10.75\ Kn\ (1 + 8.064\ Kn)}{\{1 + 13.789\ Kn + 86.682\ Kn^2\}} \tag{14}$$

In Eqs. (5), (13) and (14), the mean free path (λ_A) for DBS vapor in N_2 gas has been used to calculate the Knudsen number, and $\Omega_{AB}^{(1,1)}$ was calculated to be 1.34 for DBS/N_2 at 293°K (6,7,9).

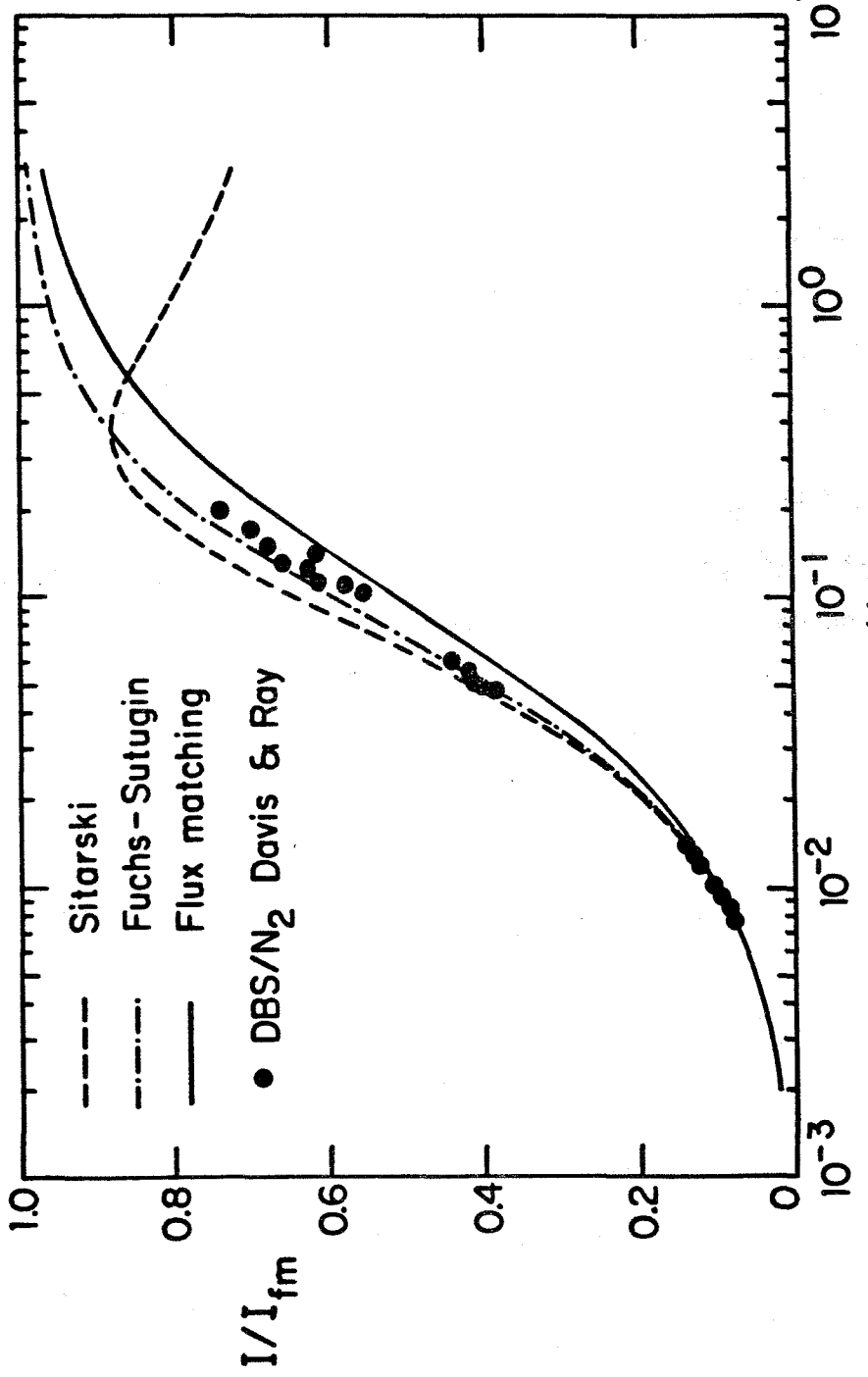

Figure 5. Comparison of theoretical formulations with experimental results for evaporation in the transition regime.

It can be seen from Fig. 5 that the flux matching approach underpredicts the experimental values by less than 10% over the entire range of Knudsen numbers. This approach, therefore, predicts mass flux reasonably well. The Fuchs-Sutugin equation gives quite a good agreement with the data, particularly for $Kn < 0.1$. The Sitarski-Nowakowski equation underpredicts the flux substantially in the regime $Kn > 1$.

The flux matching method with the boundary sphere located at the particle surface makes it possible to describe the composition and temperature fields in the region surrounding the particle using the continuum transport relationships. The boundary conditions at the particle surface are derived by matching the continuum and free molecular fluxes.

Consider a particle of radius a with surface temperature T_o and vapor concentration $x_A = x_{Ao}$ (Fig. 4). Far from the particle, $T = T_\infty$, $x_A = x_{A_\infty}$. At the boundary sphere, let $x_A' = x_A$. At $\ell = 0$, the vapor flux matching implies

$$4\pi D a (x_{A_\infty} - x_A') = a^2 \bar{V}_A (x_A' - x_{Ao}) \tag{15}$$

where D denotes the binary diffusivity D_{AB}.

Using the relations $\beta = \frac{4D}{\lambda_A \bar{V}_A}$ and $Kn = \frac{\lambda_A}{a}$, the value of x_A' for $\ell = 0$ is given as

$$x_A' = x_{Ao} + (x_{A_\infty} - x_{Ao}) \frac{\beta Kn}{1+\beta Kn} \tag{16}$$

Since $P_A << P_B$, it can be assumed that the heat conduction occurs mainly through the background gas rather than through the condensible vapor. Matching the free molecular and continuum heat fluxes yields

$$4\pi a K_T (T_\infty - T') = \pi a^2 \bar{V}_B \left(\frac{C_{vB}}{R} + \frac{1}{2} \right) (T' - T_o) \frac{P}{T} \tag{17}$$

Since $$K_T = \frac{1}{4}\gamma\lambda_A\bar{V}_B\frac{P}{T}\left(\frac{C_{vB}}{R}+\frac{1}{2}\right) \quad ,$$

we obtain

$$T' = T_o + (T_\infty - T_o)\frac{\gamma Kn}{1+\gamma Kn} \tag{18}$$

Transport of vapor and energy to the surface of the particle may now be evaluated using the continuum transport equations subject to the boundary conditions x_A' and T' at the particle surface.

2.4 Nucleation Rates in the Presence of Growing Particles.

The classical treatment of homogeneous nucleation involves the computation of the intrinsic nucleation rate, J_∞ (number of particles formed per unit volume per unit time) based upon the mean vapor concentration. Pesthy et al. (2) have recently shown that, once some particles have been formed, the reduction of the vapor concentration in the region surrounding the particle by diffusion to the particle surface can substantially reduce the total rate of homogeneous nucleation. Following the approach of Pesthy et al. (2) we may define a clearance volume for use in the evaluation of the average nucleation rate. Consider a particle with radius a at time t. At large radial distance, r, the vapor pressure is not perturbed by the particle, so the nucleation rate approaches the intrinsic rate, J_∞. Nearer to the particle surface, the nucleation rate is a function of radial distance, J(r). This is illustrated in Fig. 6.

The clearance volume is the volume inside the radial distance ρa defined such that, if the nucleation rate in the region from a to ρa is taken to be zero and that beyond ρa is taken to be J_∞, the total nucleation rate equals that determined by the exact volume integration. Thus, we have

$$\int_a^\infty J(r) 4\pi r^2 dr = \int_{\rho a}^\infty J_\infty 4\pi r^2 dr \tag{19}$$

Since $J(r) = 0$ for $r < a$, the integrals may be written as

$$\int_0^\infty J(r) 4\pi r^2 dr = \int_{\rho a}^\infty J_\infty 4\pi r^2 dr \tag{20}$$

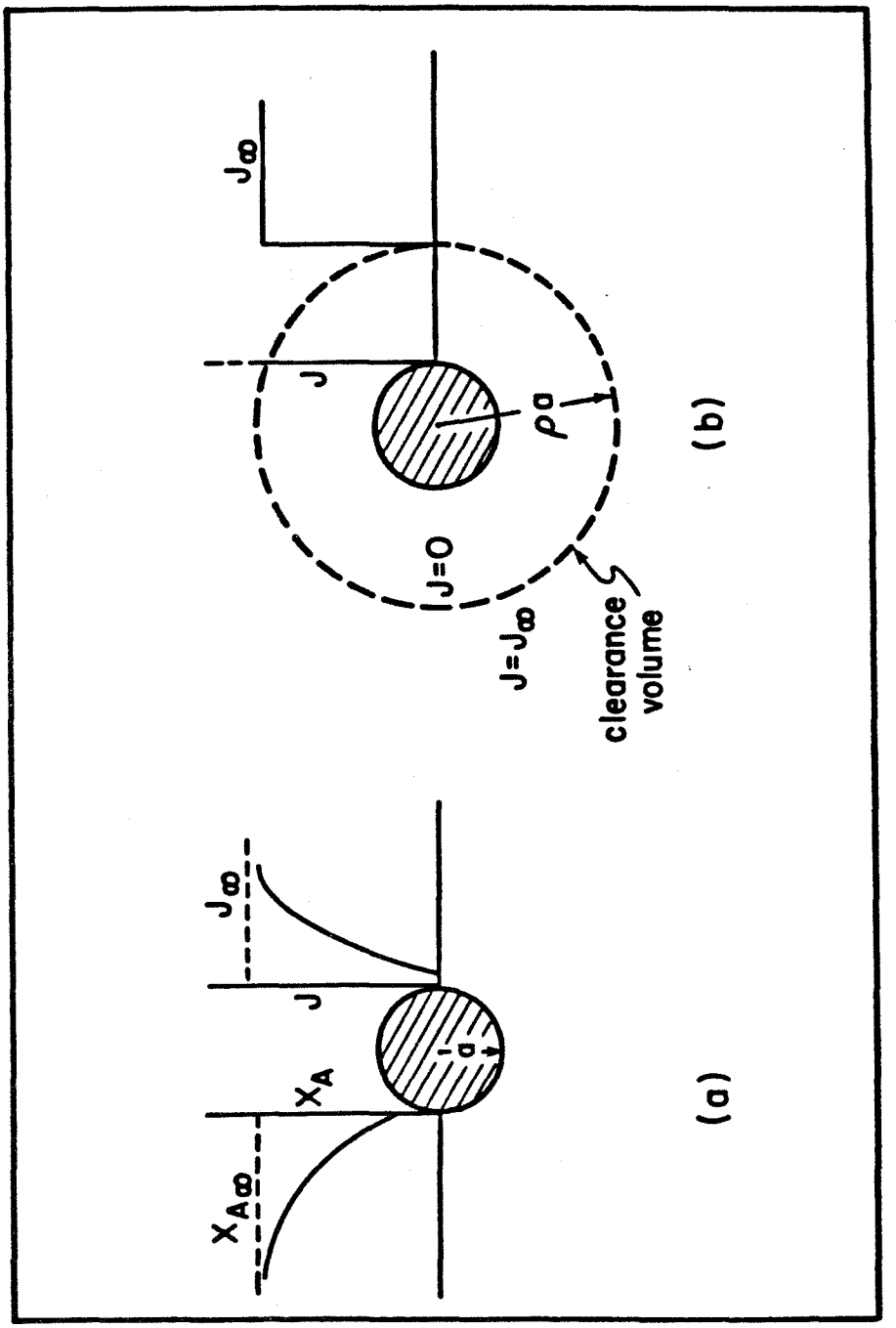

Figure 6. Illustration of the concept of clearance volume

(a) Actual vapor concentrations and nucleation rates near a particle.

(b) Nucleation rates assumed in determination of the clearance volume.

The dimensionless clearance volume may be explicity evaluated as

$$\rho^3 = \frac{3}{a^3}\int_0^\infty \left(1 - \frac{J(r)}{J_\infty}\right) r^2 dr \tag{21}$$

In terms of the dimensionless radial coordinate

$$y = \frac{r}{a(1+\beta Kn)} \tag{22}$$

Eq. (21) becomes

$$\rho^3 = 3(1+\beta Kn)^3 \int_0^\infty \left(1 - \frac{J(y,t)}{J_\infty}\right) y^2 dy \tag{23}$$

For an ensemble of particles, the regions of influence of adjacent particles may overlap. The appropriate limit of integration is, therefore, a finite radius r_c. We may write

$$\rho^3 = 3(1+\beta Kn)^3 \int_0^{\frac{r_c}{a(1+\beta Kn)}} \left(1 - \frac{J(y,t)}{J_\infty}\right) y^2 dy$$

The fractional reduction in the overall nucleation rate due to a growing polydisperse aerosol may be estimated by computing the fraction of the volume in which nucleation is quenched. This total fractional clearance volume, Ω, is calculated by integrating over the particle size distribution function, i.e.,

$$\Omega = \int_0^\infty \frac{4}{3}\pi\rho^3 a^3 n(a,t) da \tag{24}$$

In the limit of small Ω, the volume average nucleation rate is

$$J_{av} = J_{\infty} (1-\Omega) \tag{25}$$

As Ω increases, the average nucleation rate approaches zero. A detailed treatment of the final stages of nucleation quenching taking into account the spatial distribution of particles and overlapping regions of influence, is beyond the scope of the present analysis. Instead, the average nucleation rate will be approximated by

$$J_{av} \simeq \begin{cases} J_{\infty}(1-\Omega) & : \quad 0 \leq \Omega < 1 \\ \\ 0 & : \quad \Omega \geq 1 \end{cases} \tag{26}$$

i.e., nucleation is assumed to be completely supressed for fractional clearance volumes greater than unity.

2.5 Concentration and Temperature Profiles.

The chemical species and energy conservation equations may be solved subject to the boundary conditions derived by flux matching at the particle surface, Eq. (16) and (18), in order to compute the vapor concentration and temperature profiles in the region surrounding a growing particle. The problem is unsteady, but can be simplified since the time scales for nucleation, vapor diffusion, energy transport, and particle growth are widely different. This is illustrated in Table 2. For the vapors of interest to the present discussion, the time scale for heat conduction in the gas, τ_c, is much shorter than that for conduction within the particle. Most of the heat can, therefore, be assumed to be conducted away from the particle. The development of vapor concentration and temperature profiles will occur on similar time scales. The time required for particle growth is much longer than the time for relaxation of the temperature and composition fields surrounding the particle. For this reason, fluxes to the particle may be described by a quasi-steady-state model of transport into the gas surrounding the particle.

The classical treatment of homogeneous nucleation predicts the rate of new particle formation after a quasi steady cluster population has been established. Collins (10) derived the following expression for the time lag τ_{sn} in developing this steady state population of clusters in self-nucleation:

$$\tau_{sn} = 4\pi \left(\frac{\sigma}{RT}\right) \frac{\sqrt{2\pi M_A RT}}{P_A (\ell n S)^2}$$

Table 2. Characteristic times for growing particle processes.

	Heat Conduction in Air	Heat Conduction in Particle	Vapor Diffusion	Particle Growth
Characteristic Time τ	$\frac{a^2}{\alpha_T} \equiv \tau_c$	$\frac{a^2}{\alpha_d}$	$\frac{a^2}{\mathcal{D}}$	$\frac{c_d a^2 (1+\beta Kn)}{c\mathcal{D}x_{A\infty}}$
τ/τ_c	1	$\frac{\alpha_T}{\alpha_d}$	$\frac{\alpha_T}{\mathcal{D}} \equiv Le$	$\frac{c_d Le(1+\beta Kn)}{cx_{A\infty}}$
Typical Values of τ/τ_c in Air				
Water	1	145	0.86	$> 10^2$
Organics	1	200	2 - 4	$> 10^2$
Metals	1	~ 5	1.5	$> 10^4$

For most vapors of interest, the characteristic nucleation times are very small compared to the time scale of particle growth, so that steady state nucleation theory may be applied.

The steady state mass, chemical species, and energy conservation equations are:

$$\frac{1}{r^2}\frac{d}{dr}(cr^2V^*) = 0 \tag{27}$$

$$V^*\frac{dx_A}{dr} = \mathcal{D}\frac{1}{r^2}\frac{d}{dr}\left(r^2\frac{dx_A}{dr}\right) \tag{28}$$

$$\zeta V\frac{dT}{dr} = \alpha_T\frac{1}{r^2}\frac{d}{dr}\left(r^2\frac{dT}{dr}\right) \tag{29}$$

where the mass and chemical species conservation equations are written in molar units to take advantage of the simplification which the constant molar density affords in calculation of the molar average radial velocity, V^*. ζ is the ratio of specific heats, C_{pA}/C_{pB}.

The mass balance for the particle is

$$cV_o^*4\pi a^2 + c_d\frac{d}{dt}\left(\frac{4}{3}\pi a^3\right) = 0 \tag{30}$$

The particle energy balance may be written

$$cV_o^*\Delta H_v\,(4\pi a^2) - K_T\frac{dT}{dr}\Big|_a(4\pi a^2) = 0 \tag{31}$$

Equations (27) and (28) are solved subject to the boundary conditions

$$x_A = x_A' \quad , \quad r = a$$

$$x_A = x_{A\infty} \quad , \quad r \to \infty$$

The molar average velocity at the particle surface is then found to be

$$V_o^* = - \frac{\mathcal{D}}{a} \ln \left(\frac{1-x_A'}{1-x_{A\infty}} \right) \tag{32}$$

Limiting our consideration to a dilute system, $x_{A\infty} << 1$, and utilizing the flux matching condition, Eq. (16); Eq. (32) may be written

$$V_o^* \simeq - \frac{\mathcal{D}}{a} \frac{(x_{A\infty}-x_{Ao})}{1+\beta Kn} \tag{33}$$

Substituting into Eq. (30), the particle growth rate becomes

$$a(1+\beta Kn) \frac{da}{dt} = \frac{c\mathcal{D}}{c_d} (x_{A\infty}-x_{Ao}) \tag{34}$$

For binary system containing a dilute vapor, the mass average velocity is related to the molar average velocity by

$$V \simeq V^* \frac{M_A}{M_B} \tag{35}$$

For a dilute vapor, Eq. (33) and Eq. (18) may be combined with Eq. (29) to obtain

$$K_T(T_o-T_\infty) = \Delta H_v c\mathcal{D}(x_{A\infty}-x_{Ao}) \frac{1+\gamma Kn}{1+\beta Kn} \tag{36}$$

Eq. (36) will be solved to determine T_o. It is important to note that, because of the Kelvin effect, the equilibrium concentration at the surface is

$$x_{Ao} = x_{sat}(T_o) e^{\frac{\phi}{aT_o}} \tag{37}$$

where

$$\phi = \frac{2\sigma v_m}{k}$$

The time dependent vapor concentration and temperature profiles may now be determined by solving the full conservation equations, viz.,

$$\frac{\partial x_A}{\partial t} + V^* \frac{\partial x_A}{\partial r} = \frac{\mathcal{D}}{r^2} \frac{\partial}{\partial r} \left(r^2 \frac{\partial x_A}{\partial r} \right) \tag{38}$$

$$\frac{\partial T}{\partial r} + \zeta V \frac{\partial T}{\partial r} = \frac{\alpha_T}{r^2} \frac{\partial}{\partial r} \left(r^2 \frac{\partial T}{\partial r} \right) \tag{39}$$

subject to the boundary conditions

$$\begin{aligned} x_A &= x_A' \quad , \quad T = T' \quad \text{at } r = a(t) \\ x_A &= x_{A_\infty} \quad , \quad T = T_\infty \quad \text{at } r \to \infty \end{aligned} \tag{40}$$

and initial conditions

$$x_A = x_{A_\infty} \quad , \quad T = T_\infty \quad \text{at } t = 0 \tag{41}$$

The complications introduced by the moving boundary, a = a(t) may be simplified by rescaling the radial coordinate. Pesthy et al. (2) used r/a(t). The present problem requires the radial coordinate defined in Eq. (22), i.e., $y = r/[a(1+\beta Kn)]$, in order to account for the Knudsen number dependence. Equations (38) and (39) are then transformed to

$$\frac{a^2(1+\beta Kn)^2}{\mathcal{D}} \frac{\partial x_A}{\partial t} - \left\{ y \frac{a(1+\beta Kn)}{\mathcal{D}} \frac{\partial a}{\partial t} + \frac{1}{y^2} \frac{x_{A\infty}-x_{Ao}}{(1+\beta Kn)^2} \right\} \frac{\partial x_A}{\partial y} = \frac{1}{y^2} \frac{\partial}{\partial y} \left(y^2 \frac{\partial x_A}{\partial y}\right) \tag{42}$$

$$\frac{a^2(1+\beta Kn)^2}{\alpha_T} \frac{\partial T}{\partial t} - \left\{ y \frac{a(1+\beta Kn)}{\alpha_T} \frac{\partial a}{\partial t} + \frac{\zeta}{y^2} \frac{\mathcal{D}}{\alpha} \frac{M_A}{M_B} \frac{(x_{A\infty}-x_{Ao})}{(1+\beta Kn)^2} \right\} \frac{\partial T}{\partial y} = \frac{1}{y^2} \frac{\partial}{\partial y} \left(y^2 \frac{\partial T}{\partial y}\right) \tag{43}$$

Defining parameters A and B as

$$A \equiv \frac{1}{2} \frac{c}{c_d} (x_{A\infty}-x_{Ao}) \tag{44}$$

$$B \equiv \frac{(x_{A\infty}-x_{Ao})}{(1+\beta Kn)^2} \tag{45}$$

equations (42) and (43) become

$$\frac{\partial x_A}{\partial \theta} - \left[2Ay + \frac{B}{y^2}\right] \frac{\partial x_A}{\partial y} = \frac{1}{y^2} \frac{\partial}{\partial y} \left(y^2 \frac{\partial x_A}{\partial y}\right) \tag{46}$$

$$\frac{\partial T}{\partial \theta} - \left[2Ay + \frac{B\zeta}{y^2} \frac{M_A}{M_B}\right] \frac{\partial T}{\partial y} = \frac{Le}{y^2} \frac{\partial}{\partial y} \left(y^2 \frac{\partial T}{\partial y}\right) \tag{47}$$

The initial and boundary conditions are now given by,

$$\left.\begin{aligned} x_A &= x_A' \quad , \quad T = T' \quad \text{at } y = \frac{1}{1+\beta Kn} \\ x_A &\to x_{A_\infty} \quad , \quad T = T_\infty \quad \text{as } y \to \infty \end{aligned}\right\} \tag{48}$$

$$x_A = x_{A_\infty} \quad , \quad T = T_\infty \quad \text{at } \theta = 0 \tag{49}$$

The new time scale for the quasi steady state, θ, is defined such that

$$d\theta = \frac{\mathcal{D}\, dt}{a^2(1+\beta Kn)^2} \tag{50}$$

θ may be calculated by integrating Eq. (50) over the particle history. The particle growth rate is given by Eq. (34) which may be written in the form

$$\frac{da}{dt} = \frac{2\, A\, \mathcal{D}}{a(1+\beta Kn)} \tag{51}$$

where A is the dimensionless growth parameter given in Eq. (44). Recall that $x_{Ao} = x_{sat}(T_o)\exp(\frac{\phi}{aT_o})$ and that the radius of the freshly nucleated particle is

$$a^* = 2\sigma v_m/(kT_o \ln S) = \phi/(T_o \ln S)$$

It is obvious, therefore that A = 0 when a = a*. In the nucleation theory, it is assumed that the droplet current is independent of cluster size. Thus, the nucleation rate is the same for particles somewhat

larger than a*; and for particles of size somewhat greater than a*, it is reasonable to assume that $x_{A_o} \cong x_{sat}(T_o)$, so that A is independent of the particle radius, i.e., the Kelvin effect is neglected. Equation (51) may therefore be integrated to yield

$$a^2(1+\beta Kn)^2 = 4ADt + a^{*2}\,(1+\beta Kn^*)^2 \tag{52}$$

where $Kn^* = \frac{\lambda_A}{a^*}$, and $a = a^*$ at $t = 0$.

Substituting Eq. (52) into Eq. (50), we get

$$d\theta = \frac{D\,dt}{4ADt + a^{*2}(1+\beta Kn^*)^2}$$

Setting $\theta = 0$ at $t = 0$ and integrating, the time scale for quasi-steady particle growth becomes

$$\theta = \frac{1}{4A} \ln \left\{ 1 + \frac{4ADt}{a^{*2}(1+\beta Kn^*)^2} \right\} \tag{53}$$

Near the particle surface, the convection terms are small compared to the other terms, and the Eqns. (46), (47) are approximated by

$$\frac{\partial x_A}{\partial \theta} = \frac{1}{y^2} \frac{\partial}{\partial y} \left(y^2 \frac{\partial x_A}{\partial y} \right) \tag{54}$$

$$\frac{\partial T}{\partial \theta} = \frac{Le}{y^2} \frac{\partial}{\partial y} \left(y^2 \frac{\partial T}{\partial y} \right) \tag{55}$$

These equations apply only until the concentration and temperature gradients begin to change beyond $y > \frac{1}{2A}$. During this interval of time, $\theta \leq 1/4A$, very little particle growth occurs so this initial transient may be neglected.

The particle growth phase is therefore the quasi-steady state given by

$$-(2Ay + \frac{B}{y^2}) \frac{\partial x_A}{\partial y} = \frac{1}{y^2} \frac{\partial}{\partial y} (y^2 \frac{\partial x_A}{\partial y}) \tag{56}$$

$$-(2A + \frac{B\zeta}{y^2} \frac{M_A}{M_B}) \frac{\partial T}{\partial y} = \frac{Le}{y^2} \frac{\partial}{\partial y} (y^2 \frac{\partial T}{\partial y}) \tag{57}$$

Since vapor concentration is assumed to be dilute, the term $\frac{B\zeta}{y^2} \frac{M_A}{M_B}$ can be neglected, and the equations simplify to

$$-2Ay \frac{\partial x_A}{\partial y} = \frac{1}{y^2} \frac{\partial}{\partial y} (y^2 \frac{\partial x_A}{\partial y}) \tag{58}$$

$$-2Ay \frac{\partial T}{\partial y} = \frac{Le}{y^2} \frac{\partial}{\partial y} (y^2 \frac{\partial T}{\partial y}) \tag{59}$$

with boundary conditions given by Eq. (48).

Solutions to equations (58) and (59) are

$$\frac{x_A(y)-x_A'}{x_{A_\infty}-x_A'} = 1 - F\ (y;A,Kn) \tag{60}$$

$$\frac{T(y)-T_\infty}{T'-T_\infty} = F\ (y; \frac{A}{Le}, Kn) \tag{61}$$

where

$$F(y;A,Kn) = \frac{\frac{1}{y} e^{-Ay^2} - \sqrt{\pi A}\ \mathrm{erfc}(\sqrt{A}y)}{(1+\beta Kn)\exp\left\{\frac{-A}{(1+\beta Kn)^2}\right\} - \sqrt{\pi A}\ \mathrm{erfc}\left(\frac{\sqrt{A}}{1+Kn}\right)} \tag{62}$$

since $x_A << 1$, A is small and F can be approximated by

$$F(y;A,Kn) \cong \frac{e^{-Ay^2}}{y(1+\beta Kn)(2Ay^2 + \sqrt{2A}y + 1)} \tag{63}$$

The following definitions are now introduced

$$\Delta_T = \frac{T_o - T_\infty}{T_o} \tag{64}$$

$$\Delta_x = \frac{x_{A\infty} - x_{Ao}}{x_{A\infty}} \tag{65}$$

To determine Δ_T, the integrated Clausius-Clapeyron expression is used, i.e.,

$$x_{sat}(T_o) = x_{sat}(T_\infty)\ \exp\left[\frac{\Delta H_v}{RT_\infty}\left(1 - \frac{T_\infty}{T_o}\right)\right] \tag{66}$$

Equation (36) may now be rewritten as

$$\Delta_T = \left(\frac{\Delta H_v}{RT_\infty}\right)\cdot\left(\frac{R}{M_B C_p}\right)\cdot Le^{-1}\left(\frac{1+\gamma Kn}{1+\beta Kn}\right)\left[x_{A_\infty} - x_{sat}(T_\infty)\exp\left\{\frac{\phi}{aT_o} + \left(\frac{\Delta H_v \Delta_T}{RT_\infty}\right)\left(\frac{1}{1+\Delta_T}\right)\right\}\right] \tag{67}$$

The Kelvin effect has been introduced in Eq. (67). As discussed earlier, the Kelvin effect introduces a short time lag in the solution and may be neglected. Since $x_{A_\infty} >> x_{sat}$ for most cases of interest,

$$\Delta_T \simeq \left(\frac{\Delta H_v}{RT_\infty}\right)\left(\frac{R}{M_B C_p}\right) \; Le^{-1} \quad \left(\frac{1+\gamma Kn}{1+\beta Kn}\right) \; x_{A_\infty} \tag{68}$$

Δ_x can now be computed to be

$$\Delta_x = 1 - \frac{x_{sat}(T_\infty)}{x_{A_\infty}} \; \exp\left[\frac{\Delta H_v}{RT_\infty} \; \frac{\Delta_T}{(1+\Delta_T)}\right] \tag{69}$$

The vapor concentration and temperature profiles, therefore, are given by

$$\chi(y) \equiv \frac{x_A(y)}{x_{A_\infty}} = 1 - \Delta_x \left(\frac{1}{1+\beta Kn}\right) F\,(y;A,Kn) \tag{70}$$

$$\Gamma(y) \equiv \frac{T(y)}{T_\infty} = 1 + \Delta_T \left(\frac{1}{1+\gamma Kn}\right) F\left(y;\frac{A}{Le},Kn\right) \tag{71}$$

The saturation ratio S(y) is

$$S(y) = \chi(y) \; \frac{x_{A_\infty}}{x_{sat}(\Gamma(y))} \tag{72}$$

Using the integrated Clausius-Clapeyron equation,

$$\frac{S(y)}{S_\infty} = \chi(y) \; \exp\left[-\frac{\Delta H_v}{RT_\infty}\left(1 - \frac{1}{\Gamma(y)}\right)\right] \tag{73}$$

where

$$S_\infty = \frac{x_{A_\infty}}{x_{sat}(T_\infty)}$$

2.6 Clearance Volume and Average Nucleation Rates.

The results of the previous section give the vapor concentration and temperature profiles around a growing particle. These results will now be combined with the formulations of section (3) to obtain the clearance volume of a particle.

From nucleation theory (1), the local steady state nucleation rate is given by

$$J(y) = \frac{2P_A}{(2\pi M_A RT)^{1/2}} \left(\frac{P_A v_m^{2/3}}{kT}\right) \cdot \left(\frac{\sigma v_m^{2/3}}{kT}\right)^{1/2} \exp\left[-\frac{16\pi\sigma^3 v_m^2}{3(kT)^3(\ell nS)^2}\right] \quad (74)$$

Therefore,

$$\frac{J(y)}{J_\infty} = \left\{\frac{\chi(y)}{\Gamma(y)}\right\}^2 \exp\left[-\frac{16\pi}{3(\ell nS_\infty)^2}\left(\frac{\sigma v_m^{2/3}}{kT_\infty}\right)^3 \left\{\Gamma(y)^{-3}\left(\frac{\ell nS_\infty}{\ell nS(y)}\right)^2 - 1\right\}\right] \quad (75)$$

The dimensionless clearance volume ρ is then given by eqn. (23)

$$\rho^3 = 3\,(1+\beta Kn)^3 \int_0^\infty \left(1 - \frac{J(y)}{J_\infty}\right) y^2 dy$$

Figure 7 shows the dimensionless clearance volume ρ^3 as a function of the Knudsen number for water droplets in air. The values used in the simulation are shown in Table 3.

It can be seen from the figure that the dimensionless clearance volume ρ^3 is constant at small values of Kn and ρ^3 decreases with increasing monomer pressure. These results are consistent with the previous analysis (2).

Table 3. Parameter values for condensing water vapor

Parameter	Value	Parameter	Value
$\Delta H_v/R$	323°K	c/c_d	7.98×10^{-4}
T_∞	275°K	σ	0.072 N/m
Le	0.88	$P_{sat}(T_\infty)$	705 Pa
β	1.91	P	101.3 kPa
γ	2.8	c_d	55.5 kmole/m^3
λ_A	5.95×10^{-8} m	$\frac{R}{M_B c_p}$	0.274

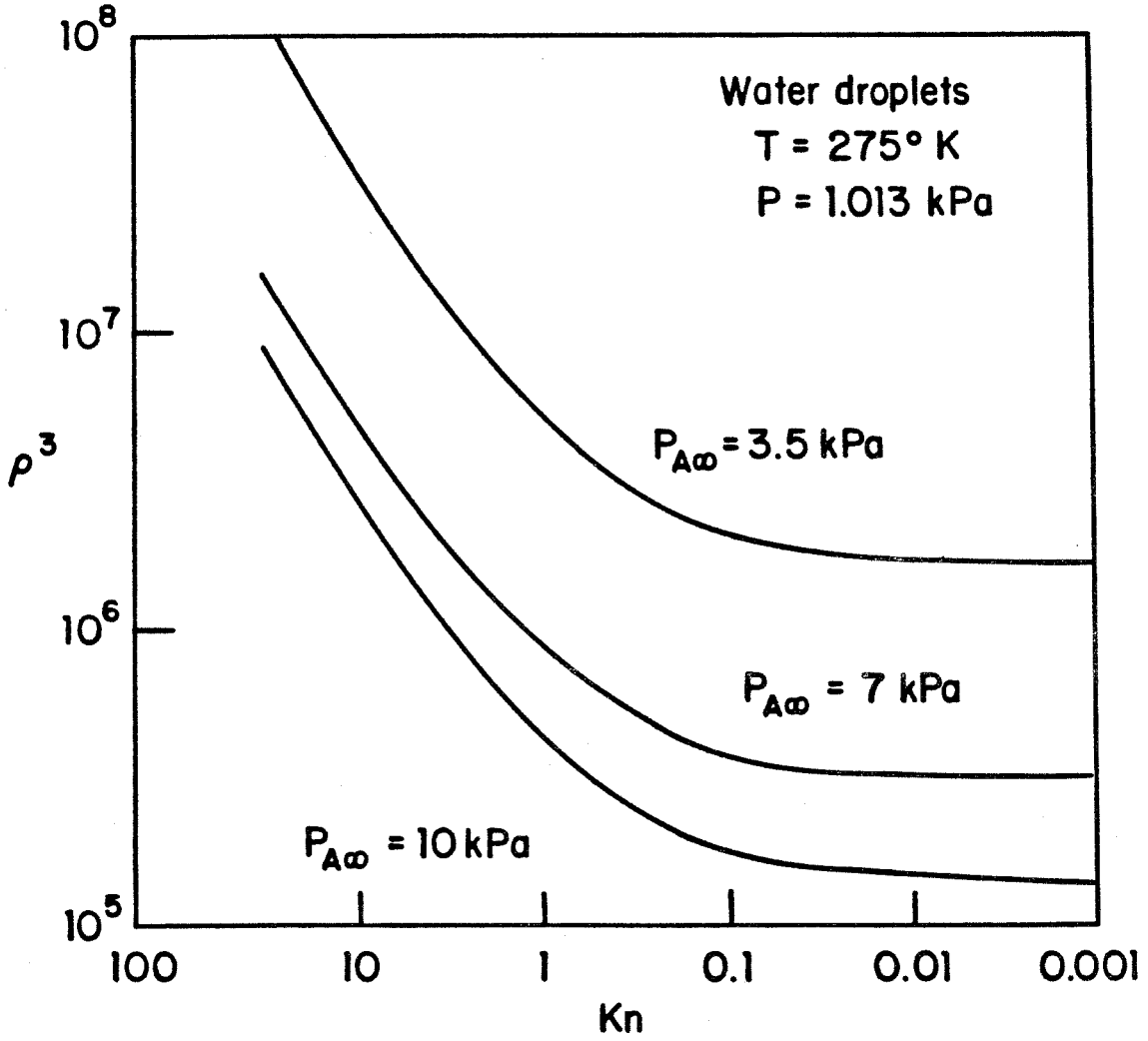

Figure 7. Dimensionless clearance volume ρ^3 for water droplets as a function of Knudsen number.

The most interesting feature is the behavior of ρ^3 at large Knudsen numbers; in this regime, ρ^3 vs. Kn is linear on the log scale with almost unit slope. In fact, ρ^3 as a function of Kn for all values of Kn can be approximated by the function

$$\rho^3 = \rho_o^3 (1 + \zeta Kn) \tag{76}$$

where ρ_o^3 is the dimensionless clearance volume for Kn → 0, and ζ is a constant which may vary with different vapors and different ambient vapor pressures, but usually has a value close to β, the constant used in flux matching method.

Thus, in the free molecular regime

$$\rho^3 \alpha Kn \tag{77}$$

This would seem to indicate that in the limit of Kn → ∞, ρ^3 → ∞ and nucleation would therefore be totally suppressed when aerosol is in the free molecular regime. That is, of course, not reasonable.

This apparent contradiction is easily resolved by noting that ρ^3 increases slowly compared to the decrease in the volume of the particle. Consequently, although ρ^3 increases with Knudsen number, the clearance volume of the particle which is $\frac{4}{3}\pi a^3\rho^3$ is decreasing, as can be seen from

$$\frac{4}{3}\pi a^3\rho^3 = \frac{4}{3}\pi a^3\rho_o^3 (1 + \zeta Kn) \tag{78}$$

For large Kn,

$$\frac{4}{3}\pi a^3\rho^3 = \frac{4}{3}\pi\rho_o^3\zeta\lambda_A^3 Kn^{-2}$$

2.7 Dimensionless Clearance Volume in the Free Molecular Regime.

The clearance volume calculations showed that the dimensionless clearance volume, ρ^3, of particles in the free molecular regime is approximately proportional to the Knudsen number. Particles in the free molecular size range can influence the kinetics of the condensing vapor because of collisions with vapor molecules and clusters. The collision frequency is given by the kinetic theory.

Consider a particle (Fig. 8) of radius a surrounded by vapor and non-condensing gases. From a distance r, vapor molecules in the differential element of volume $4\pi r^2 dr$ may be intercepted by the particle. The probability of interception depends on

(i) The fraction of the solid angle that is intercepted by the particle. This is approximated by $\pi a^2/(4\pi r^2) = a^2/(4r^2)$.

(ii) Collisions with vapor molecules and clusters in the cone between the vapor molecules at distance r and the particle. The characteristic frequency of monomer/monomer collisions which may contribute to nucleation is approximately given by

$$w \simeq \sigma_{AA} \bar{V}_A n_A \tag{79}$$

where σ_{AA} is the collision cross section and $\bar{V}_A$ is the mean molecular speed. For the vapor molecules to reach the particle from a distance r, the characteristic time is $r/\bar{V}_A$. Therefore, the probability of the molecules being intercepted by the particle is $\sigma_{AA} n_A r$.

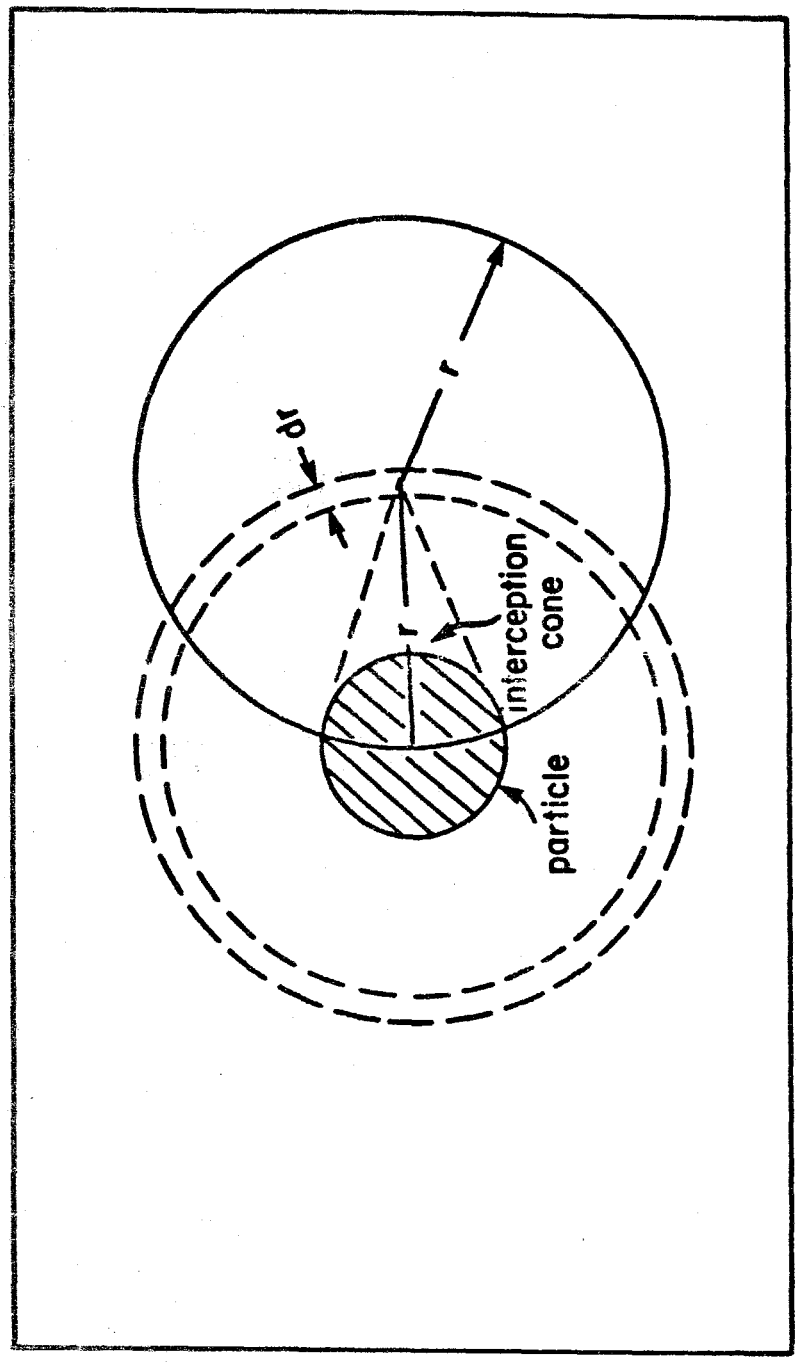

Figure 8. Interception effect of a particle in the free molecular size range on vapor molecules surrounding it.

The above two effects combine, and we obtain the change in nucleation rate to be

$$1 - \frac{J(r)}{J_\infty} = \frac{a^2}{4r^2} \cdot \frac{1}{\sigma_{AA} r n_A} \tag{80}$$

Equation (80) has been derived from very simplified arguments, but it is sufficient to indicate the dependence of clearance volume on the Knudsen number.

From Section 2.4

$$\rho^3 = \frac{3}{a^3} \int_a^{r_c} \left(1 - \frac{J(r)}{J(\infty)}\right) \cdot r^2 dr$$

using (80),

$$\rho^3 = \frac{3}{4\sigma_{AA} n_A} \cdot \left(\frac{1}{a}\right) (\ell n r_c - \ell n a) \tag{81}$$

Since $r_c >> a$,

$$\rho^3 = \frac{3}{4\sigma_{AA} n_A} \cdot \left(\frac{1}{a}\right) \ell n r_c \tag{82}$$

Thus, we see that the dimensionless clearance volume is proportional to the Knudsen number in the large Knudsen number limit.

2.8 Time Evolution of Aerosol.

It is now possible to determine the evolution of aerosol from a spatially homogeneous mixture of aerosol and vapor present in noncondensing gases. It will be assumed that bulk gas conditions change much more slowly than the rate at which the aerosol and its surrounding layers can adjust to the change. Temperature changes in the bulk gas are now incorporated in equation (83) as follows

$$\frac{\partial n}{\partial t} + \frac{\partial}{\partial a}\left[\dot{a}n(a,t)\right] = J_{av}\delta(a-a^*) + \frac{n}{\rho_g}\frac{\partial \rho_g}{\partial t} \tag{83}$$

where it is assumed

$$J_{av} = \begin{cases} J_\infty (1-\Omega) & 0 \leq \Omega \leq 1 \\ 0 & \Omega > 1 \end{cases}$$

We need one more equation to complete the system of ordinary differential equations. This is the vapor conservation equation which may be written

$$\frac{d\overline{P}_A}{dt} = \frac{\Delta\overline{P}_A}{\rho_g}\frac{\partial \rho_g}{\partial t} - 4\pi RTc_d\left[\int_{a^*}^{\infty} na^2\left(\dot{a} + \frac{a}{3\rho_g}\frac{\partial \rho_g}{\partial t}\right)da + \frac{1}{3}a^{*3}J_{av}\right] + R_p$$

In the above equation $\overline{P}_A$ is the average vapor pressure and

$$\Delta\overline{P}_A = \overline{P}_A(t=0) - \overline{P}_A(t=t) + \int_0^t R_p dt \tag{84}$$

R_p is the rate of vapor pressure increase due to reactions that may occur in the system. The solutions for monomer concentrations were obtained on the basis of P_{A_∞}, which was the ambient vapor pressure. For most systems, nucleation is quenched before a significant amount of vapor has condensed, so $\overline{P}_A \cong P_{A_\infty}$ during the nucleation phase.

The particle growth rate may be evaluated using Eq. (34)

$$\dot{a} \equiv \frac{da}{dt} = \frac{\mathcal{D}c\ (x_{A_\infty} - x_{Ao})}{ac_d\ (1+\beta\ Kn)} \tag{85}$$

Eq. (83) may be rewritten as

$$\frac{\partial n}{\partial t} + \dot{a}\ \frac{\partial n}{\partial a} = J_{av}\ \delta\ (a-a^*) - n\ \frac{\partial \dot{a}}{\partial a} + \frac{n}{\rho_g}\ \frac{\partial \rho_g}{\partial t} \tag{86}$$

Applying the method of characteristics to convert this partial differential equation to a set of ordinary differential equations, we find, along the characteristic

$$\frac{da}{dt} = \dot{a}$$

$$\frac{dn}{dt} \equiv \frac{\partial n}{\partial t} + \dot{a}\ \frac{\partial n}{\partial a} = J_{av}\ \delta(a-a^*) - n\ \frac{\partial \dot{a}}{\partial a} + \frac{n}{\rho_g}\ \frac{\partial \rho_g}{\partial t} \tag{87}$$

The terms $\frac{\partial \dot{a}}{\partial t}$, $\frac{\partial \rho_g}{\partial t}$ are available as analytical expressions from eqn. (85) and from the time-temperature history of the system.

The coupled ordinary differential equations which describe the system are, therefore,

$$\frac{d\overline{P}_A}{dt} = \frac{\Delta\overline{P}_A}{\rho_g}\frac{\partial \rho_g}{\partial t} - 4\pi RTc_d\left[\int_{a^*}^{\infty} na^2\left(\dot{a} + \frac{a}{3\rho_g}\frac{\partial \rho_g}{\partial t}\right)da + \frac{1}{3}a^{*3}J_{av}\right] + R_p \qquad (88)$$

$$\frac{da}{dt} = \frac{\mathcal{D}}{a}\frac{c}{c_d}\frac{x_{A\infty} - x_{A0}}{(1 + \beta Kn)} \qquad (89)$$

$$\frac{dn}{dt} = J_{av}\,\delta(a-a^*) - n\left(\frac{\partial \dot{a}}{\partial a}\right) + \frac{n}{\rho_g}\left(\frac{\partial \rho_g}{\partial t}\right) \qquad (87)$$

The characteristics have the initial conditions

$$a = a^* \quad \text{at} \quad t = t^*$$

and

$$P_A = P_{A\infty} \quad \text{at} \quad t = 0.$$

Figure 9 shows the results of a calculation of the size evolution of water droplets from a supersaturated vapor. It is assumed that at $t = 0$, supersaturated water vapor starts to nucleate and condense. The parameters used for this simulation are given in Table 3.

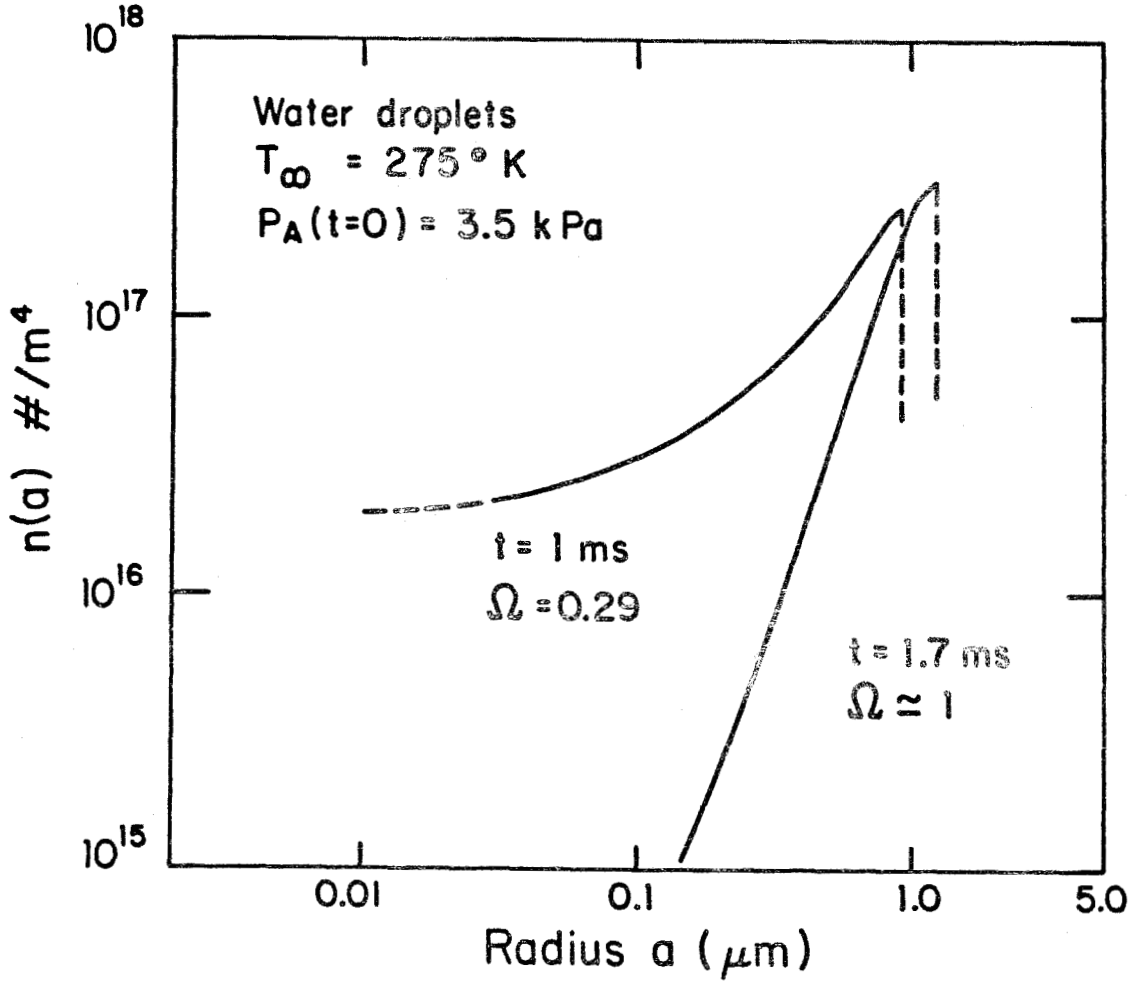

Figure 9. Evolution of size distribution of condensing water vapor.

Size distributions at two different times are shown. After 1 msec, $\Omega = 0.29$, and nucleation quenching has become significant. Very little time is required for the particles to grow to the 0.1 to 1 micron size from the critical size which is in the free molecular range. After 1.7 msec , $\Omega = 1$, and nucleation is quenched. Approximately 2% of the water vapor is converted into aerosol by this time. As the quenching point nears, the size distribution changes dramatically; the number of small particles drops sharply due to the decline in the nucleation rates. Beyond this period, the dominant process is condensation. Coagulation will become important only much later. Modelling the final stages of aerosol evolution requires consideration of coagulation and is beyond the scope of the present work.

2.9 Discussion

The present analysis is applicable to the formation and growth of particles in the continuum, transition and free molecular size ranges. Transport processes in the transition regime have been described by using flux matching (5) at the surface of particles. Although previous applications of this method have resulted in substantial errors in transport rates, when the correct formulations for mean free path and transport properties are used, flux matching at the surface gives satisfactory results.

It has been assumed that a quasi-steady-state exists for fluxes to the particles since the time required for particle growth is much longer than the times for relaxation of the temperature and composition fields surrounding the particle.

The effect of cluster diffusion to the particle on the nucleation rate has not been considered in the analysis. McGraw and McMurry (11) have shown that the effect of cluster diffusion can be important in the region close to the particle. Since nucleation suppression far from the particle ($r/a \gg 1$) contributes substantially to the total change in nucleation rates, the effect of cluster diffusion on clearance volume (Eq. 21) is difficult to ascertain, but it may not be significant.

In the sample calculation for condensing water vapor, it was observed that new particles are formed only for a very short period of time. Similar results are obtained in the simulation of other systems where vapor nucleation occurs, i.e., there is a short initial interval of simultaneous nucleation and condensation. Nucleation may continue to occur in systems

where vapor is produced by reactions, or saturation vapor pressure is lowered due to thermal changes. Nucleation may also occur if the vapor and aerosol distributions are not uniform. The present analysis neglects the effects on nucleation rates of overlapping regions of influence of adjacent particles. A detailed treatment of the final stages in the quenching of nucleation must consider the spatial distribution of particles and the vapor concentration and temperature profiles in these regions.

The concept of the total fractional clearance volume discussed in Section 2.4 can be utilized on its own without calculations of size distribution evolution. To a first approximation, Ω indicates the fraction by which nucleation is reduced by a growing aerosol. Nucleation can be eliminated in systems where seed particles are present in such concentrations that $\Omega > 1$. This is obviously the condition for maximum growth of particles. The final size of the particles is determined by the amount of vapor that is available for condensation. In order to grow large particles, the vapor concentration must be high, and the number of pre-existing particles must be small. However, these conditions also tend to produce nucleation. Careful control of vapor concentration is thus required for maximum growth of particles.

References (Chapter 2)

1) G. S. Springer, "Advances In Heat Transfer," T. F. Irvine and J. P. Hartnett, eds., Vol 14, pp 281-346, Academic Press, New York (1978).

2) A. J. Pesthy, R. C. Flagan and J. H. Seinfeld, J. of Coll. and Interface Sci., Vol 82, pp 465-479 (1981).

3) J. Jeans, "The Dynamical Theory of Gases," Dover Publications, New York (1954).

4) N. A. Fuchs, "The Mechanics of Aerosols," Macmillan, New York (1964).

5) N. A. Fuchs and A. G. Sutugin, "Highly Dispersed Aerosols," Ann Arbor Sci. Publications, London (1970).

6) J. O. Hirschfelder, C. F. Curtiss and R. B. Bird, "Molecular Theory of Gases and Liquids," John Wiley & Sons (1964).

7) E. J. Davis and A. K. Ray, J. Aerosol Sci., Vol 9, pp 411-422 (1978).

8) E. J. Davis, P. Ravindran and A. K. Ray, Chem. Engg. Commun., Vol 5, pp 251-268 (1980).

9) E. J. Davis, "Single Aerosol Particle Studies, "ACS Winter Symposium, Tucson, Arizona (1981).

10) F. C. Collins, Z. Electrochem, Vol 59, pp 404-407 (1955).

11) R. McGraw and P. H. McMurry, J. Coll. and Interface Sci., In press.

12) J. Frenkel, "Kinetic Theory of Liquids," Dover, New York (1955).

13) J. Zeldovich, Sov. Phys.-JETP, Vol 12, p 525 (1942).

14) M. Volmer, Z. Elektrochem., Vol 35, pp 555-561 (1929).

15) R. Becker and W. Doering, Ann. Phys. (Leipzig), Vol 24, pp 719-752 (1935).

16) F. F. Abraham, J. Appl. Phys., Vol 8, pp 20-23 (1940).

17) F. Kuhrt, Z. Phys., Vol 131, pp 185-204 (1952).

18) J. Lothe and G. M. Pound, J. Chem. Phys., Vol 36, pp 2080-2085 (1962).

CHAPTER 3

QUENCHING OF NUCLEATION

3.1 Introduction

The theory developed in the last chapter provides a criterion for controlling nucleation. It was shown that nucleation will be substantially reduced when a system is operated with aerosol and vapor concentrations such that the total clearance volume fraction Ω is greater than unity. The determination of the total clearance volume fraction involved a complex integration (Eq. 23, Eq. 75) which could only be done numerically. In its present form, the clearance volume concept is somewhat difficult to incorporate into calculations of aerosol nucleation and growth. It is therefore desirable to have a simplified expression for the dimensionless clearance volume.

In this chapter, the clearance volume formulation is further analyzed and simplified by determining asymptotic expansions of the integrals and a simple analytical criterion is established for the quenching of nucleation. Using this expression, a calculation is carried out to determine the growth of nucleated aerosols.

3.2 The Quenching Criterion

The total clearance volume fraction Ω, as defined in section 2.4, is the sum of individual clearance volumes of the particles in a system. For a monodisperse aerosol of radius a and containing N_∞ number of

particles per unit volume, the clearance volume fraction is given by

$$\Omega = \frac{4}{3}\pi N_\infty a^3 \rho^3$$

The criterion for nucleation to be quenched is $\Omega > 1$. In essence then, it is possible to predict quenching of nucleation in an aerosol system if clearance volumes are calculated. In the previous chapter, clearance volumes were calculated by numerical integration of the following equation:

$$\rho^3 = 3(1+\beta Kn)^3 \int_0^\infty \left(1 - \frac{J(y,t)}{J_\infty}\right) y^2 dy \qquad (23)$$

$J(y)$ is the nucleation rate at a distance $y = \frac{r}{a(1+\beta Kn)}$ from the particle. $J(y)/J_\infty$ is given by:

$$\frac{J(y)}{J_\infty} = \left\{\frac{\chi(y)}{\Gamma(y)}\right\}^2 \exp\left[-\alpha\{\Gamma(y)^{-3}\left(\frac{\ln S_\infty}{\ln S(y)}\right)^2 - 1\}\right] \qquad (88)$$

In the above equation,

$$\alpha = \frac{16\pi}{3(\ln S_\infty)^2} \cdot \left(\frac{\sigma v_m^{2/3}}{kT_\infty}\right)^3 \qquad (89)$$

$$\chi(y) \equiv \frac{x_A(y)}{x_{A_\infty}} = 1 - \Delta_\chi \left(\frac{1}{1+\beta Kn}\right) F\,(y;A,Kn) \qquad (70)$$

$$\Gamma(y) \equiv \frac{T(y)}{T_\infty} = 1 + \Delta_T \left(\frac{1}{1+\gamma Kn}\right) F\,(y;\frac{A}{Le},Kn) \qquad (71)$$

$$A \equiv \frac{1}{2}\frac{c}{c_d}\left(x_{A\infty}-x_{A0}\right) \tag{44}$$

$$F(y;A,Kn) \cong \frac{e^{-Ay^2}}{y(1+\beta Kn)(2Ay^2+\sqrt{2A}y+1)} \tag{63}$$

$$\frac{S(y)}{S_\infty} = \chi(y)\ \exp\left[-\frac{\Delta H_v}{RT_\infty}\left(1-\frac{1}{\Gamma(y)}\right)\right] \tag{73}$$

We shall now determine an approximate analytical value for the integral in Eq. (23), thereby obtaining a simple criterion for quenching of nucleation. The method by which the integration will be done is valid for $\alpha \lesssim \ell n\ S_\infty(1+\beta Kn)^2/\sqrt{2A}$. This restriction does not limit the usefulness of the result since most systems operate in this range.

It is convenient to introduce the following definitions:

$$\left.\begin{aligned}
\Delta_1 &= \frac{\Delta_x}{(1+\beta Kn)}\ F\ (y;\ A,\ Kn)\\
\Delta_2 &= \frac{\Delta_T}{(1+\gamma Kn)}\ F\ (y;\ \frac{A}{Le},\ Kn)\\
\Delta_3 &= 2(\Delta_1+\frac{\Delta H_v}{RT_\infty}\Delta_2)/\ln S_\infty
\end{aligned}\right\} \tag{90}$$

Consequently

$$\chi(y) = 1-\Delta_1 \qquad \Gamma(y) = 1+\Delta_2 \tag{91}$$

Recall from section 2.5 that:

$$\Delta_x \equiv 1 - \frac{P_{sat}}{P_{A_\infty}} \exp\left\{\frac{\Delta H_v}{RT_\infty}\ \frac{\Delta T}{1+\Delta T}\right\}$$

$$\Delta_T \equiv \frac{\Delta H_v}{RT_\infty}\left(\frac{R}{M_B C_p}\right)\cdot Le^{-1}\left(\frac{1+\gamma Kn}{1+\beta Kn}\right)\ \Delta_x\, x_{A_\infty}$$

It also follows from Eq.(44) that,

$$A = \frac{1}{2}\frac{P_{A_\infty} v_m}{kT}\Delta_x \tag{92}$$

Typically, for a dilute vapor

$$\Delta_T << \Delta_x \text{ and } A < 10^{-4}$$

The integrand in Eq. (23) is negligible except when y>>1. And for y>>1, it can be shown that Δ_1, Δ_2 and Δ_3 are all much less than unity. Eq.(73) can then be simplified to

$$\frac{\ln S(y)}{\ln S_\infty} \simeq 1 - \frac{1}{2}\Delta_3 \tag{93}$$

Using the above equation, Eq.(88) can be simplified:

$$\frac{J(y)}{J_\infty} \simeq (1-2\Delta_1-2\Delta_2)\exp\{-\alpha(-3\Delta_2+\Delta_3)\} \tag{94}$$

For systems with $\alpha \lesssim \ell n\, S_\infty(1+\beta Kn)^2/\sqrt{2A}$, the following approximation holds,

$$1 - \frac{J(y)}{J_\infty} = 2\Delta_1\left(1 + \frac{\alpha}{\ln S_\infty}\right) + 2\Delta_2\left\{1-1.5\alpha + \frac{\frac{\Delta H_v}{RT_\infty}\alpha}{\ln S_\infty}\right\} \tag{95}$$

The integral for clearance volume (Eq. 23) now takes the form

$$\rho^3 = 3(1+\beta Kn)^3 \int_0^\infty \{2\Delta_1 (1 + \frac{\alpha}{\ln S_\infty}) + 2\Delta_2 \ (1-1.5\alpha + \frac{\Delta H_v \alpha}{RT_\infty \ln S_\infty})\} y^2 dy \qquad (96)$$

Eq.(96) can be integrated analytically if it is possible to integrate each of the following expressions:

$$\int \Delta_1 y^2 dy \quad \text{and} \qquad \int \Delta_2 y^2 dy$$

These integrals are similiar, and Laplace's method (1) can be applied to obtain an approximate analytical value. We proceed as follows:

$$\int_0^\infty \Delta_1 y^2 dy \equiv \int_0^\infty \frac{\Delta_x}{(1+\beta Kn)^2} \frac{y e^{-Ay^2} dy}{(2Ay^2 + \sqrt{2A}\, y + 1)} \equiv \frac{\Delta_x}{(1+\beta Kn)^2} \int_0^\infty e^{q(y)}\, dy \qquad (97)$$

where $q(y) = -Ay^2 + \ln y - \ln (2Ay^2 + y/2A + 1)$

It can be shown that

$$\frac{dq}{dy} \equiv q'(y) = 0 \quad \text{at} \quad y = y^* \equiv \frac{0.585}{\sqrt{2A}}$$

Consequently, the integral in Eq. (97) may be approximated (1) by the first term in the asymptotic expansion:

$$\int_0^\infty \Delta_1 y^2 dy \equiv \frac{\Delta_x}{(1+ Kn)^2} e^{q(y^*)} \int_{-\infty}^\infty \exp\{\tfrac{1}{2} q''(y^*)(y-y^*)^2\}\, dy$$

The integral on the right is a simple transformation of the Gamma function

with the argument 1/2; thus the integral (Eq. 97) is approximated by

$$\int_0^\infty \Delta_1 y^2 dy \approx \frac{\Delta_x}{(1+\beta Kn)^2} e^{q(y^*)} \sqrt{\frac{-2\pi}{q''(y^*)}} = \frac{\Delta_x}{(1+Kn)^2} \frac{0.172}{A} \tag{98}$$

Similarly

$$\int_0^\infty \Delta_2 y^2 dy \approx \frac{\Delta_T Le}{(1+\gamma Kn)(1+\beta Kn)} \cdot \frac{0.172}{A} \tag{99}$$

From Eqs. (96), (98), (99) and (92), the value of ρ^3 is seen to be,

$$\rho^3 \approx 2.064\ (1+\beta Kn)\ \frac{kT_\infty}{P_{A_\infty} V_m} \left[\left(1 + \frac{\alpha}{\ln S_\infty}\right) + \left(1-1.5\alpha + \frac{\Delta H_v}{RT_\infty} \cdot \frac{\alpha}{\ln S_\infty}\right) \frac{\Delta H_v}{RT_\infty} \cdot \frac{R}{M_B C_P} \cdot \frac{P_{A_\infty}}{P} \right] \tag{100}$$

A correction term can be obtained by integrating a second order term, and this correction term $\rho^{3'}$ is

$$\rho^{3'} = -\frac{3\Delta_x^2 \alpha^2}{(\ln S_\infty)^2 (1+\beta Kn)} \cdot \frac{1}{\sqrt{2A}} \tag{101}$$

Thus ρ^3 is given by

$$\rho^3 \approx 2.064\ (1+\beta Kn)\ \frac{kT_\infty}{P_{A_\infty} V_m} \left[\left(1 + \frac{\alpha}{\ln S_\infty}\right) + \left(1-1.5\alpha + \frac{\Delta H_v}{RT_\infty} \frac{\alpha}{\ln S_\infty}\right) \frac{\Delta H_v}{RT_\infty} \cdot \frac{R}{M_B C_P} \cdot \frac{P_{A_\infty}}{P} \right] - \frac{3\Delta_x^2 \alpha^2}{(\ln S_\infty)^2 (1+\beta Kn)} \cdot \frac{1}{\sqrt{2A}} \tag{102}$$

Fig. 10 compares the analytical result of Eq.(102) with the numerical

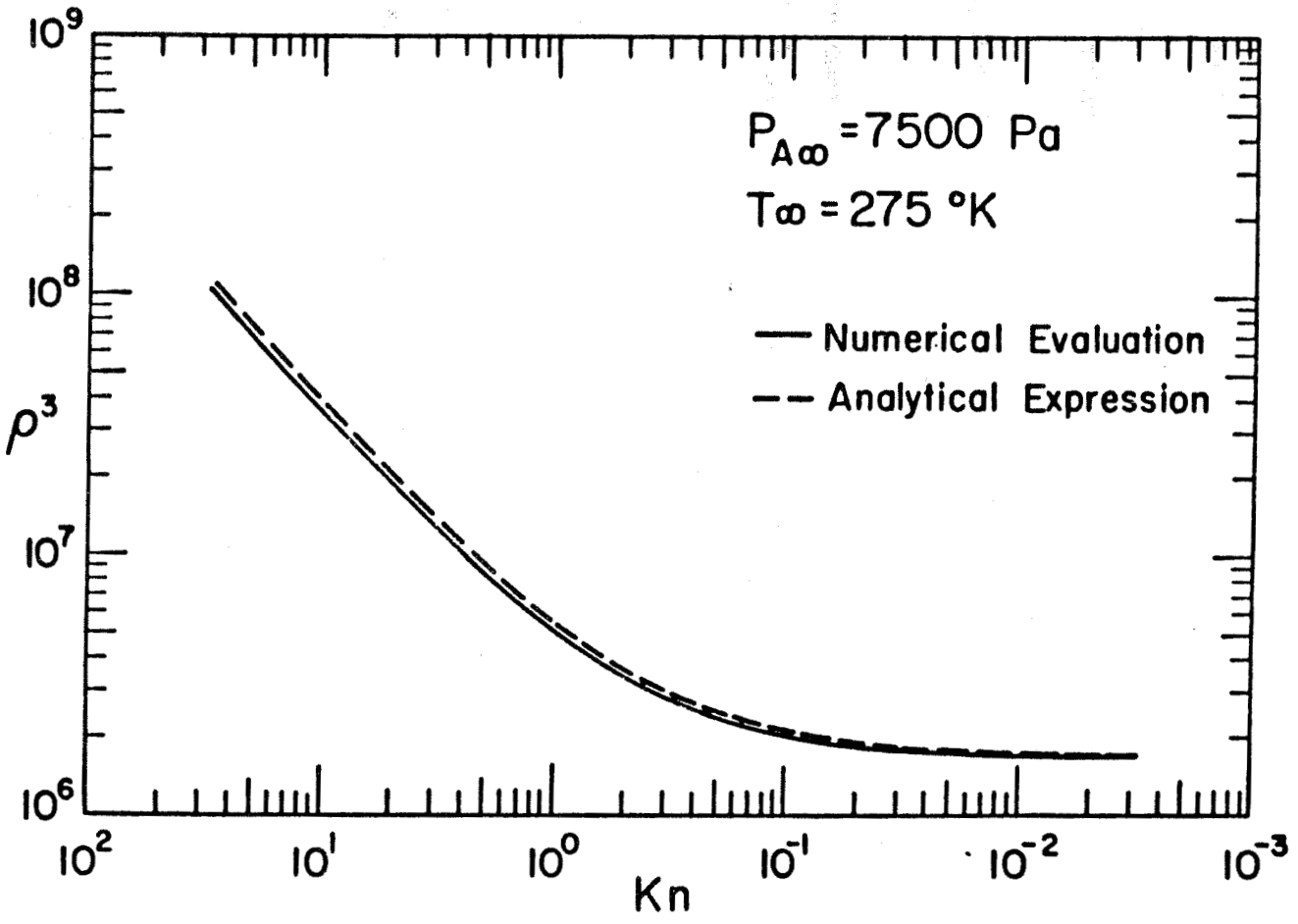

Figure 10. Comparison of analytical approximation of the dimensionless clearance volume with numerical evaluation of the exact expression.

results in section 2.6. The curves are drawn with the parameters given in Table 4. It can be seen that the two evaluations differ by less than 10% at all points. At Kn=1, for example, the numerical integration gives a value of $\rho^3=5.2X10^6$. The analytical expression in Eq.(102) gives a value of $5.6X10^6$ for ρ^3 at the same point; and the difference between the two is about 7%.

Further examination of Eq.(102) shows that the first order terms are:

$$\rho^3 = 2.064\ (1+\beta Kn)\ \frac{kT_\infty}{P_{A_\infty} v_m} \cdot \frac{\alpha}{\ln S_\infty} \qquad (103)$$

The above equation confirms the results obtained in section 2.4 regarding the behaviour of ρ^3 as a function of Kn and P_{A_∞}. It can be seen that

$$\rho^3 \propto (1+\beta Kn)$$

and

$$\rho^3 \propto \frac{1}{P_{A_\infty}}$$

i.e., the dimensionless clearance volume increases linearly with Knudsen number at large Knudsen numbers, and is inversely proportional to the vapor pressure. Substituting the value of α from Eq.(89) into Eq.(103) we obtain

$$\rho^3 = 34.583\ \frac{(1+\beta Kn)}{(\ln S_\infty)^3}\ \ \frac{\sigma^3 v_m}{(kT_\infty)^2} \cdot \frac{1}{P_{A_\infty}} \qquad (104)$$

We now have a simple criterion for determining whether significant nucleation will occur in a system or not. There will be no significant

nucleation in a system if

$$\frac{144.86\, N_\infty a^3 (1+\beta Kn)\, \sigma^3 v_m}{(\ln S_\infty)^3 (kT_\infty)^2 P_{A_\infty}} > 1 \qquad (105)$$

where N_∞ is the total number of particles in the system and a is the average particle radius. The above criterion can be made more accurate by using Eq. 102 for the dimensionless clearance volume and by integrating the clearance volumes over the size distribution.

It is interesting to observe that the parameter γ used in flux matching of heat transfer and the term ΔH_v are both absent from the above expression for dimensionless clearance volume. This implies that the change in the temperature around a particle (due to condensation) is not as important a factor in quenching as the decrease of vapor pressure in a dilute system. In other words, quenching is determined primarily by the loss of vapor to the particles.

The dimensionless clearance volume ρ^3 is also seen to be very strongly dependent on the surface tension σ of the condensed phase. Since surface tension varies with temperature and is somewhat difficult to evaluate accurately in cases where cluster sizes are small, this introduces a certain amount of uncertainty in calculation of the clearance volume.

3.3 Growth of Self-nucleated Aerosol

This simple criterion for quenching of nucleation (Eq. 105) can be used to calculate particle nucleation and growth in a manner similiar to that of Sec. 2.8. In this section, we shall simplify the calculations

even further and, in particular, examine the size limits of aerosols formed by homogeneous nucleation and grown by heterogeneous condensation.

Aerosols which are formed by homogeneous nucleation subsequently grow by condensation of the remaining vapor. Unless additional condensible vapor is produced in the system after the nucleation phase, growth of the nucleated aerosol will be limited by the amount of vapor available in the system at the end of nucleation.

Consider a system in which nucleation phase can be assumed to occur during a period t_n during which most of the nucleated particles are formed. The system contains $n_A = P_A/kT$ vapor molecules at the beginning. The total number of particles produced by nucleation is N_∞. A typical nucleation rate profile, as shown in Fig. 11(a), shows a steep rise and fall with a well defined peak value. For the purpose of this calculation, the nucleation rate will be approximated by a step function (Fig. 11(a)) with a maximum value $\bar{J}$ of duration t_n. The total number of particles produced by the assumed nucleation rate profile is also N_∞. The value of $\bar{J}$ is then given by

$$N_\infty = \bar{J}\, t_n \tag{106}$$

Nucleation produces critical clusters, each containing g^* vapor molecules, where

$$g^* = \frac{4}{3}\frac{\pi a^{*3}}{v_m} = \frac{\pi}{6}\frac{\sigma^3 v_m^2}{(kT\ln S)^3} \tag{107}$$

During the nucleation phase, the fraction of vapor depleted is usually

small, as we have seen in the previous chapter. We can, therefore, use the steady state growth law (Eq. 52) for growth of particles during the nucleation phase. Thus the average radius of the aerosol at the end of the nucleation phase is given by

$$a_n = \{2v_m n_A D t_n + [(\frac{3}{4\pi} v_m \beta^*)^{1/3} + \beta\lambda_A]^2\}^{1/2} - \beta\lambda_A \qquad (108)$$

The above equation is obtained by combining Eqs. (52), (92) and (107).

Since nucleation is quenched when particles reach size a_n, the total clearance volume fraction at this point is unity. Thus

$$N_\infty \frac{4}{3} \pi a_n^3 \rho^3 = 1$$

Using equations (104) and (107), the above condition may be written as:

$$1.032\ N_\infty (\frac{4}{3}\pi a_n^3)\, g^* \frac{(1+\beta Kn)}{n_A v_m} = 1 \qquad (109)$$

After this phase, nucleation becomes negligible, and the aerosol grows by condensation. The final average radius of the particles is determined by vapor species conservation, i.e.,

$$a_f = (\frac{n_A}{N_\infty}\ v_m \frac{3}{4\pi})^{1/3} \qquad (110)$$

Eqs.(106) through (110) are a set of algebraic equations which are easily solved for a set of given parameters. If the monomer concentration (n_A)

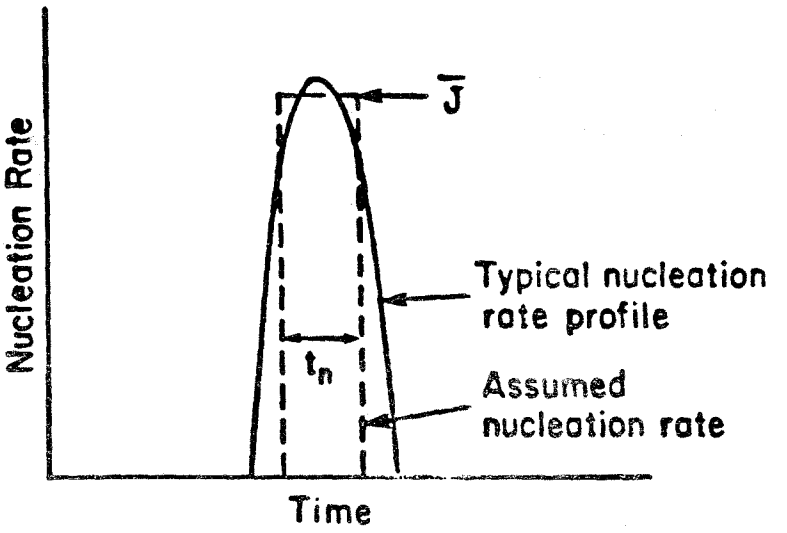

Figure 11. (a) Illustration of nucleation rates used in calculation of aerosol growth.

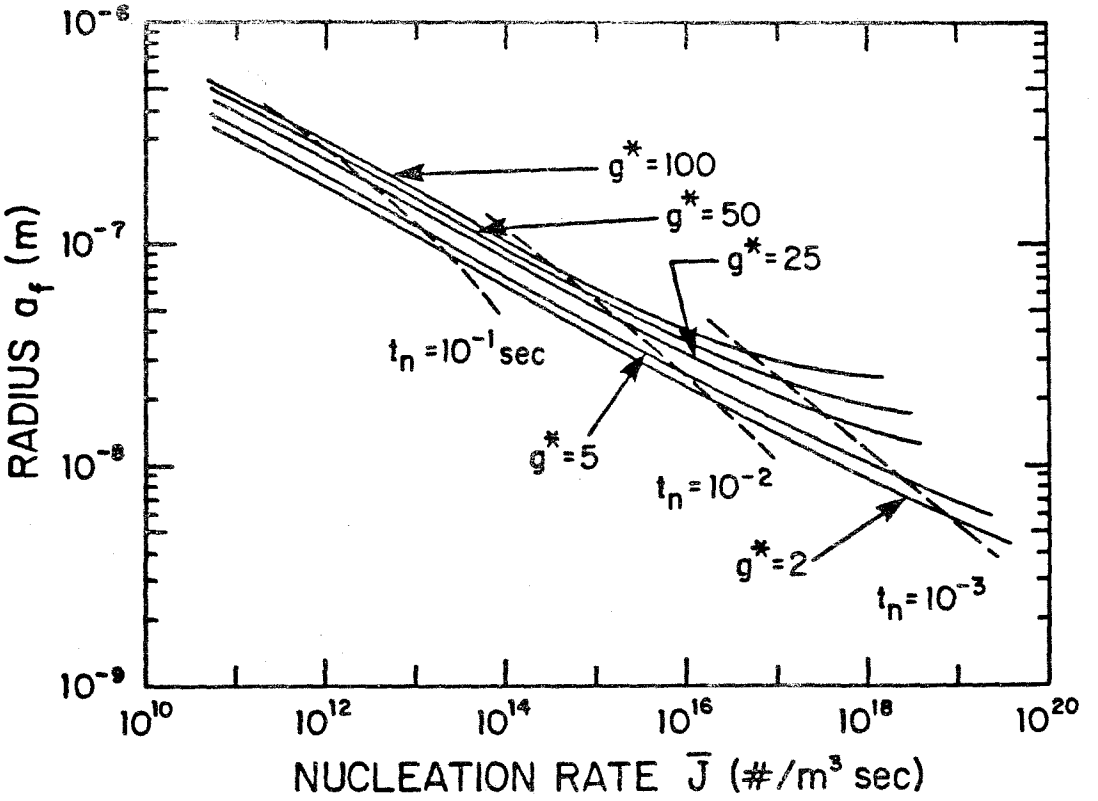

Figure 11. (b) Growth of aerosol in a combustion process (a_f is the maximum size of the aerosol)

molecular volume (v_m), temperature and the diffusivity of the condensing species are known, it is possible to make calculations of the final size of the aerosol as a function of the other parameters, $\bar{J}$, t_n, and g^*.

As an example, we can consider the aerosol produced by the vaporization and condensation of mineral matter during coal combustion. Typically, 0.1 kg of coal is burnt per cubic meter of air, producing about 0.1 gram of condensible vapor.

The final size of the aerosol due to nucleation and condensation of this vapor is shown in Fig. 11(b). The manner in which the problem has been formulated gives a monodisperse aerosol as the product. The following parameters were used for this calculation:

Density of condensed phase: 2.3×10^3 kg/m^3 T = 2000 °K

Diffusivity = 10^{-5} m^2/s $\beta = 2.$ $\lambda_A = 7 \times 10^{-8}$ m

$n_A = 1.5 \times 10^{20}$/m^3 at 2000 °K $v_m = 4.34 \times 10^{-29}$

From the figure it can be seen that the aerosol produced grows to a larger size if nucleation rates are low and the critical cluster is big. Typical values (2) for $\bar{J}$ are in the range $10^{14} - 10^{17}$ /m^{3}sec. For lower values of nucleation rates the nucleation phase becomes unduly long. At very high number concentrations the condensed aerosol will undergo substantial coagulation. If coagulation occurs at a lower temperature, i.e., below the ash fusion temperature, the product may be composed of chain agglomerates in which the basic unit is the condensed particle. The critical cluster size for the ash vapor is usually no more than 50. The aerosol size is very strongly dependent on the nucleation rate and the

duration of nucleation phase; it shows a weaker dependence on the critical cluster size. It should be noted that the nucleation rate and the critical cluster size are not independent variables and that they are both strongly dependent on the surface tension of the condensing species. Therefore, it can be concluded that surface tension of the condensing vapor is a primary determinant of the size of the product aerosol.

It is also seen from Figure 11(b) that the aerosol produced by nucleation and condensation of ash vapor cannot be expected to exceed 1 um in size. This conclusion is verified by experimental observations (4) which showed that the aerosol produced by nucleation and condensation of ash vapor is a submicron aerosol. It should be mentioned here that the size ranges predicted by this calculation is typical of the aerosols produced in high temperature systems, including the silicon produced in the free space reactors at JPL and Union Carbide.

References (Chapter 3)

1) G. F. Carrier, M. Krook and C. E. Pearson, "Functions of a Complex Variable", McGraw Hill, New York (1966)

2) K. W. Im and P. M. Chung, J. AIChE, Vol 26, pp 655-663, (1980)

3) M. J. McNallan, G. J. Yurek and J. F. Elliot, Comb. Flame, Vol 42, pp 45-60, (1981).

4) D. D. Taylor and R. C. Flagan, Aerosol Science and Technology, Vol 1, pp 103-117, (1982).

CHAPTER 4

AEROSOL REACTOR FOR SILICON PRODUCTION

4.1 Introduction

Production of silicon aerosol by gas phase reaction is a promising alternative to the conventional methods for producing polycrystalline silicon for photovoltaic and electronic applications. At present most of the high purity silicon is produced by epitaxial reactors in the form of films, or in bell jar or tubular reactors in bulk form. These are batch operation reactors with high energy and labor consumption. Consequently the cost of production is high (1). Recently Union Carbide (2) and the Jet Propulsion Laboratory (12) have developed a continuous flow reactor in which silicon aerosol is obtained from silane gas by thermal decomposition:

$$(1) \qquad SiH_4 \text{ -----> } Si + 2H_2$$

The basic concept of the continuous flow reactor is shown in Fig. 2. In the Union Carbide process, silane is introduced at the top of the reactor and heated by recirculating hydrogen. The silane thus produced nucleates due to its low vapor pressure, and forms a very fine powder of submicron particles. This process has the potential of being a continuous operation, and the energy consumption is lower than conventional methods by a factor of ten or more.

Unfortunately, the submicron silicon aerosol that is generated in the flow reactor is very difficult to separate from the gas flow and to handle

in subsequent processing. Moreover, the large surface area of the small silicon particles makes the collected powder susceptible to contamination. If larger particles could be produced in the aerosol reactor, the separation, handling and contamination problems could be greatly reduced; and the process could then become a truly continuous one.

As we have seen in previous chapters, particle formation and growth from a vapor are initially controlled by: (I) homogenous nucleation, and, (II) heterogenous condensation or reaction on particle surfaces. The JPL and Union Carbide reactors were operated at sufficiently high temperatures to ensure complete pyrolysis of the silane feed gas within a limited residence time (about 5 seconds). The high rate of generation of condensible products of reaction results in a high nucleation rate and the formation of a large number of very small particles. Even after condensation of the remaining vapor on these nuclei these particles remain submicron in size. Much of the previous work on the free space reactor has been devoted to increasing the size of the silicon particles. These efforts to increase particle size have focussed on particle growth by coagulation (Levin (17), Praturi, et al. (15), Lay and Iya (2)).

Particle growth by coagulation was examined by applying the sectional model developed by Gelbard, et al. (13) to simulate particle growth in a typical flow reactor. Fig. 12 shows the calculated evolution of particle size distribution in normal operation of the continuous flow pyrolyzer developed at the Jet Propulsion Laboratory. The mean diameter of the product at the end of about 4 seconds residence time is about 0.2 micron. It is apparent that particle growth by coagulation is too slow to grow particles out of the submicron range.

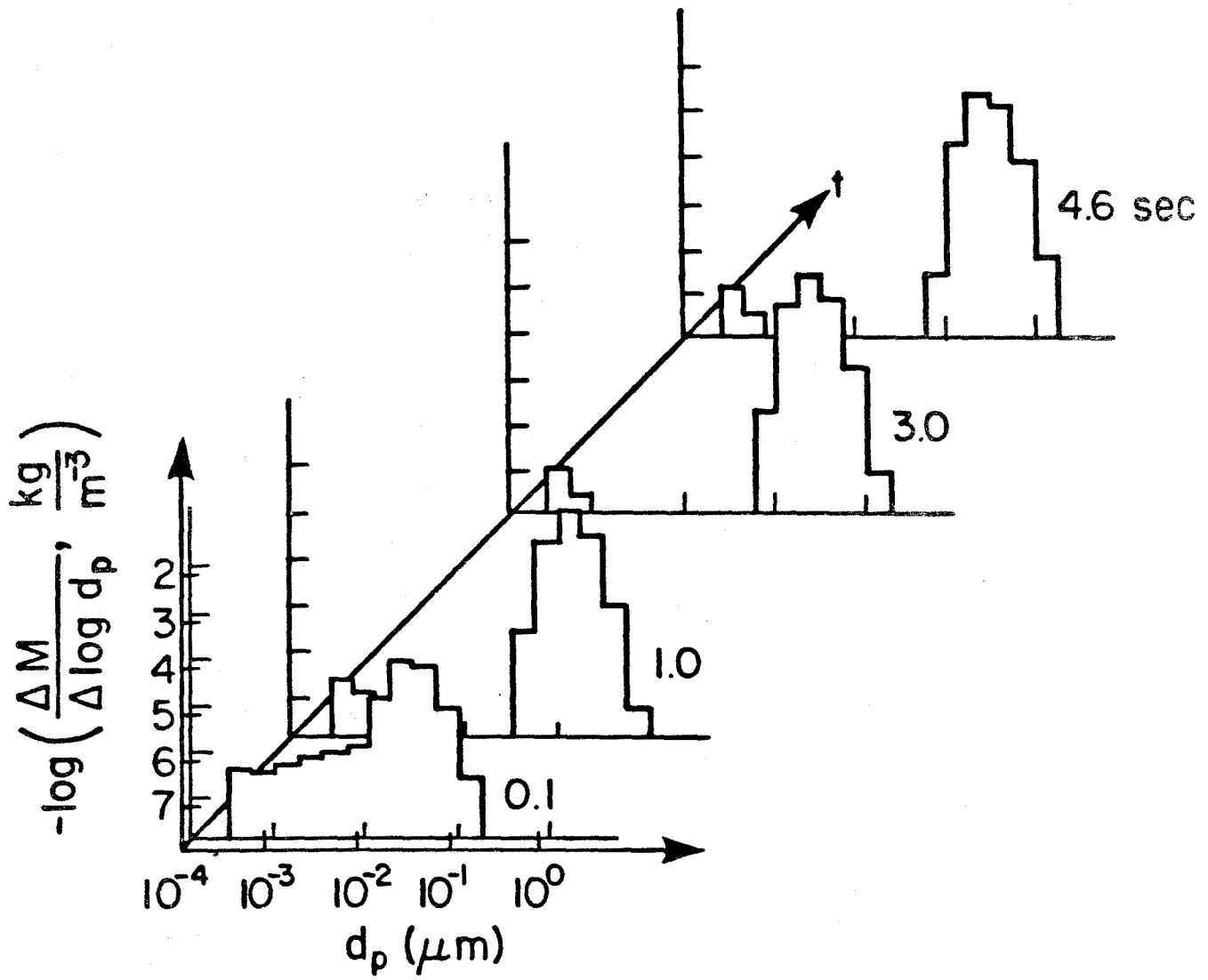

Figure 12. Sectional model calculations of aerosol evolution in the JPL reactor.

Particle growth must, therefore, be achieved by vapor deposition on the particles. However, given the large number concentrations produced in the initial burst of nucleation, growth significantly beyond the submicron range is not practical. Large aerosol particles can be grown if the number concentration can be reduced by several orders of magnitude and maintained at this low level throughout this growth process. This requires that additional nucleation be prevented.

From the theory developed in the previous chapters, the method to prevent nucleation is to keep the total clearance volume fraction, Ω, greater than unity. In general, this condition can be met by doing any of the following :

I) Maintain aerosol concentration at a sufficiently high level,

II) Keep the vapor pressure low, or

III) Increase the temperature.

For the silane system, the aim is to decrease the number concentration of the aerosol as much as possible in order to maximize particle size. Vapor concentration can be kept low by limiting the rate of silane decomposition. This would then disqualify the third option, since silane undergoes a thermal decomposition, and the rate of decomposition increases with temperature.

A possible means of producing large particles in the silicon aerosol reactor is to start with a small number of seed particles and to control the temperature of the reaction at a lower level than the present systems, thereby limiting the rate of silane decomposition and allowing the seed aerosol to grow. An understanding of the kinetics of silane decomposition is, therefore, very important for control of the system.

4.2 Kinetics of Silane Decomposition

The kinetics of the thermal decomposition of silane (SiH_4) are not yet fully understood. Purnell and Walsh (3) made a pioneering study (1966) in which pyrolysis of silane was carried out at 650°K to 700°K in a static system. The products were seen to be hydrogen, disilane (Si_2H_6) and a solid product with the composition $(SiH_x)_n$. The hydrogen to silicon ratio x had the value 2 when the solid product was first formed, but decreased with reaction time, and ultimately pure silicon is obtained.

A detailed analysis by Purnell and Walsh of the initial part of the reaction during which 0 to 3 percent decomposition occurs suggested a unimolecular decomposition with a temperature and pressure dependent rate constant. Two mechanisms were postulated. On the basis of thermodynamic considerations, Purnell and Walsh favored the following mechanism:

(2) $$SiH_4 + M \xrightarrow{k_{+2}} SiH_2 + H_2 + M$$

(3) $$SiH_2 + SiH_4 \underset{k_{-3}}{\overset{k_{+3}}{\rightleftharpoons}} Si_2H_6$$

(4) $$Si_2H_6 + SiH_4 \underset{k_{-4}}{\overset{k_{+4}}{\rightleftharpoons}} Si_3H_8$$

It has been since confirmed (5,6) that this mechanism is operative for the initial part of the reaction. The Arrhenius parameters of these reactions are shown in Table 4. These parameters are taken from a more recent study by Ring et al.(9).

The later part of the reaction mechanism is not well understood. During this stage, the decomposition of disilane and trisilane are

TABLE 4.

Arrhenius Parameters for Silane Decomposition

Reaction	$\log_{10}$ A	E_{act}(MJ/kmole)	Ref.
2	15.5	249.6[a]	(6)
-3	14.4	--	(9)
+3	10.3	4.186	(9)
-4	15.7	222	(9)
5	15.3	230	(8)
6	14.7	206	(8)

a) The parameters are for the high pressure limit (k_∞). The actual value of k_1 depends on pressure and temperature. The following chart gives the ratio k_1/k_∞ :

Pressure (torr)	Temperature (^oK) 650	710	1050
80	0.15	0.12	0.01
400	0.36	0.30	0.03
4000	0.73	0.67	0.16

expected to become important. The following mechanisms have been proposed for these decomposition reactions.

(5) $$Si_2H_6 \xrightarrow{k_5} Si_2H_4 + H_2$$

(6) $$Si_3H_8 \xrightarrow{k_6} SiH_4 + SiH_3SiH$$

The kinetic parameters of these reactions are also shown in Table 4.

Above 500°C, the polyhydrides of silicon tend to decompose to silicon and hydrogen (7). Of particular interest in the later stages of silane pyrolysis is the solid product $(SiH_x)_n$ where $0 < x < 2$. It has been suggested that (5) this could be a mixture of $(SiH_2)_n$, $(SiH)_n$ and silicon. Purnell and Walsh theorized that the solid product is formed by the successive insertion of SiH_2 in the lower silanes which then diffuses to a surface. This would involve the following mechanism:

(7) $$SiH_2 + (SiH_2)_{n-1} \longrightarrow (SiH_2)_n$$

(8) $$SiH_2 + Si_{n-1}H_{2n} \longrightarrow Si_nH_{2n+2}$$

At large values of n the above two formulae become experimentally indistinguishable.

Ring and O'Neal (9) have proposed that, during the later stages of the reaction, heterogenous mechanisms become important and reaction occurs at the wall surfaces of the reaction vessel. They proposed the following additional reactions:

(9) SiH_2 ------> $Wall\text{-}SiH_2$

(10) $SiH_2\text{-}Wall$ ------> $Wall\text{-}SiH_2^*$

(11) $Wall\text{-}SiH_2^* + SiH_4$ ------> $Wall\text{-}SiH_3 + SiH_3^*$

(12) $SiH_3^* + SiH_4$ ------> $Si_2H_6 + H^*$

(13) $H^* + SiH_4$ ------> $H_2 + SiH_3^*$

(14) $SiH_3^* + SiH_3^*$ ------> Si_2H_6

The reactions (9-11) initiate SiH_3^* radical formation, which then reacts with additional silane. This may explain the observed increase in reaction rate in the final stages of the pyrolysis.

If surface reactions are important, the formation of the aerosol may become important to the kinetics of the system, since it would provide a surface for the reactants. No study of this aspect of the silane pyrolysis has been made to date. It is possible that surface reactions on aerosols could explain the difference in silane decomposition rates that have been observed by different authors in the later stages of the reaction.

From the above discussion it is obvious that the final stages of silane pyrolysis are uncertain. Most of the dynamic processes in the aerosol reactor occur before a significant amount of condensation has occurred. If nucleation can be controlled during this period, control in the later stages follows quite easily. Surface reactions will enhance the particle growth rate and minimize the risk of further nucleation. The important reaction is, therefore, the initial silane decomposition reaction. The rate of silane consumption is

$$\rho_g d([SiH_4]/\ \rho_g)/dt = -k_1[SiH_4] \qquad (111)$$

The rate constant k_1 depends on temperature as well as pressure; and at atmospheric pressure, this constant can be approximated by:

$$k_1 = (0.96 - 8.735X10^{-4}T) \exp(35.69 - 30024/T) \quad sec^{-1}$$

In the temperature range 650°K to 1050°K.

4.3 Clearance Volume for Silicon Aerosol

To determine the clearance volume of the aerosol in this system, it is required to determine whether the condensing species is a polysilane, Si_nH_x, or silicon, and whether surface reactions are important in the process. Studies of silane pyrolysis have not addressed this issue. In the absence of better information, it will be assumed that silicon is the condensing species. Since silicon will have much lower vapor pressure than a condensing polysilane and surface reactions will promote aerosol growth, it is obvious that the worst case is being considered.

With the above assumption, the parameters for aerosol evolution in the flow reactor are shown in Table 5. These values are for a system where a small amount (1% to 10%) of silane in nitrogen is pyrolyzed. For parameters which vary with temperature, the value at 800°K has been taken. The vapor pressure expression has been obtained by extrapolation of the vapor pressure curve shown in Fig. 13.

The assumptions made in obtaining the parameters are somewhat extreme. It is important to note that, irrespective of the values of physical properties of this system, the method for producing large aerosol particles will remain the same. There must be a small amount of seed aerosol, and a controlled, slow reaction rate to promote seed growth and prevent nucleation.

TABLE 5.

Parameter Values for Silicon Aerosol Growth

Parameter	Value	Parameter	Value
$\Delta H_v/R$	$9.9X10^4$	σ	0.87 N/m
Le	1.1	P	101.3 kPa
β	3.1	c_d	82.7 Kmole $/m^3$
γ	3.7	$R/M_B c_p$	0.28

$$P_{sat} = 133.4\exp(25.232-55894./T) \quad Pa$$

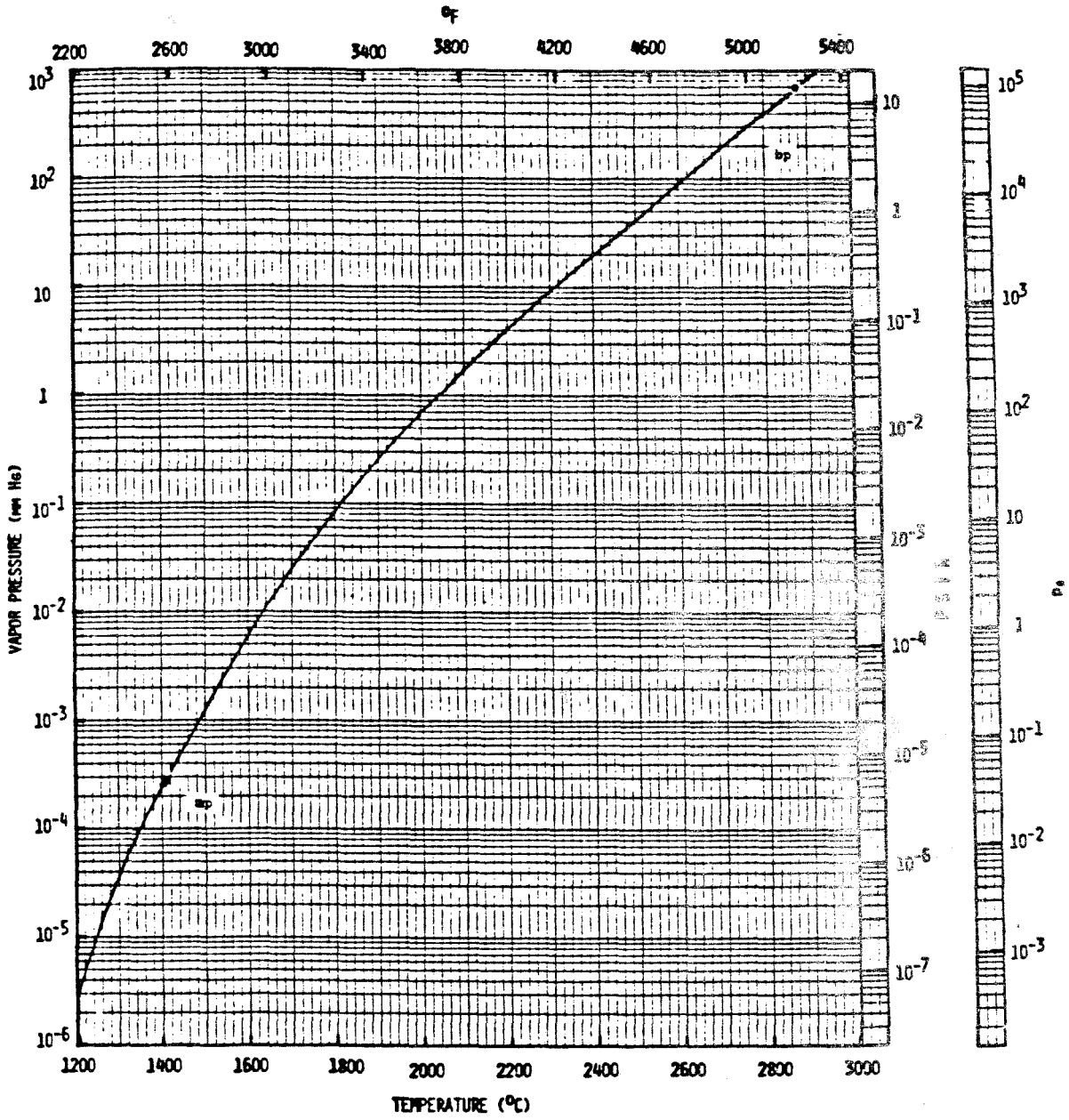

Figure 13. Vapor pressure curve for silicon.

(Source: Yaws, et al. (16))

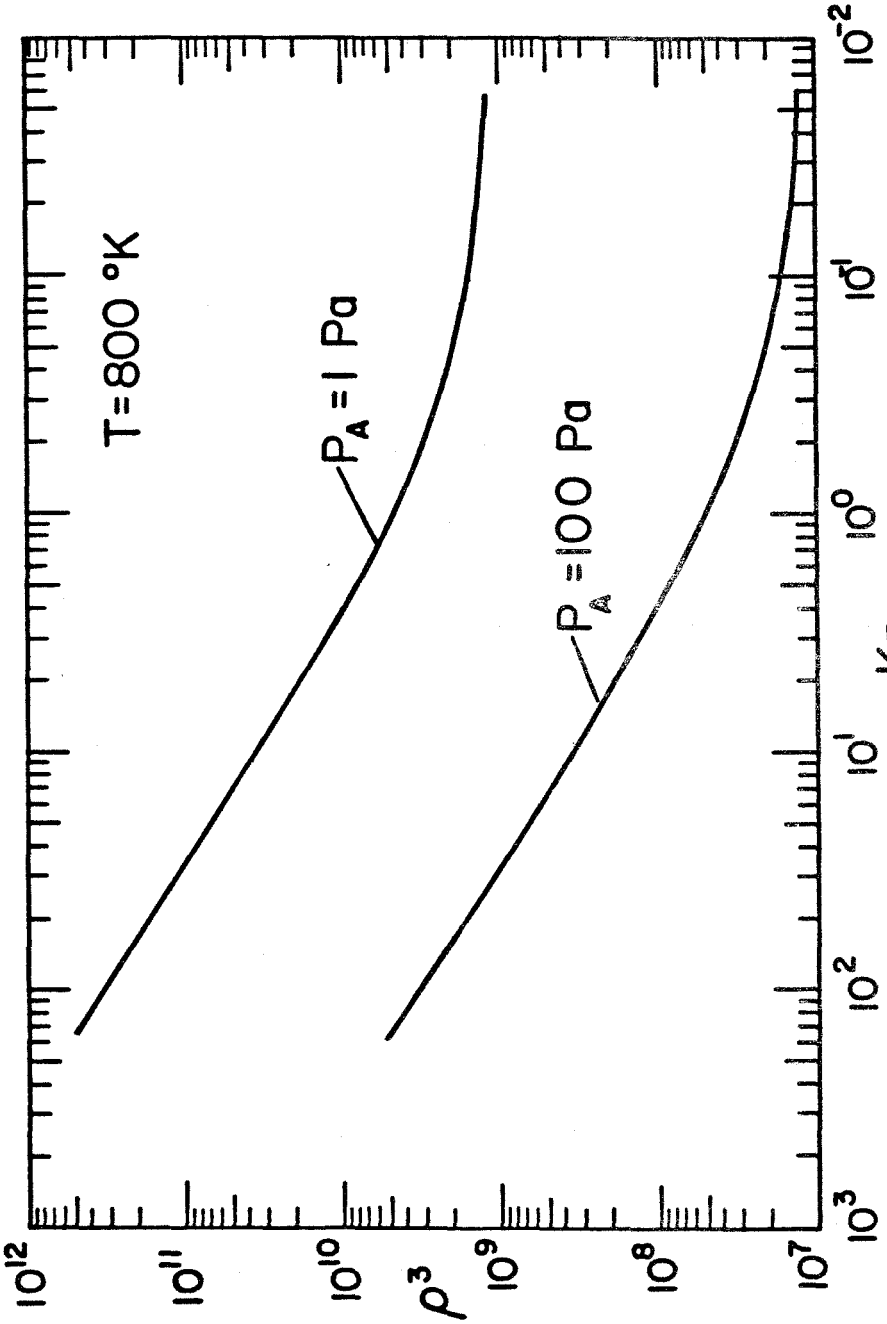

Figure 14. Dimensionless clearance volume for silicon aerosol.

The dimensionless clearance volume of silicon aerosol was calculated on the basis of the parameters in Table 5 and the results are plotted in Fig. 14. The behaviour of ρ^3 as a function of Knudsen number is similiar to that of the H_2O aerosol system. Following the results of the clearance volume analysis in chapters 2 and 3, we can correlate the plots of ρ^3 by the analytical expression given below:

$$\rho^3 = 5.95X10^6(1+3.1Kn)(T/P_A) \qquad 600^oK < T < 1100^oK$$

4.4 Controlled Rate Silicon Aerosol Reactor

The kinetics of silane decomposition can now be integrated into the model of simultaneous nucleation and particle growth to simulate the previous silicon free space reactors and to identify operating conditions which would allow growth of large particles. The first case to be considered is the flow reactor operated at high temperature (high reaction rate) with no seed aerosol. When 20% silane is pyrolyzed in this system at 875 °K, nucleation occurs almost instantly, producing $1.17X10^{17}$ /m^3 particles before nucleation is quenched. The nucleated particles then grow by deposition of vapor. As shown in Fig. 17, the particles grow to a size of about 0.12 micron. In fact, simulations carried out for conditions under which substantial nucleation occurs always give a product between 0.05 and 0.3 micron in size, as observed in the flow reactors at Union Carbide and the Jet Propulsion Laboratory (2, 17).

A flow reactor for the growth of large silicon particles by silane decomposition requires a much slower reaction rate than was achieved in the free space reactors. Because of the extreme reactivity of silane gas and for reasons of conversion efficiency, the amount of silane in the

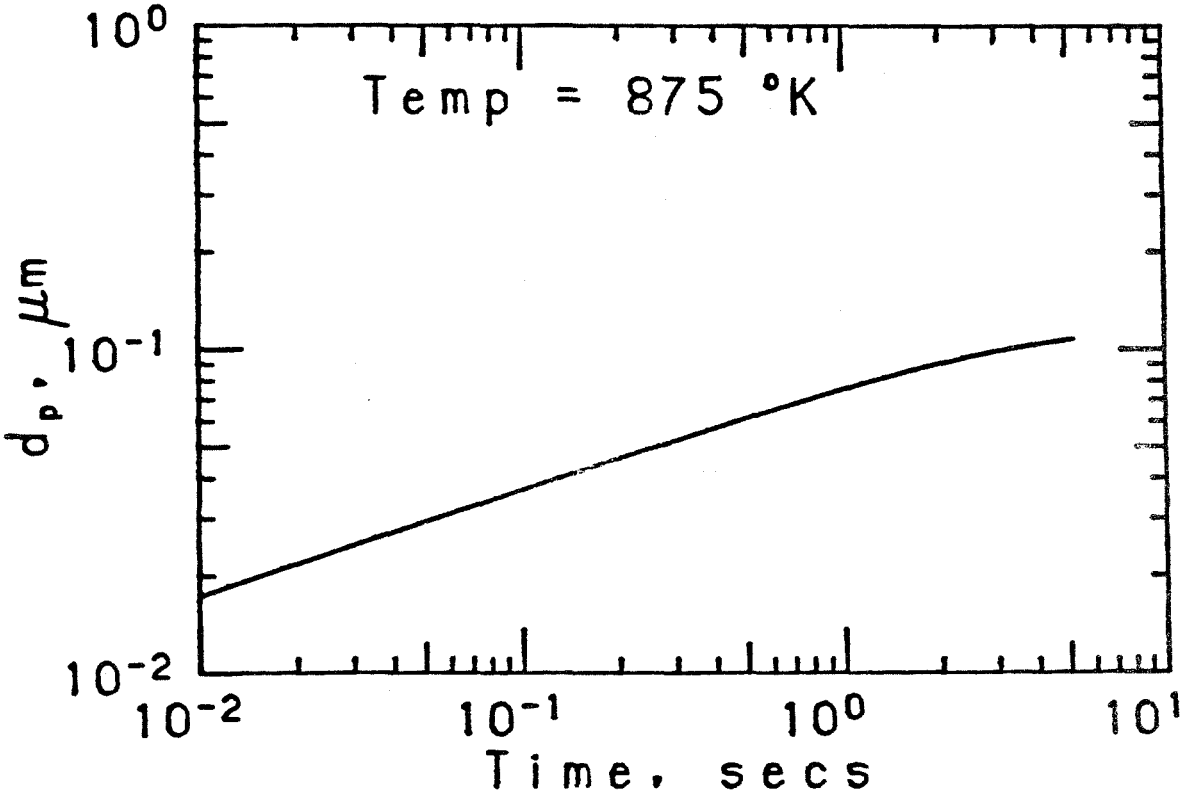

Figure 15. Particle growth in a conventional free space reactor

gases leaving the reactor should be kept very small. Thus, it is desirable to accelerate the reaction to ensure complete conversion within the reactor. To do this, the reactor wall temperature may be increased along its length. In general, the temperature profile in the reactor may be written as a function of axial position, z, i.e.,

$$T = f(z) \tag{112}$$

The point z=0 is chosen where the silane reaction is negligible; in the present simulations this was taken to be at a temperature T_i=775 °K. The end point for simulations is at time $t=t_f$, when the aerosol flow reaches the point z=L in the reactor. The temperature at this point is T_f.

It can be shown that the temperature profile in the reactor as a function of time is given by

$$t = \frac{\pi d^2 T_i}{4U_i} \int_0^T \frac{dT}{T\left(\frac{df}{dz}\right)_T} \tag{113}$$

where U_i is the volume flow rate at z=0 and d is the diameter of the reactor tube.

The temperature profiles chosen for the reactor were of the form:

$$T = T_i\sqrt{1 + C_0 z} \tag{114}$$

where $$C_o = \frac{1}{L}\{(\frac{T_f}{T_i})^2 - 1\}$$

The above equation can be substituted in Eq.(113) to find:

$$T = T_i[1 + \frac{2C_o U_i}{\pi d^2} t] \qquad (115)$$

i.e. the temperature profile is linear in time and parabolic along the length of the reactor. The total residence time in the reactor is then given by

$$t_f = (\frac{T_f}{T_i} - 1) \frac{\pi d^2}{2C_o U_i} \qquad (116)$$

The temperature profile chosen is by no means the optimum for the reactor, but was selected for the simplicity with which it may be implemented in the experiments and simulations. A set of parameters for which experiments were carried out is shown in Table 6.

Figures 16-21 show the results of a simulation of a flow reactor in which 1% to 2% silane is reacted in presence of seed aerosol. The temperature profile for this calculation is given by the parameters in Table 6. The seed aerosol size distribution for this simulation is shown in Fig. 16. This size distribution is obtained from experimental data and will be discussed later. The seed is a submicron aerosol very similiar to the product obtained in the JPL and Union Carbide reactors; but the number concentration has been reduced by a very large factor. Fig. 17 shows the

TABLE 6.

Temperature Parameters for Silicon Reactor

Parameter	Value	Parameter	Value
L	0.37 m	t_f	0.98 sec
T_i	775 °K	U_l	$2.2X10^{-5}$ m^3/sec
T_f	1100 °K	d	0.0095 m
C_o	2.7424	u_l	0.3104 m/sec

$$T = 775\sqrt{1+C_o z}$$

$$T = 775+332.6t$$

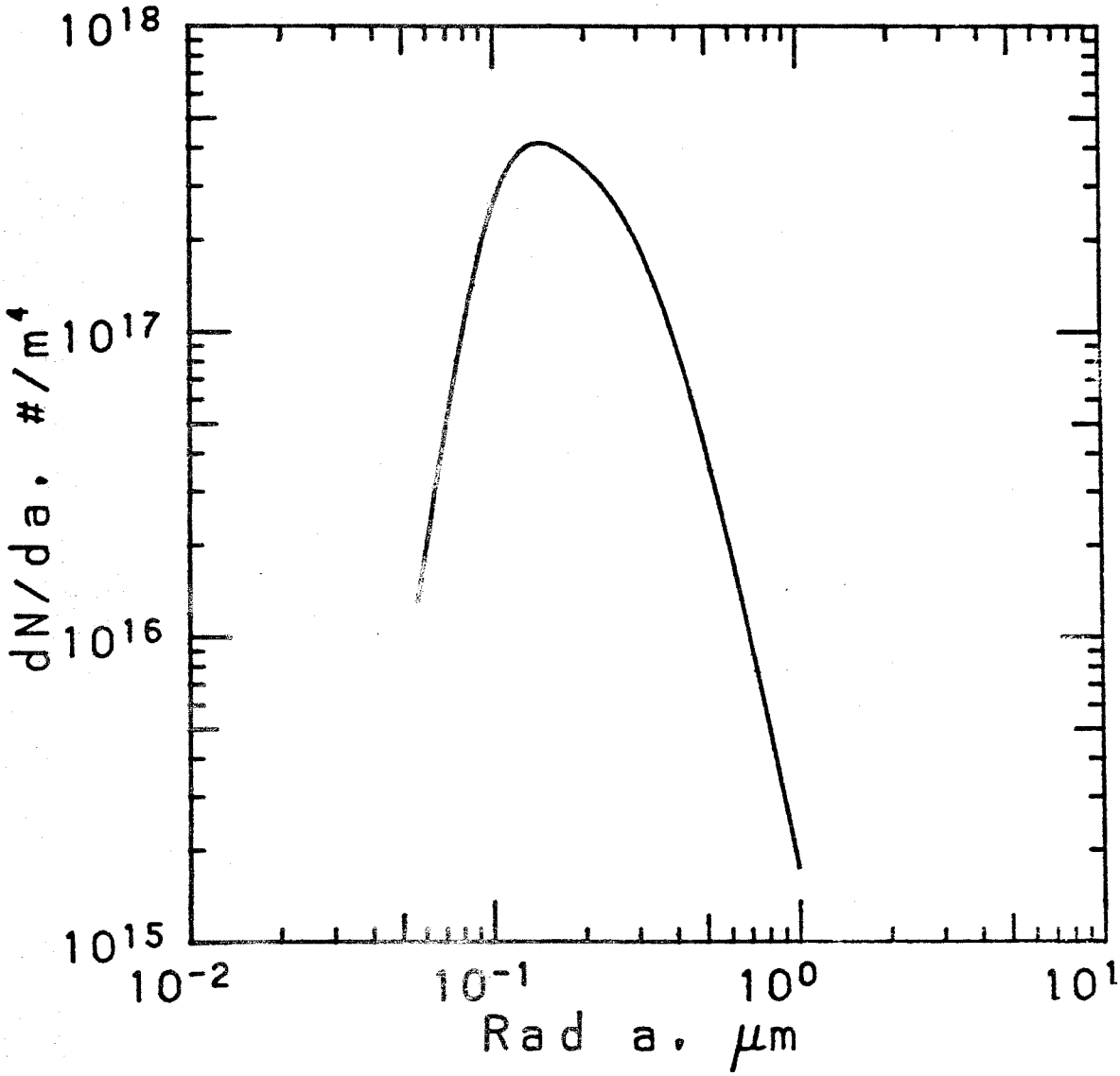

Figure 16. Size distribution of seed aerosol (T=775 °K)

Total number concentration=$1.02 \times 10^{11}/m^3$

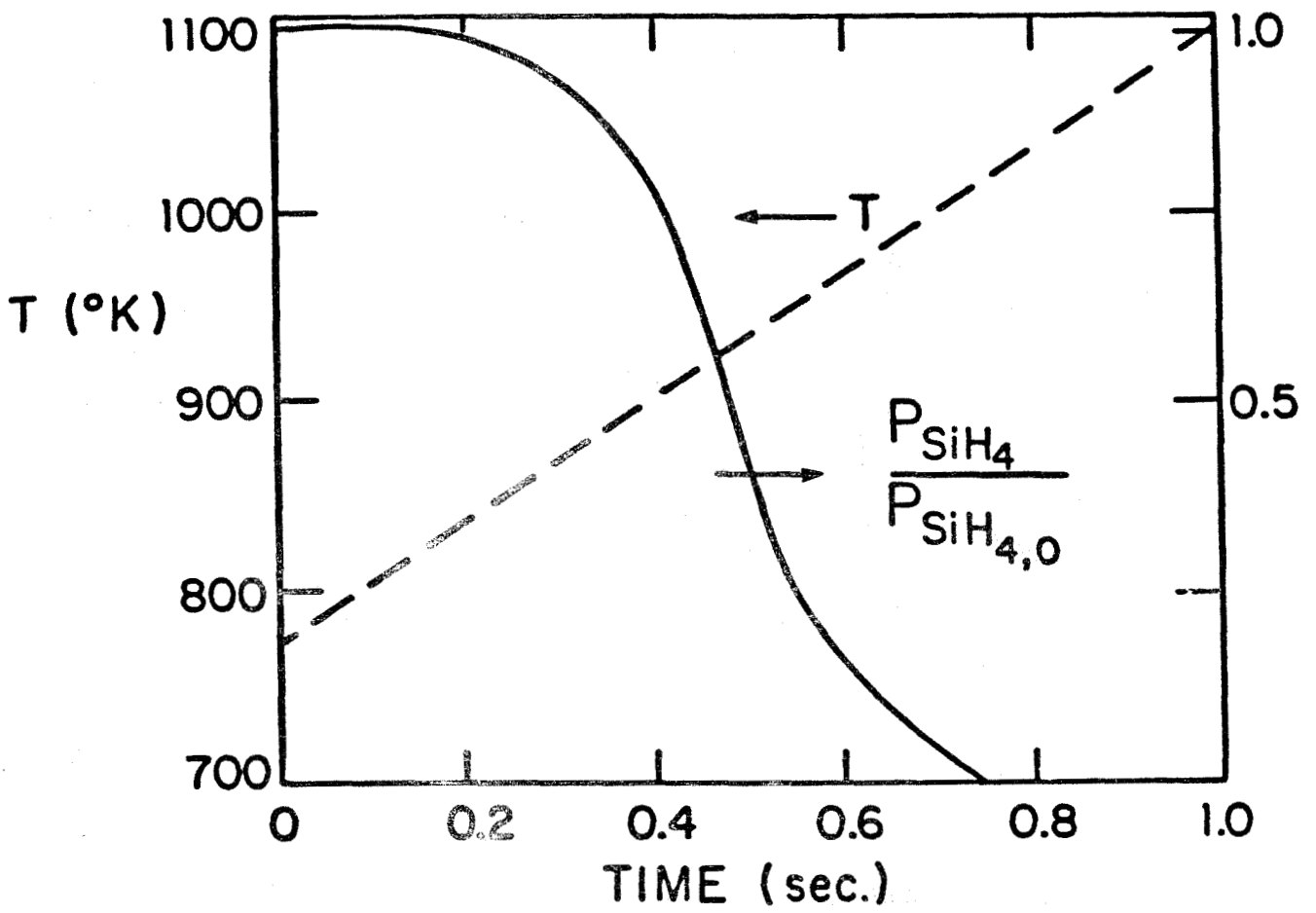

Figure 17. Temperature profile and reaction kinetics in the aerosol reactor.

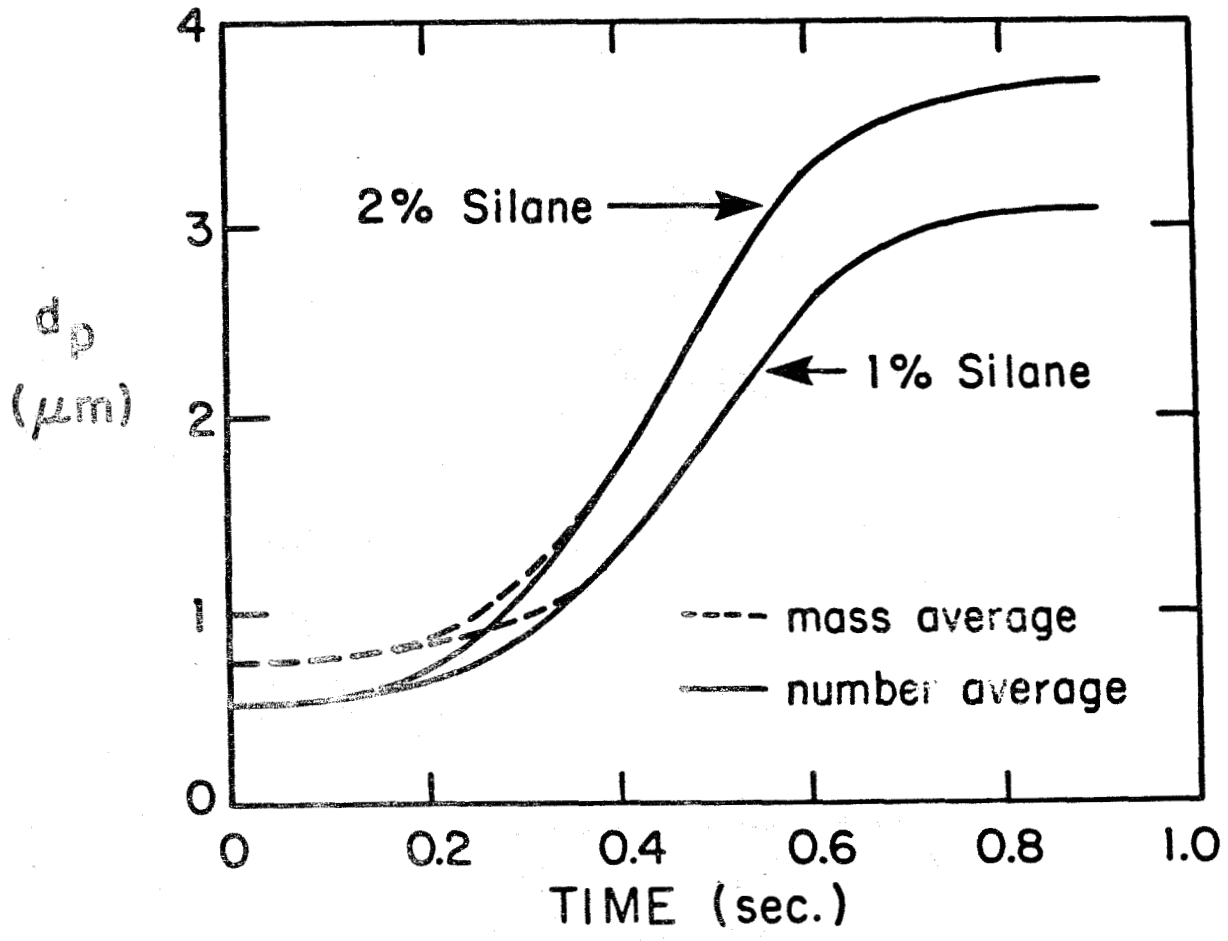

Figure 18. Particle growth in the silicon aerosol reactor.

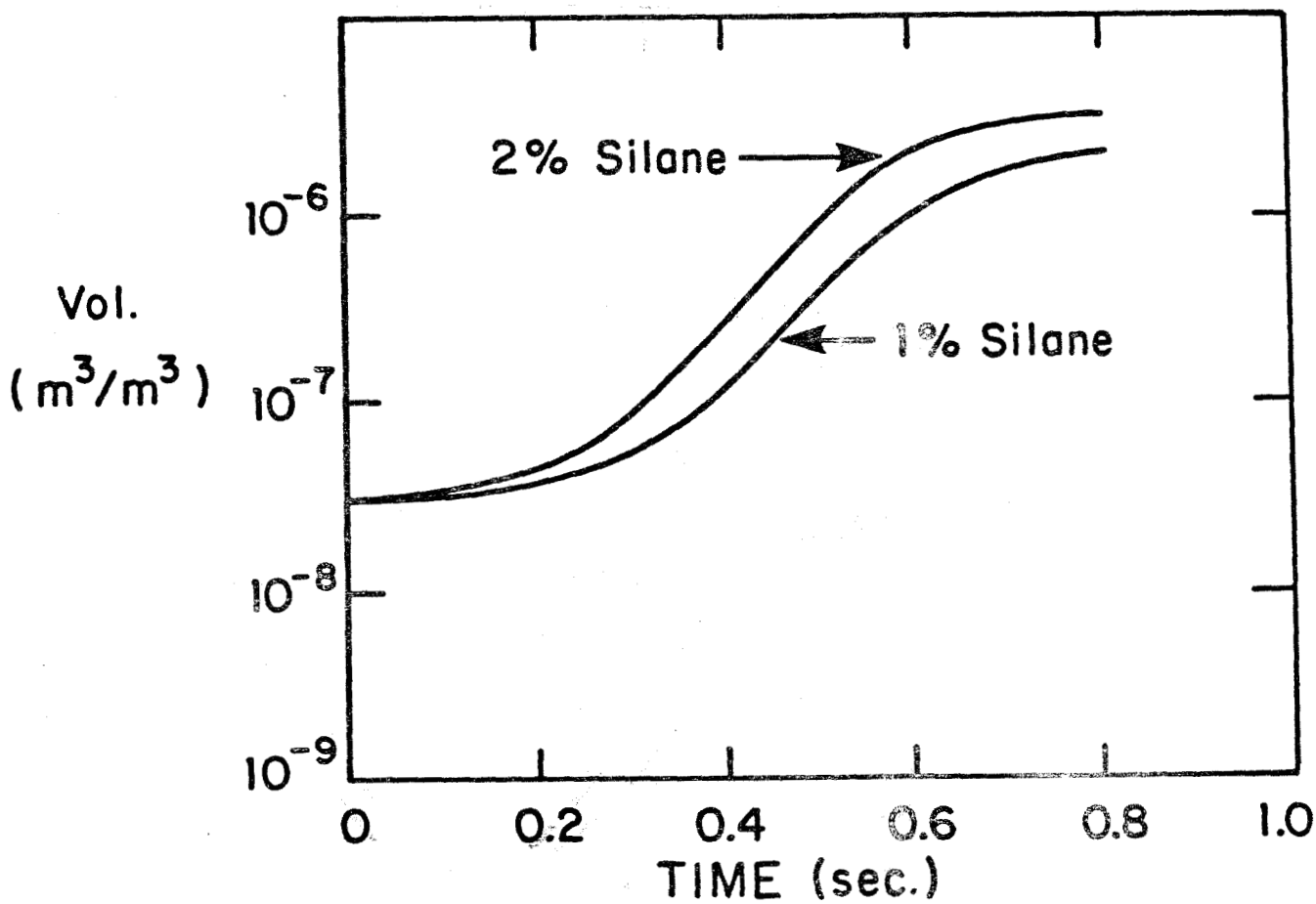

Figure 19. Aerosol volume fraction evolution in the aerosol reactor

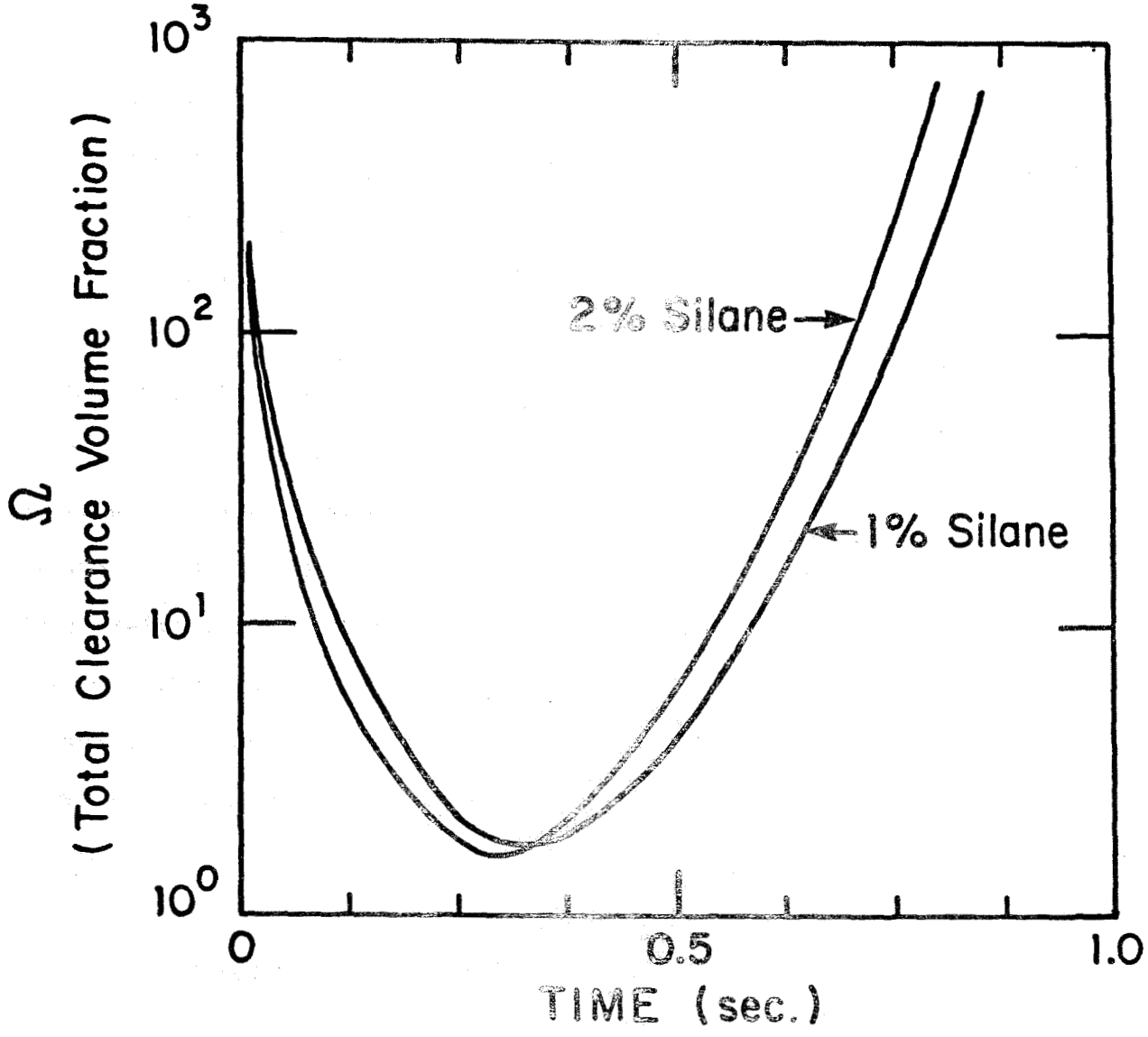

Figure 20. Total clearance volume fraction Ω in the reactor

temperature and the kinetics of the reaction in the reactor as a function of time. The total residence time in the reactor is approximately 1 sec. During the initial period (t<0.3 sec), very little reaction occurs, and the seed particles grow to about 0.5 micron. As the particles grow in size, they become more efficient in scavenging the vapor, and the faster reaction rate does not result in nucleation. The aerosol also becomes monodisperse, as is seen in Fig. 18. The mean diameter of the product is 3.01 microns with 1% silane and 3.7 microns with 2% silane. This is a sufficiently large size for collection by inertial deposition or, perhaps, by sedimentation. Fig. 20 shows the total clearance volume fraction as a function of time. As the aerosol volume fraction increases (Fig. 19), the condensation process finally dominates the reaction rate, and the total clearance volume fraction goes up steadily. In the final stages very little silane is left; the high temperatures in this region serve mainly to react all traces of silane.

Some silane is expected to be lost to the walls due to surface reactions. The rate constant for the surface reaction was found by Iya, et al. (14) to be:

$$k = 5.14 \times 10^{9} \exp(-19526.9/T) \quad \text{sec}^{-1} \qquad (117)$$

Surface reaction rates have been incorporated in the simulation. Fig. 21 shows the losses due to wall reaction. About 6% is lost to the walls when 1% silane is reacted and this fraction remains the same when 2% silane is reacted.

These calculations suggest that the controlled-rate flow reactor can

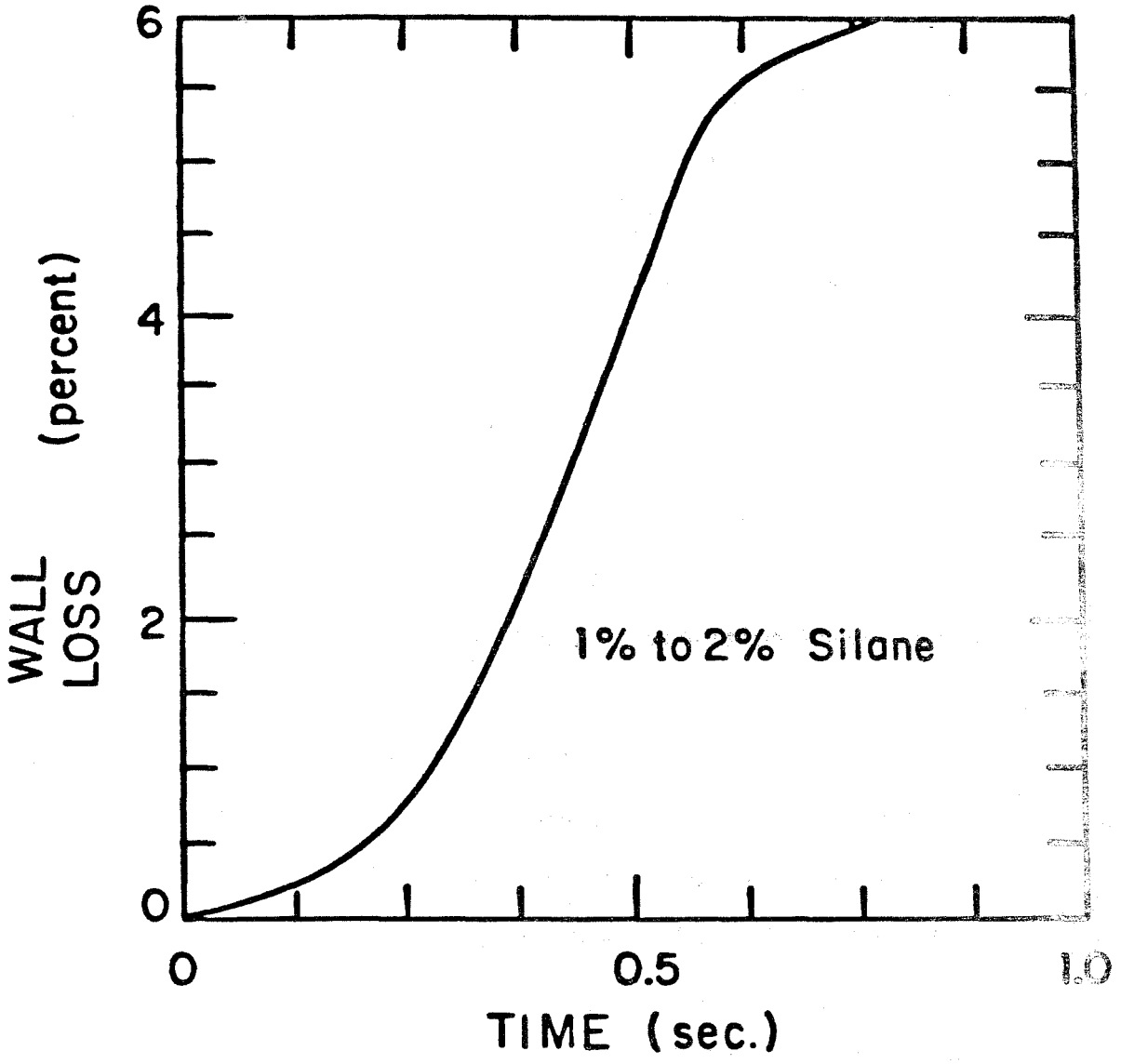

Figure 21. Wall losses due to reaction on the wall surface

grow substantially larger particles than were produced in the Union Carbide or JPL experiments. An experimental system developed to test these predictions will be discussed in the next chapter.

It is important to note that these simulations do not take into account particle growth by coagulation and the variation of the reaction rate with radial position in the reactor. Hence the size range of particles may be broader than these simplified calculations indicate.

References (Chapter 4)

1) Milorad Dudukovic, "Reactor Models for CVD of Silicon", The Science of Silicon material Workshop (LSA project of the Jet Propulsion Laboratory), Phoenix, Arizona (1982).

2) J. R. Lay and S. K. Iya, "Silane Pyrolysis in a Free Space Reactor", Proc. of the 15th IEEE Photovoltaic Specialists Conference, June, 1981.

3) J. H. Purnell and R. Walsh, Proc. Royal Soc., Vol 293, 543-561 (1966)

4) J. H. Purnell and P. John, J. Organometal. Chem., Vol 29, pp 233-266, (1971).

5) P. Neudorfl, A. Jodhan and O. P. Strausz, J. Phy. Chem., Vol 84, pp 338-339, (1980).

6) C. G. Newman, H. E. O'Neal, M. A. Ring, F. Leska, and N. Shipley, Int. J. Chem Kin., Vol XI, pp 1167-1182, (1979).

7) A. G. MacDiarmid, Adv. Inorg. Chem & Radiochem., Vol 3, pp 207-251, (1961).

8) K. Stokland, Trans. Faraday Soc., Vol 44, pp 545, (1948).

9) M. A. Ring and H. E. O'Neal, "Kinetics and Mechanism of Silane Decomposition", The Science of Silicon Material Workshop (LSA project of the Jet Propulsion Laboratory), Phoenix, Arizona, (1982).

10) P. S. Neudorfl and O. P. Strausz, J. Phys. Chem., Vol 82, pp 241, (1978).

11) F. C. Eversteijn, Phillips Res. Reports, Vol 26, pp 134-144, (1971).

12) A. K. Praturi, R. Jain and G. C. Hsu, Report # 5101-106 of LSA project of Jet Propulsion Laboratory, Pasdena, CA, April (1979).

13) F. Gelbard, Y. Tambour and J. H. Seinfeld, J. Colloid Interface Sci., Vol 76, No 2, pp 15-34, (1980)

14) S. K. Iya, R. N. Flagella and F. S. DiPaolo, Journal of the Electrochemical Society, Vol. 129, pp 1531-1535, (1982).

15) A. K. Praturi, G. C. Hsu and R. Lutwack, "Modelling of Silicon Particle Growth," JPL Report # 5101-105, (1979)

16) C. L. Yaws, K. Li, J. R. Hopper, C. S. Fang and K. C. Hansen, Lamar University, JPL Report # 9950-502, (1981)

17) H. Levin, "Proceedings of Symposium on Materials and New Processing Technologies for Photovoltaics," The Electrochemical Society, (1980).

CHAPTER 5

EXPERIMENTAL SYSTEM

5.1 Introduction

Application of the theory of simultaneous nucleation and condensation has clearly shown that an aerosol reactor for production of large particles of silicon must have the following:

I) A low number concentration seed aerosol. The number concentration must be low enough such that substantial growth of the seed is possible.

II) Reaction rate controlled to minimize the nucleation rate while the seed aerosol is grown. The reactor wall temperature may be varied to control the reaction rate. From the simulations carried out earlier, the initial temperatures may be as low as 775 °K. At these low temperatures, the rate of vapor production is slow enough to be scavanged by the aerosol.

An experimental system incorporating these features was designed to demonstrate the feasibility of controlled growth of silicon particles.

5.2 Design Considerations of the Experimental System

An important consideration in the design of the reactor is the fact that silane is a highly reactive toxic gas. It burns spontaneously in contact with air or oxygen, producing silica (SiO_2):

$$SiH_4 + O_2 \longrightarrow SiO_2 + 2H_2O$$

In order that silica be not formed in the system, all gases

introduced into the experiment must be free of oxygen. All joints were, therefore, regularly tested for leaks. Nitrogen, which was used as a diluent gas, was cleaned of oxygen by passing it through a purging unit. The purging unit consisted of a stainless steel vessel containing copper turnings and maintained at a temperature of 400 - 450 °C. Quartz reactor tubes and mixing sections were connected by vacuum o-ring joints. At the start and the end of every experiment, the system was put through a number of cycles in each of which it would be first pressurized with pure nitrogen and then evacuated with a vacuum pump. Finally, a constant flow of nitrogen was maintained through the reactor for the duration of the experiment.

Because of the extreme care necessary in the handling of silane, the experiment was designed to use small quantities of silane. The reactor tube inside diameter was 9.5 mm. To minimize loss of aerosol by sedimentation the primary reactor flow was directed vertically downwards. Because the temperature must increase along the length of the reactor, buoyancy induced flow instabilities are a potential problem. If the flow momentum is greater than the buoyancy force, this problem can be avoided, i.e., this requires that

$$\frac{g_a \Delta T d}{u^2 T} < 1$$

where g_a is the acceleration due to gravity, ΔT is the temperature difference, d is the diameter of the reactor tube and u is the mean velocity of gases in the reactor tube. In the seed generator, the flow velocities are too small for this condition to hold. Fortunately, the

degree of control required of the seed generator is not as severe as for the primary reactor. Furthermore, the particles in this reactor are too small for sedimentation to be significant. Consequently the seed aerosol reactor was designed for a vertically upwards flow with buoyancy effects dominating the flow.

The seed aerosol must be uniformly mixed throughout the gases entering the primary reactor so that particle-free pockets of fluid do not lead to homogenous nucleation of new particles and the disruption of the process. Seed particles are expected to be in the submicron range. These particles are too big for effective mixing by brownian motion within a reasonable period of time. Static mixing units were used to provide rapid mixing within a small volume. A significant amount of the seed aerosol is lost in the mixing zone, but this amount is extremely small compared to aerosol production in the primary reactor. Since these losses do not significantly influence the efficiency of the process, they have been tolerated in the design of the present apparatus.

5.3 Experimental System

The experimental setup is illustrated in Fig. 22. It is a vertically mounted two stage system; the first stage serves as the aerosol seed generator, and the second stage is the the primary reactor. The two stages are placed on parallel mounts. The main components of the reactor system are:

I) Reactor and Mixer Units

II) Zone Furnaces

III) Flow Control Systems

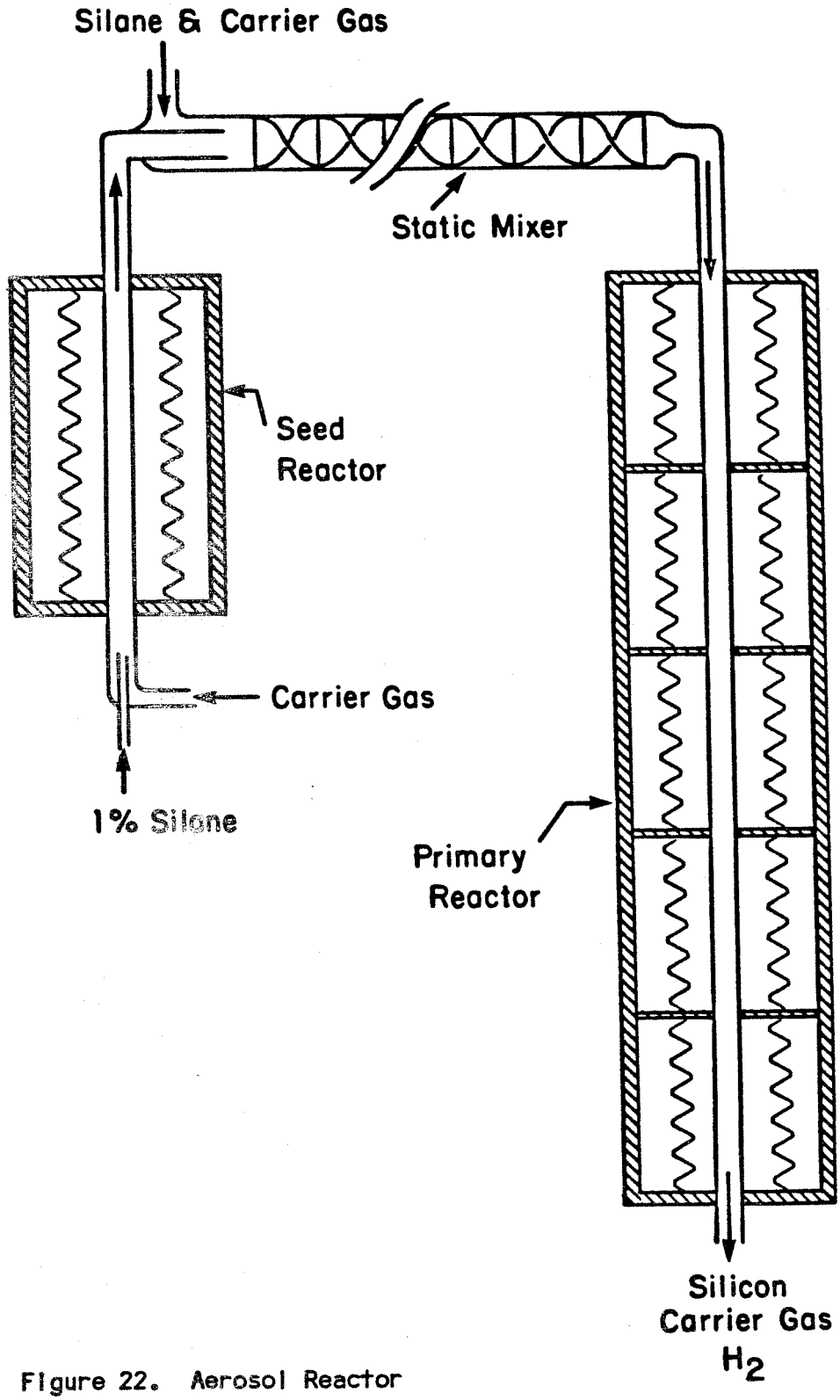

Figure 22. Aerosol Reactor

iv) Dilution and Sampling Systems

I) Reactor and Mixer Units: The seed aerosol reactor and the primary reactor share a common basic design and construction. Each is made up of a 9.5 mm I.d. (11 mm o.d.) quartz tube. The seed aerosol reactor has a 12 cm long heating zone. This stage is connected to the primary reactor through the mixer tube (pyrex tube, 16 mm I.d., 40 cm long). Pure silane with carrier gas (nitrogen) enters the mixing tube around the seed aerosol. The mixer tube contains 16 static mixing elements (Luwa static mixer, 3/8 inch o.d.) in series, and these elements mix the seed aerosol, silane and the carrier gases into a homogenous two phase flow. This flow then enters the primary reactor tube (50 cm long). Leak tight connections between these sections are made through 'o' ring flanges and viton 'o' rings.

II) Furnaces: The seed aerosol generator is heated by a small resistance type split furnace containg a 5 cm long (5.5 cm I.d.) heater element (Thermcraft). The heater is capable of delivering 200 watts at 28 volts. The heater is enclosed in an insulated firebrick housing surrounded by a water cooled metal cover. Cooling is done by flowing water through cooling coils soldered on the metal cover. This feature reduces the time for the furnaces to reach steady state.

The primary furnace is a five zone furnace. Each zone furnace contains three heating elements identical to the one in the seed aerosol reactor furnace described above. The heater elements are separated from each other by zirconia insulation plates. This minimizes

the effect of each zone on the neighbouring one, and allows effective temperature variation in the furnace. The primary reactor has 14 theromocouples cemented along the length. Five of these are used as sensors for feedback to control units. Each heating element is powered through a temperature control unit. These control units were designed to vary the power to the element by varying the input voltage from 0 volt DC to 28 volts DC. Fig. 23 shows the desired temperature profile and the actual temperatures in the reactor.

III) Flow Control Systems: An important consideration in the design of the gas flow systems was the flow of silane gas. Silane gas reacts with oxygen to form silica (SiO_2) which could then deposit in the flow system and interfere in the proper operation of flowmeters and flow controllers. The silane supply tanks were provided with dual purge valves through which higly purified nitrogen could be introduced to remove all traces of silane.

A flow controller (Porter Instruments, DFC 1400; 10 cc/min flow element) was used to control the flow of 1% silane into the seed aerosol generator. This flow is introduced at the center of the seed reactor tube and around this flow pure nitrogen is introduced coaxially through a Tylan FC 260 flow controller. The flow of nitrogen reduces the residence times in the seed generator and decreases wall reactions.

The flow of the seed aerosol then enters the mixer tube. At the same point a mixture of silane and nitrogen enters the mixer tube coaxially around the seed aerosol flow. The new silane forms about 1% of the total flow and is metered by a Porter Instruments DFC 1400 flow controller. The gases and the aerosol are well mixed in the mixer and then they enter the

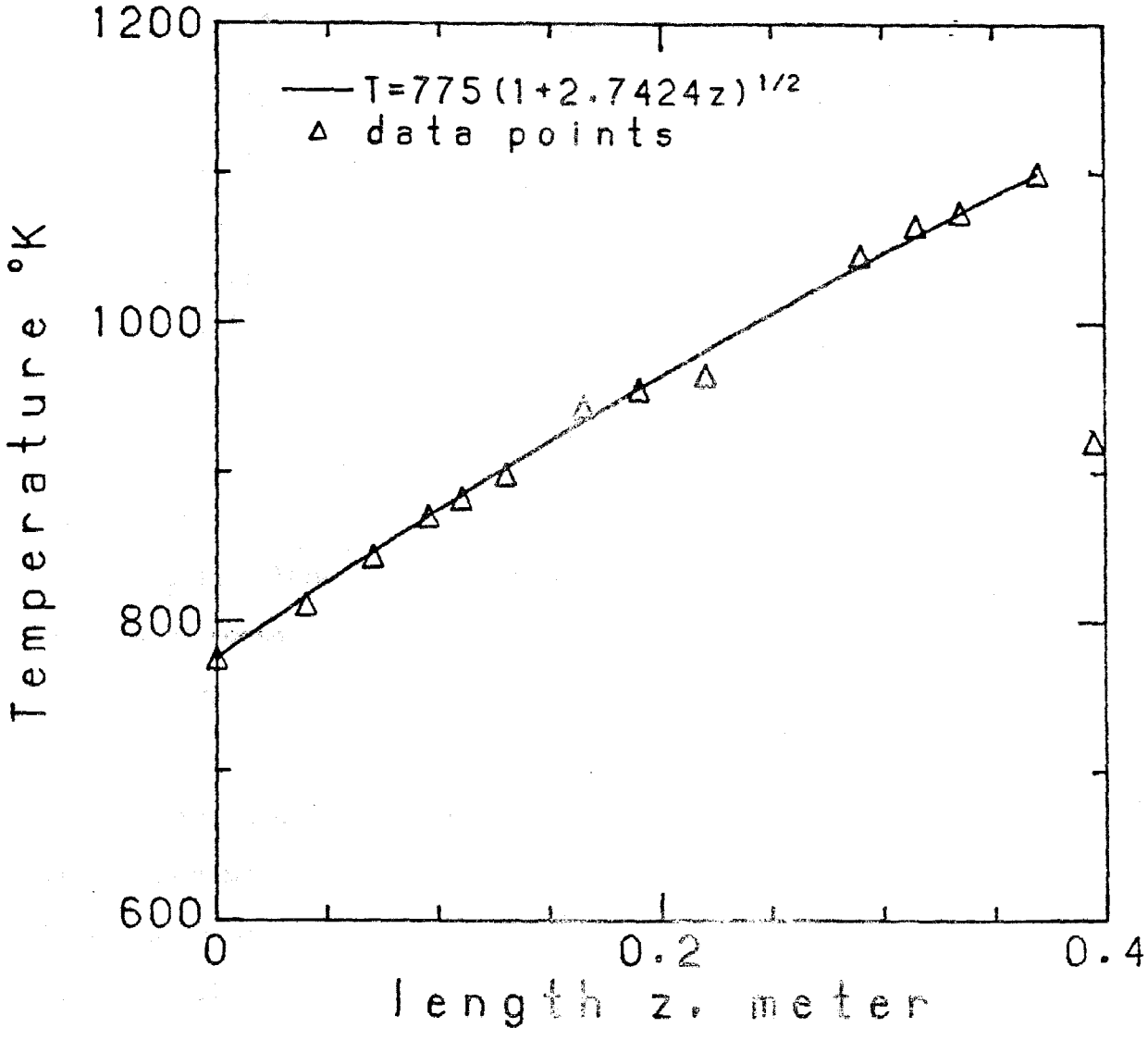

Figure 23. Temperature profile in the reactor

—— desired temperature profile

Δ measured temperature

primary reactor.

The typical flows and residence times in this system are shown below:

a) Seed aerosol reactor:

1% silane in nitrogen:	5-20 cc/min
Pure nitrogen	5-10cc/min
Residence time	10-25 secs
Temperature	900°K

b) Mixer tube

Seed Aerosol flow	10-30 cc/min
Primary silane flow	5-20 cc/min
Primary nitrogen	0.5-2 l/min
Residence time	3-4 secs

c) Primary Reactor: The inlet flows are the same as in the mixer tube.

Residence time	1 sec
Reynolds number	114
$g_a \Delta Td/(u^2T)$	0.2
Temperature	750°K to 1100°K

The flow at the exit has no silane left.

iv) Dilution and Sampling Systems: The product coming out of the reactor is silicon aerosol at a very high temperature (approx. 1100 °K). The aerosol concentration is also extremely high and must therefore be cooled and diluted before sampling. The dilution system shown in Fig. 24

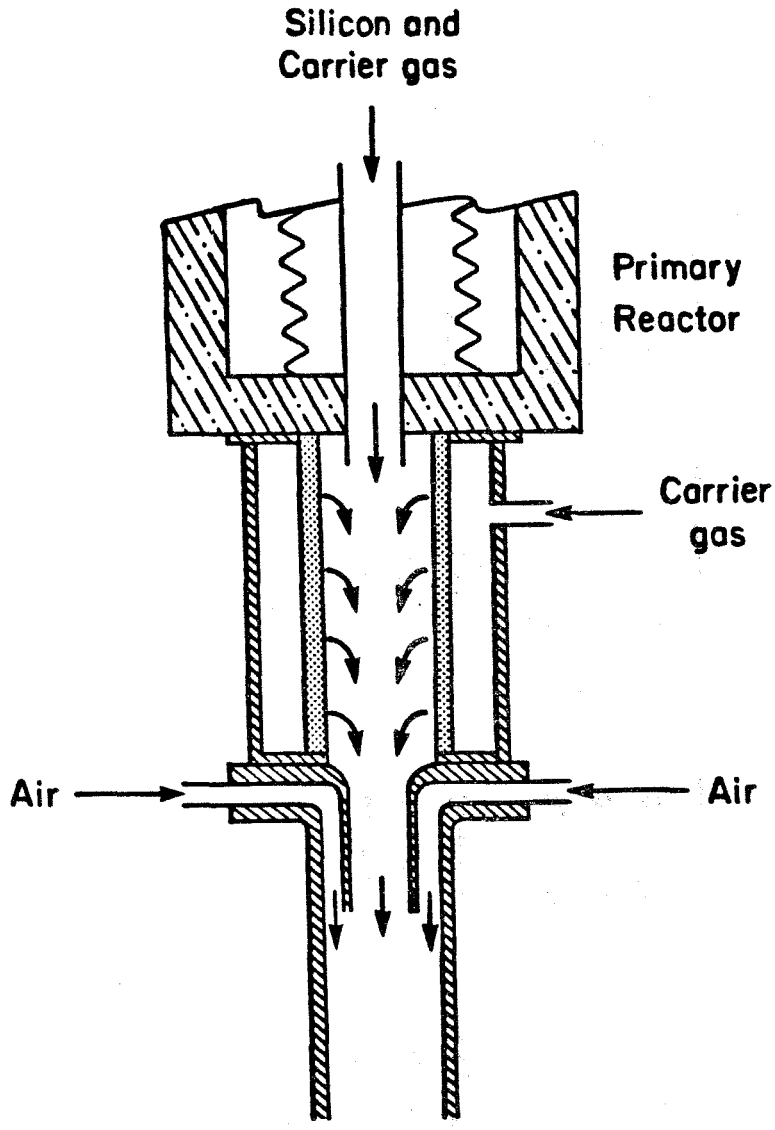

Figure 24. Dilution system for the reactor products.

TABLE 7. Size Cuts in Sampling Instruments
(all sizes in microns)

Channel	EAA	ROYCO OPC	PMS OPTICAL PARTICLE COUNTER RANGE 3	RANGE 2	RANGE 1	RANGE 0
1	.0032	0.12-0.17	0.5-1.0	1- 2	2- 4	2- 5
2	.0056	0.17-0.27	1.0-1.5	2- 3	4- 6	5- 8
3	.0100	0.27-0.42	1.5-2.0	3- 4	6- 8	8-11
4	.0178	0.42-0.62	2.0-2.5	4- 5	8-10	11-14
5	.0316	0.62-0.87	2.5-3.0	5- 6	10-12	14-17
6	.0562	0.87-1.17	3.0-3.5	6- 7	12-14	17-20
7	.1000	1.17-1.52	3.5-4.0	7- 8	14-16	20-23
8	.178	1.52-1.92	4.0-4.5	8- 9	16-18	23-26
9	.316	1.92-2.37	4.5-5.0	9-10	18-20	26-29
10	.562	2.37-2.87	5.0-5.5	10-11	20-22	29-32
11	1.00	2.87-3.42	5.5-6.0	11-12	22-24	32-35
12		3.42-4.02	6.0-6.5	12-13	24-26	35-38
13		4.02-4.67	6.5-7.0	13-14	26-28	38-41
14		4.67-5.37	7.0-7.5	14-15	28-30	41-44
15		>6.12	7.5-8.0	15-16	30-32	44-47

was developed to dilute and cool the aerosol with minimum losses. As the aerosol leaves the reactor, a coaxial flow of equal magnitude but much less momentum is introduced from the sides of a sintered tube. This prevents the aerosol from coming in contact with the colder walls and depositing due to thermophoresis. Further downstream, a large flow of diluent gas with much higher momentum joins the aerosol flow coaxially and in the same direction. The total flow rate is such that the flow becomes turbulent and the aerosol then mixes with the gases. This causes dilution and cooling to occur simultaneously.

Sampling of the aerosol was done by an Electrical Aerosol Size Analyzer (Thermo-Systems Inc., Model 3030), a Royco Model 226 Laser Optical Particle Counter and a Classical Scattering Optical Particle Counter (Particle Measurement Systems, Model CASP-100-HV (SP)). The ranges of operation of these instruments is shown in Table 7.

5.4 Results and Discussion

Most of the experimental results described below were carried out in the reactor with operating parameters given in Table 6. The only exception is the run in which the temperature (Fig. 28 and 29) is kept constant and the reaction is not controlled.

Figures 25(a) and 25(b) show the mass distributions measured with the Classical Scattering Optical Particle Counter (PMS). The seed aerosol for these runs, as shown in Fig. 26, has a number concentration of $1.02 \times 10^{11}/m^3$. The seed aerosol size distribution was obtained by inverting the data from an Electrical Aerosol Size Analyzer with the algorithm developed by Crump and Seinfeld (3). The product has a mass

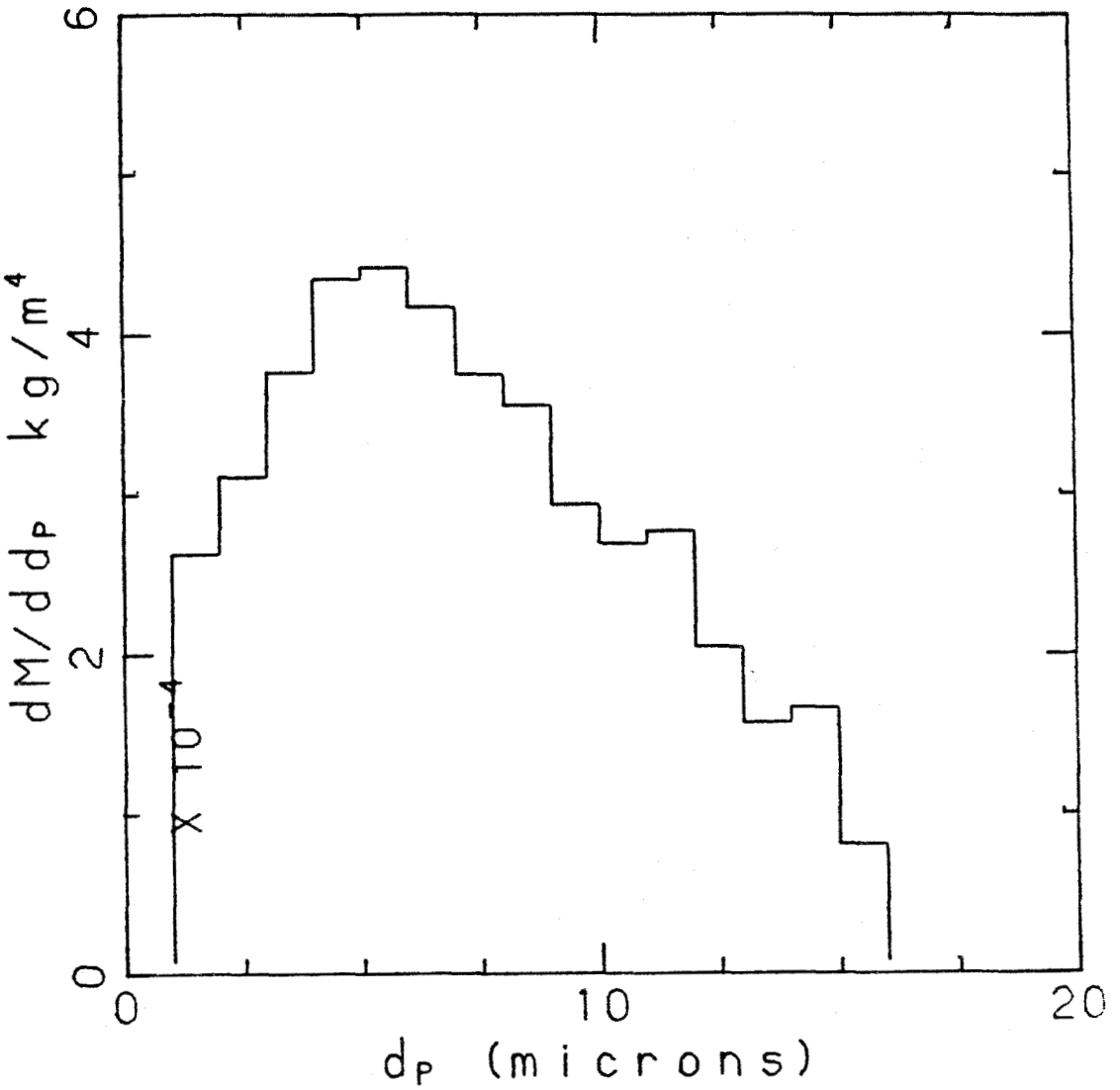

Figure 25. (a) Mass distribution of aerosol after reacting 1% silane in presence of seed aerosol (total seed concentration = $1.02 \times 10^{11}/m^3$)

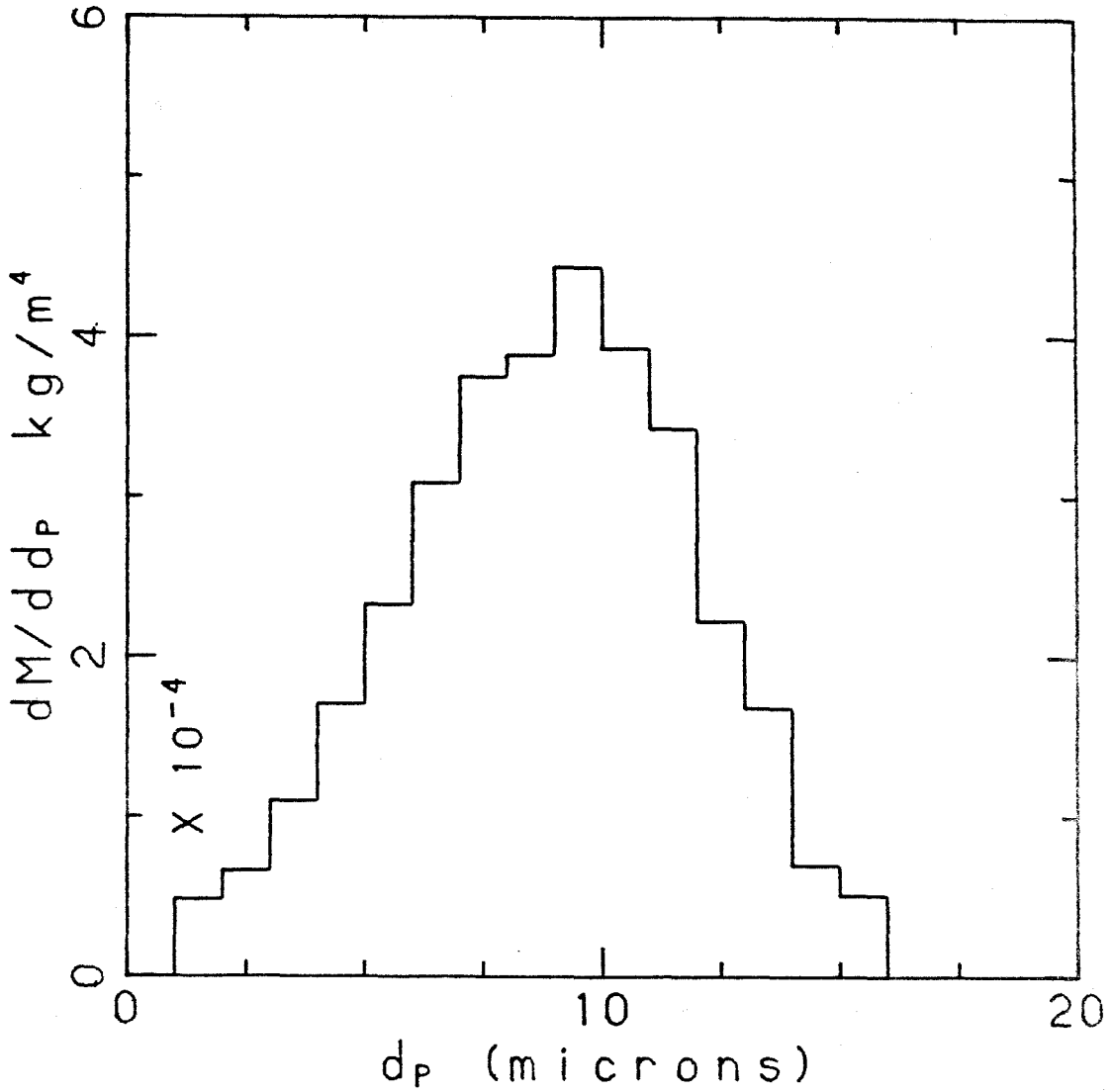

Figure 25. (b) Mass distribution of aerosol after reacting 2% silane in presence of seed aerosol (total seed concentration = $1.02 \times 10^{11}/m^3$)

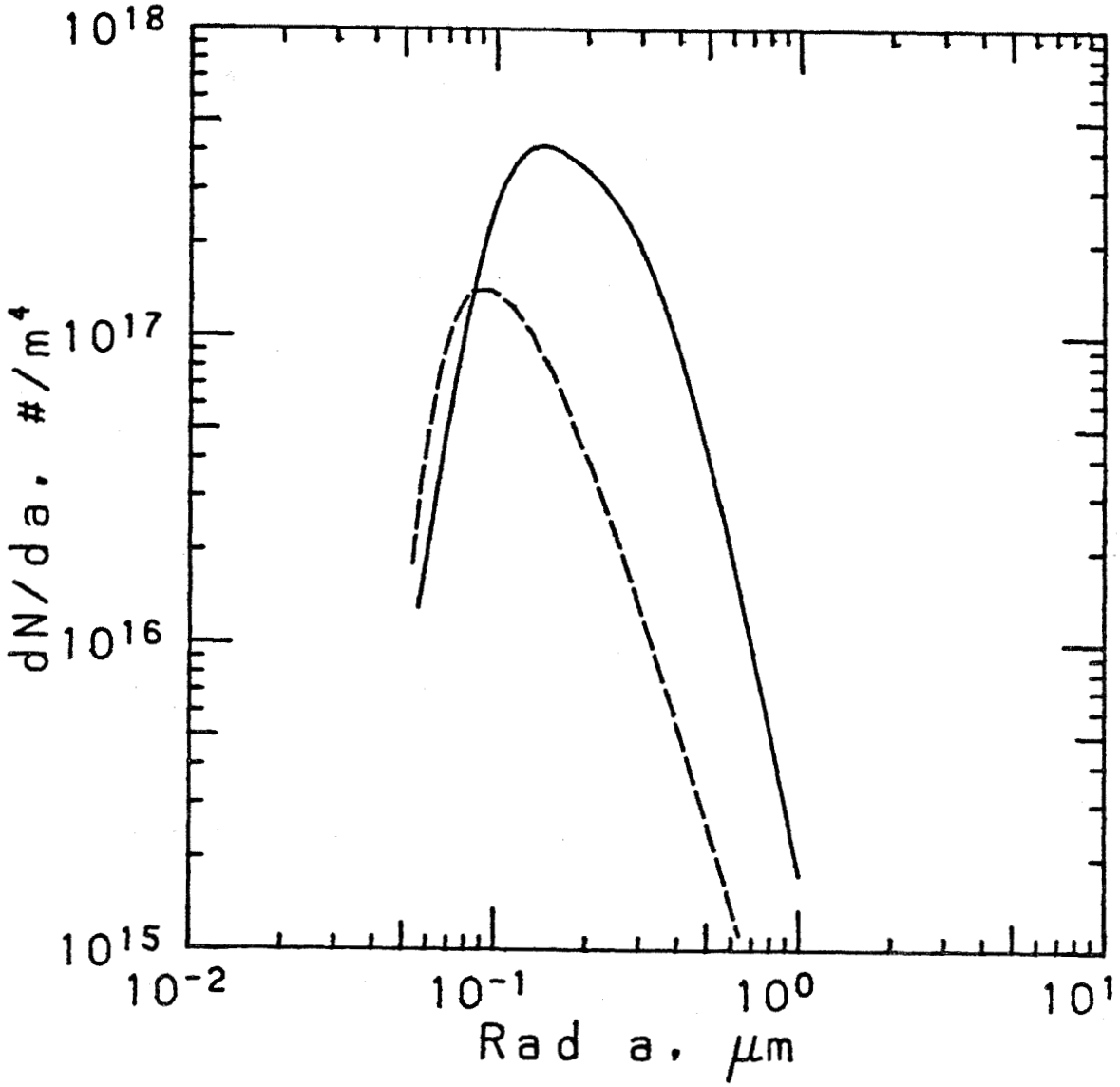

Figure 26. Size distributions of seed aerosol at 775 °K

—— (a) Reduced concentration ($2.7X10^{10}/m^3$)

—— (b) Seed aerosol of Fig. 16 ($1.02X10^{11}/m^3$)

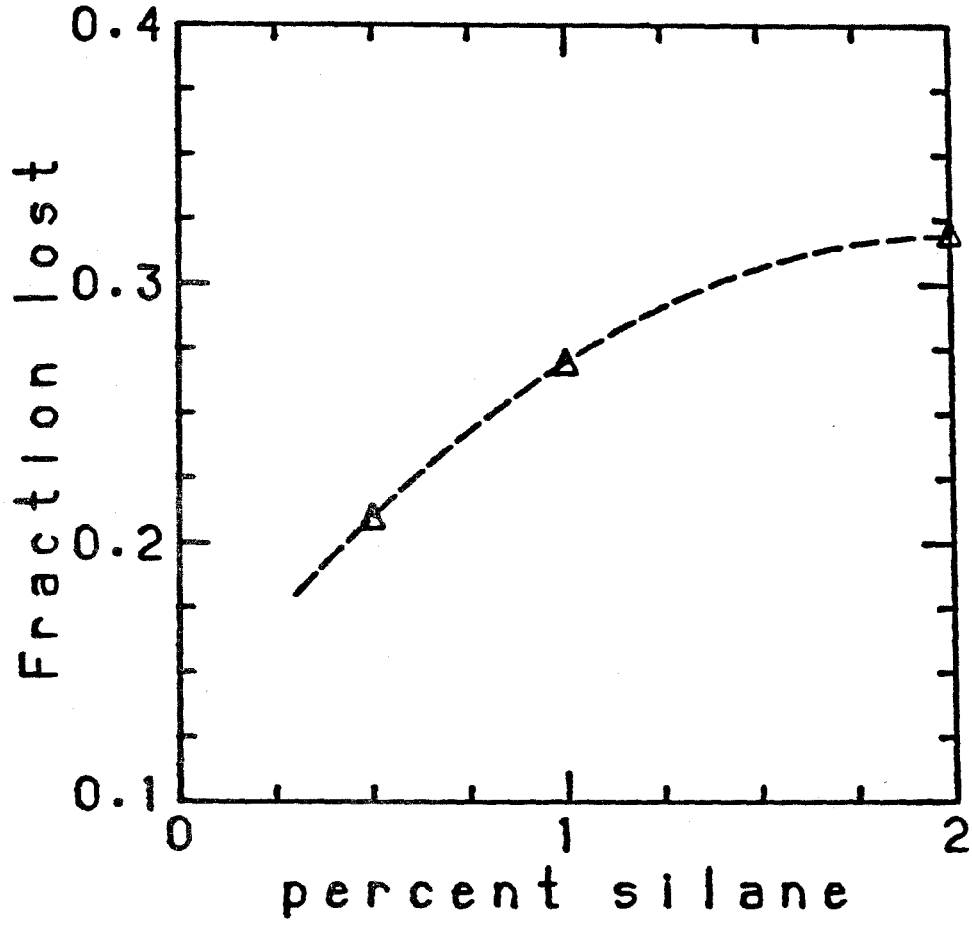

Figure 27. Silicon losses in the reactor as a function of input silane concentration.

mean diameter of 3.5 microns (mass median diameter: 6.23 microns) when 1% silane is reacted and 4.95 microns (mass median diameter: 8.98 microns) when 2% silane is reacted. Figures 17-21 of the last chapter show the results of a theoretical simulation of the reactor with the same seed aerosol. The product is predicted to have a mass mean diameter of 3.0 microns for the case of 1% silane and 3.7 microns in case of 2% silane. It must be noted here that the theory predicts a monodisperse aerosol, whereas the product is certainly polydisperse. As was mentioned earlier, this is mainly due to radial variations in the reactor and coagulation of the aerosol, none of which have been accounted for in the theory. Coagulation would also increase the size of the particles above that predicted by theory.

Elemental analysis of the product aerosol revealed that it is mainly silicon with less than 5% hydrogen.

Finally, the mass of the product was collected by a total filter to determine the loss of silicon (both as silane and silicon) in the furnace. The results are shown in Fig. 27. About 73% of silicon is recovered when 1% silane is reacted. The recovered fraction is less when silane concentration is increased. The losses in the figure include deposition in the dilution and cooling systems which are outside the reactor. In chapter 4, it was shown that when 1% silane is reacted, about 6% of the silane is expected to be lost due to reaction on the wall. It was determined experimentally that, for the same case, about 10% of the silicon is lost in the dilution system; thus, the actual losses in the reactor are about 17%.

The feasiblity of growing large silicon particles by silane

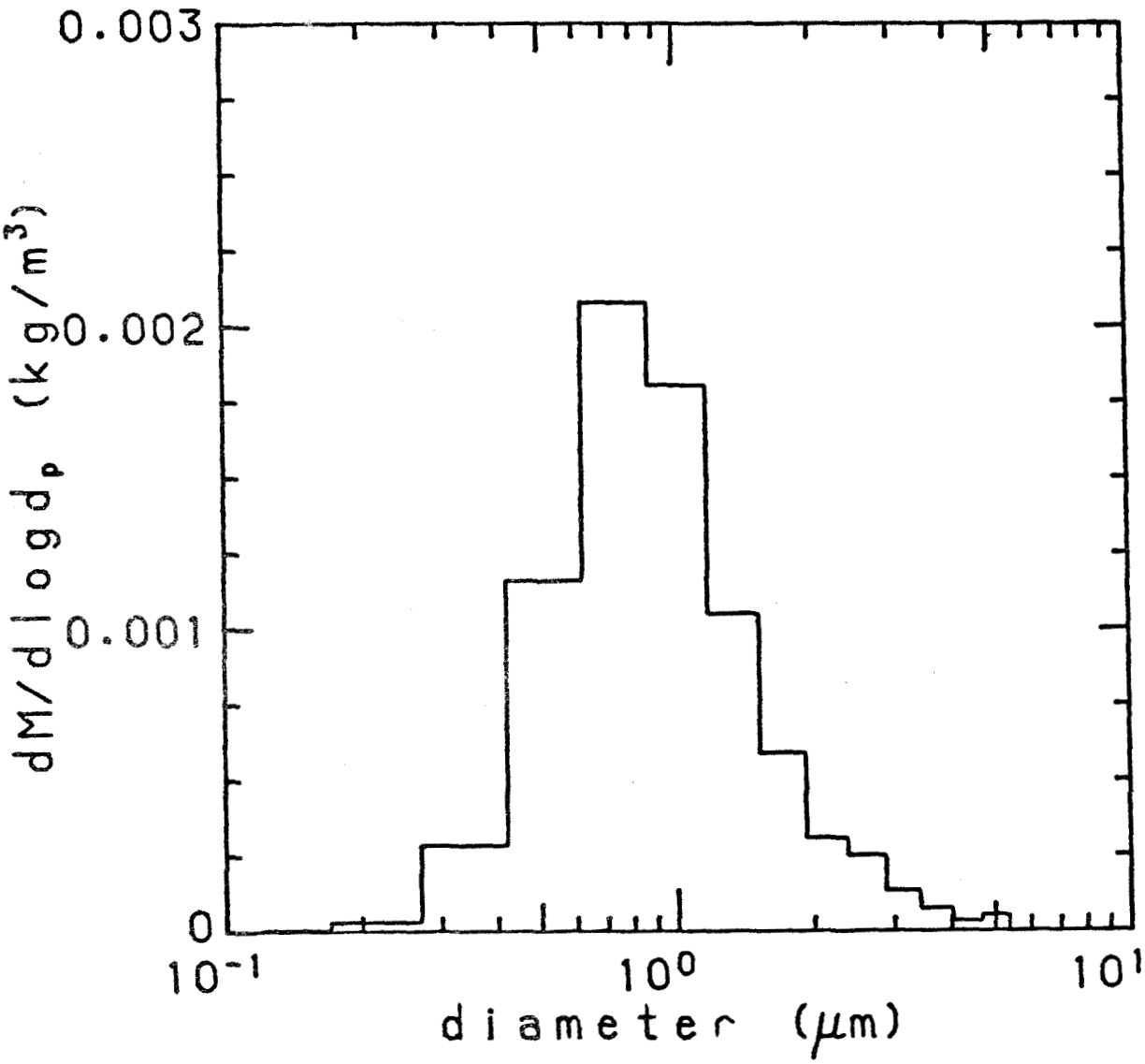

Figure 28. Mass distribution of silicon aerosol in a high temperature reactor at 900 °K without seed aerosol.

(Silane concentration 1%)

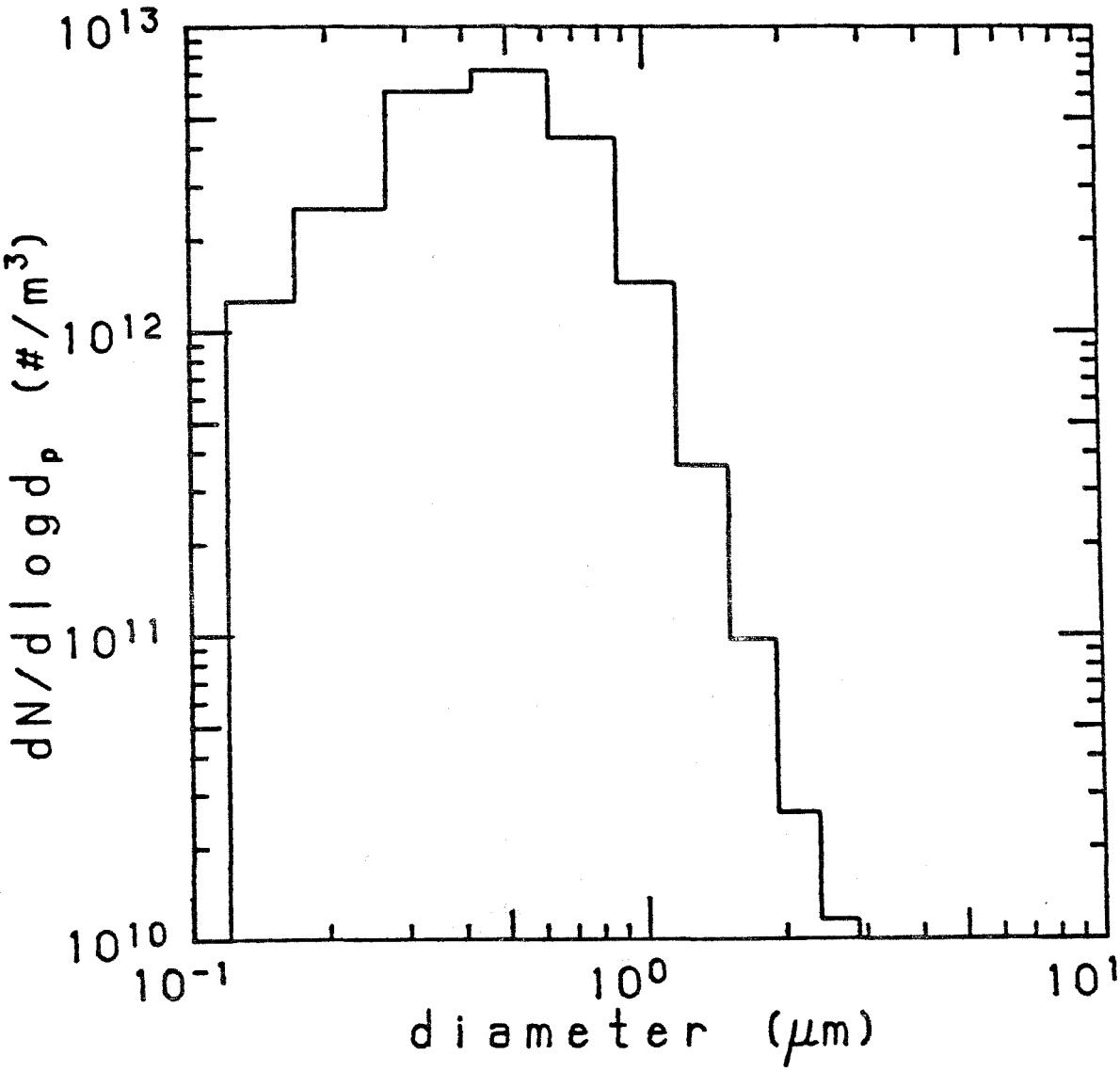

Figure 29. Size distribution of silicon aerosol in a high temperature reactor at 900 °K without seed aerosol.

(Silane concentration 1%)

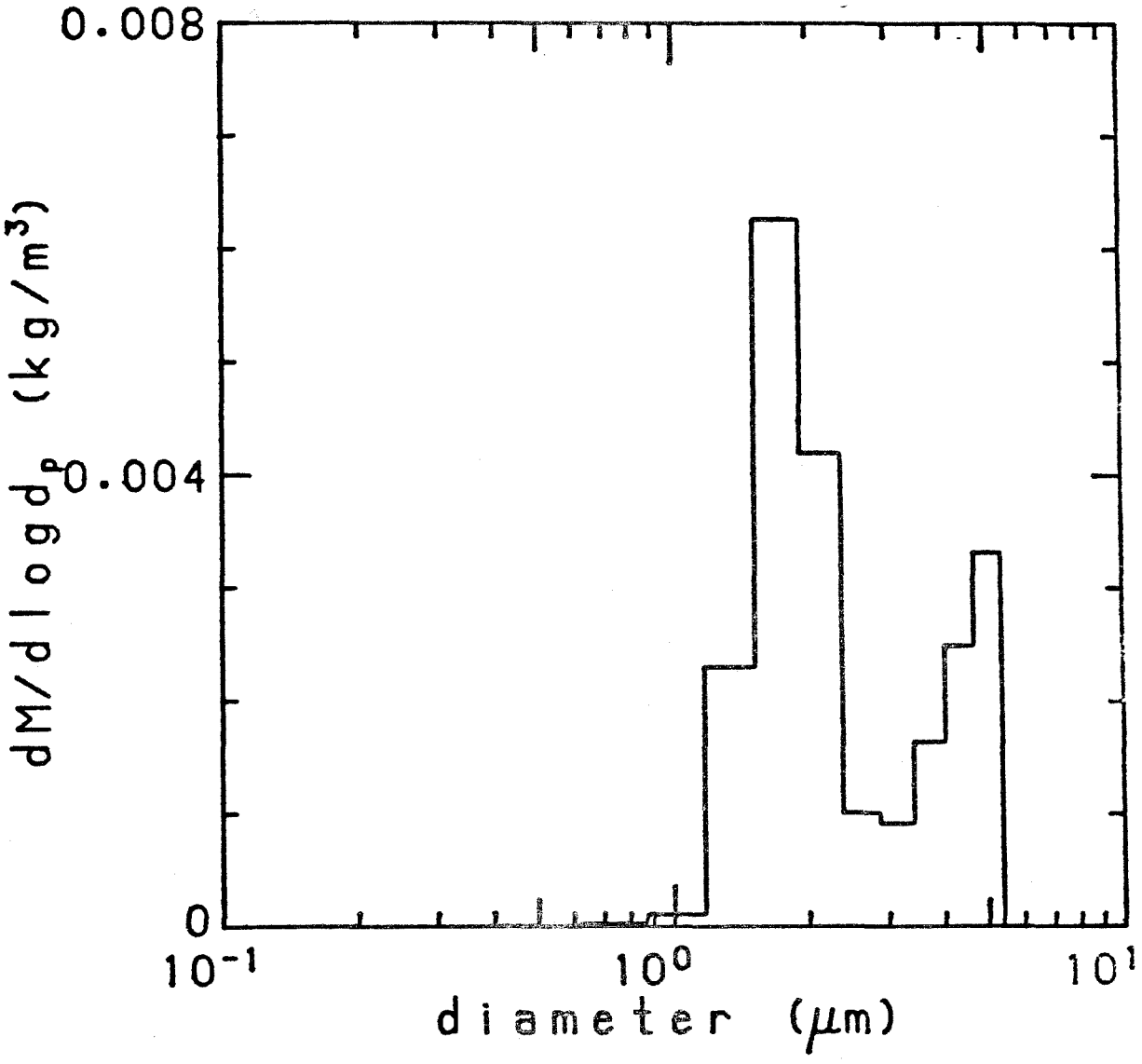

Figure 30. Mass distribution of product aerosol after reacting 1% silane with reduced seed concentration ($2.7X10^{10}/m^3$).

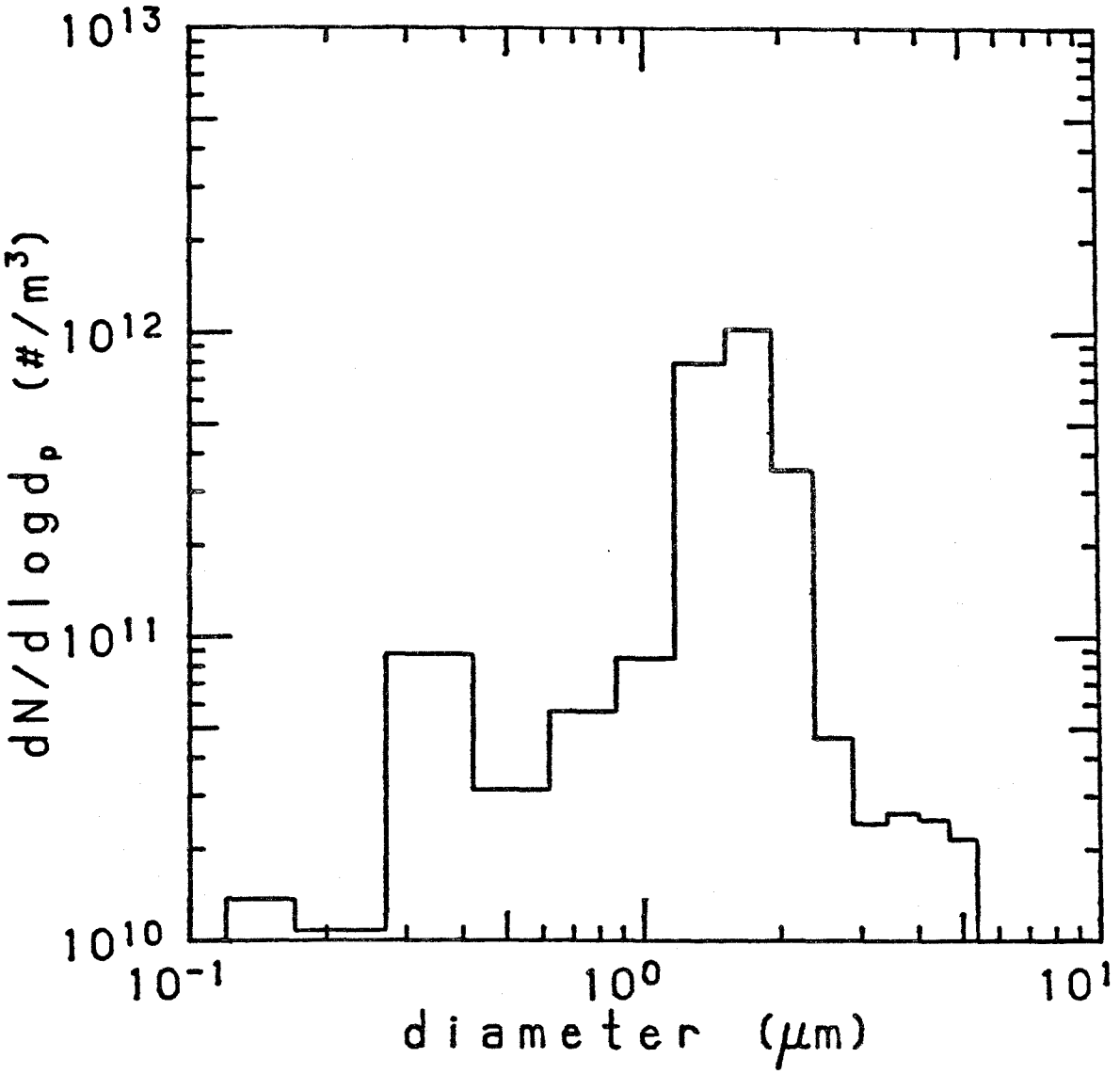

Figure 31. Number distribution of product aerosol after reacting 1% silane with reduced seed concentration ($2.7X10^{10}/m^3$)

pyrolysis has been demonstrated. Additional experiments were conducted to explore the reactor performance when its operation was not optimized to maximize particle growth.

Figures 28 and 29 show the results of running the reactor in the manner of a high temperature (high reaction rate) free space reactor as was done at the Jet Propulsion Laboratory (1) and at Union Carbide (2). The temperature for this run was 900 °K and there was no seed aerosol. The mass mean diameter is now 0.453 micron. These results are comparable to those obtained in the conventional free space reactors and it indicates that nucleation has been dominant, as was predicted by theory.

If the seed aerosol is reduced substantially, nucleation is predicted to occur by theory, and average particle size is predicted to be in the submicron range. However, when the seed aerosol is reduced to a total number concentration of $2.7X10^{10}$ $/m^3$ (i.e. reduced by a factor of 4), as shown in Fig. 26, the product aerosol becomes bimodal as shown in Fig. 30 and 31. The mass mean diameter is 1.34 um. Coagulation of seed aerosol is a possible explanation for this change in the character of the particle size distribution. Nucleation and growth of seed particles occur simultaneously in this system. Once the seed particles have grown, they efficiently scavenge the smallest of the nucleated particles. As a result, the seed particles grow at the expense of the smaller nucleated particles. Coagulation is thus an important consideration in the reactor.

References (Chapter 5)

1) H. Levin, "Proceedings of Symposium on Materials and New Processing Technologies for Photovoltaics," Electrochemical Society, 1980.

2) J. R. Lay and S. K. Iya, "Proceedings of the 15th IEEE Photovoltaic Specialists Conference," pp 565-568 (1981).

3) J. G. Crump and J. H. Seinfeld, Aerosol Sci. and Technology, Vol 1, No 1, pp 15-34, (1982).

CHAPTER 6

DISCUSSION AND CONCLUSIONS

The reactor for production of silicon appears to be successful in producing large particles of silicon. The main difference between the aerosol reactor developed and the conventional free space reactors is illustrated in Fig. 32 where the characteristic times of the different reactors is compared with the characteristic times for the silane reaction. The JPL and Union Carbide reactors operate at high temperatures where the reaction is extremely fast. This leads to nucleation of the vapors and the product is a submicron aerosol. The reactor discussed here operates under controlled reaction rates and condensation predominates. The temperatures in the aerosol reactor increase with time, but slowly enough such that the aerosol is at all times able to scavenge the vapors.

The experimental data indicate that the results from the reactor are in reasonable agreement with theory when nucleation is expected to be significantly quenched and when the system is run as a conventional high temperature free space reactor. The main reasons for the differences between theoretical predictions and experimental results are probably the radial variations in the reactor and coagulation of the aerosol. Coagulation is specially significant when large numbers of particles are expected to nucleate and it leads to additional growth of seed particles.

An improved analysis would, therefore, include coagulation as a mechanism for particle growth. The radial profiles in the reactor should

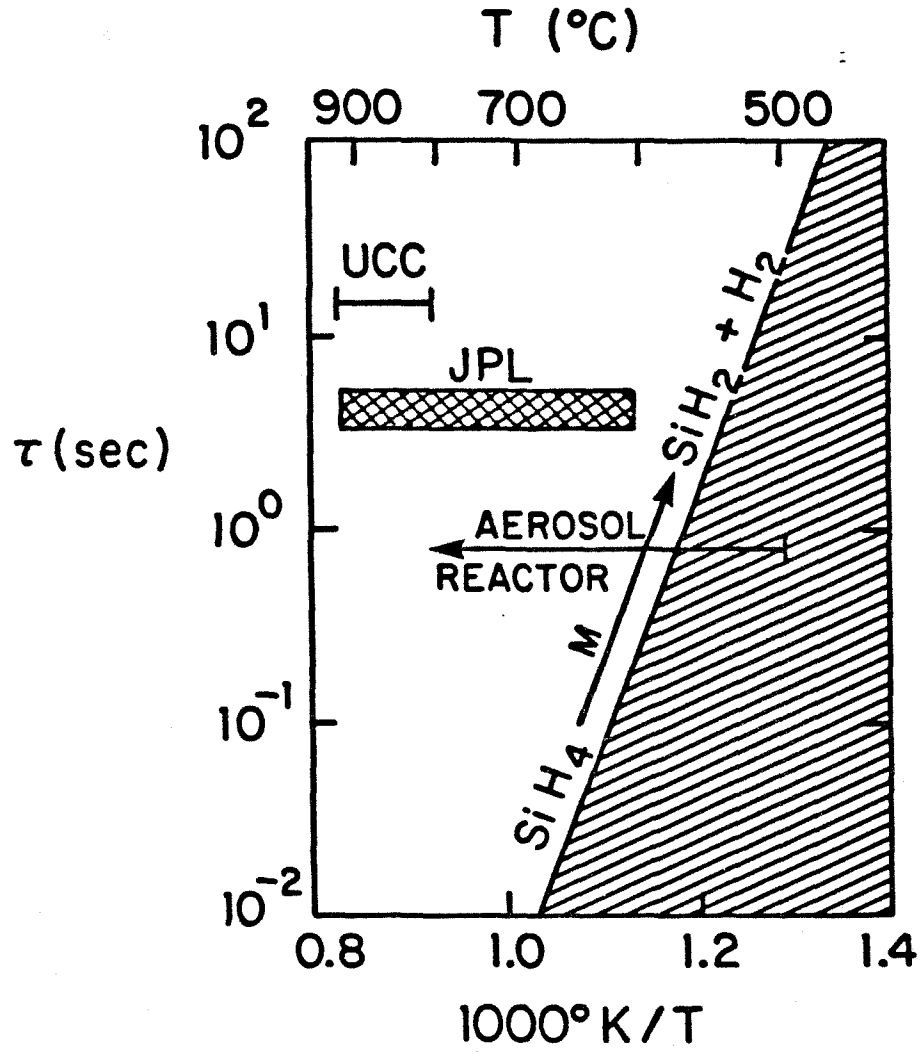

Figure 32. Comparison of characteristic times of the silane reaction with residence times in the reactor.

also be taken into account. The coagulation calculations must include both that due to brownian motion and that due to differential sedimentation. The analysis would be more complex than the present theory. Simplified computational techniques should be adopted. An option is to use the sectional model of aerosol dynamics developed by Gelbard, et al. (1). This would reduce the computational effort significantly.

The experiments with the aerosol reactor indicate that aerosol sampling methods should be a major consideration in future work. The reactor generates aerosols in high concentrations and in size ranges varying from submicron to over 10 microns. This creates problems in sampling. Preliminary experiments also indicated that particles tend to bounce off or be broken up in inertial impacters. An impactor designed to collect friable solid particles and in-situ optical particle counters with capability of sampling high aerosol concentrations would be particularly helpful in further analyses of the product.

A significant step would be to enlarge the reactor to obtain particles large enough to be collected easily by gravitational settling. It would then be possible to incorporate a collecting crucible into the system in which the particles are melted. The reactor would then be able to produce silicon melt in one operation. The melt could be processed to grow single crystals by conventional methods.

The experimental reactor utilizes silane for production of silicon. The theory can be applied to other gaseous reactants, and to other systems where control of nucleation is desired. In a modified form, the analysis may be applied to the fluidized bed reactor for silicon production.

The development of the reactor was made possible by analyzing the

process of simultaneous nucleation and condensation for particles in the free molecular, transition and the continuum size ranges. The analysis is a modification of the classical theory, and appears in the theory as the total clearance volume fraction Ω . As long as $\Omega << 1$, the two approaches are identical. As Ω becomes of the order unity, the theories diverge. It should be recalled that the present analysis was carried out by considering simultaneous nucleation and condensation around a single particle and then summing up the individual effects for all particles. The effect of the influence of adjacent particles was ignored. As the volume of influence of adjacent particles overlap, the relation between average vapor pressure, as used in the classical theory, and the background vapor pressure, as used in the clearance volume approach, is very difficult to define. Comparison of the two methods is not possible unless a detailed analysis of simultaneous nucleation and condensation is made by taking into account the spatial distribution of particles and overlapping regions of influence. When the clearance volume approach is used with such a detailed analysis it can provide an accurate analysis of nucleation and condensation. Ray and Dronamraju (2) have made an analysis of vapor concentrations in a monodisperse aerosol. Their analysis does not take into account the effect of nucleating particles on vapor concentrations. It may be possible to extend their analysis and incorporate it into the present theory.

The present analysis also provides a compact analytical criterion to determine the dominant process in nucleation and condensation (Eq. 102). This analytical expression could be used to simplify calculations when coagulation is included in the analysis. Of particular interest is the

conclusion that, for a dilute condensing vapor, the competition between nucleation and condensation onto particles is determined primarily by vapor depletion by the particles, and not by the temperature changes due to release of latent heat of condensation.

References (Chapter 6)

1) F. Gelbard, Y. Tambour and J. H. Seinfeld, J. Colloid and Interface Sci., Vol 76, pp 541-572, (1980).

2) A. K. Ray and M. Dronamraju, Aerosol Sci. and Tech., Vol 1, No 4, pp 449-462 (1982).

APPENDIX A. FORTRAN SOURCE CODE AND SAMPLE OUTPUT

A.1 Documentation

Symbols used in Program SFR.FTN

Variable	Description
A0	Ratio VM/k, m^3 $^oK/J$
ABS	Absolute error specified for RKF subroutine
AJ	Modified nucleation rate, $\#/m^3 sec$
AL	Lewis number
AQ	Aerosol volume fraction
B1	Constant used in flux matching method
C1	Constant used to specify temperature profile
CV	Total clearance volume fraction
DELT	Time of integration by RKF subroutine, sec
DIM	Ratio Diffusivity/A0, kg/ $Ksec^3$
DQ(26)	dQ/dT : derivative array
DTF	Nondimensional temp derivative $-(dTF/dt)/TF$, sec^{-1}
EJ	Material constant in expression of nucleation rate
F	Mean free path of vapor molecules, m
HVR	$\Delta Hv/R$, where ΔHv is heat of vaporisation, (^oK)
IFLAG	Flag : Indicates status of integration in RKF
IWORK(6)	Array for use by RKF
K(26)	Array used to number characteristics
L	Maximum number of characteristics (<12)
M	Maximum number of equations (M=2L+2)
N	2+(actual number of characteristics)
PHT	Material constant=2*SIG*A0, m ^oK

Variable	Description
PIC	Material constant=2*PI/A0, $J/m^3\ ^oK$
PSF	Saturation vapor pressure, Pa
PT	Total pressure, Pa
Q10	Initial value of Q(1) i.e. vapor pressure, Pa
Q20	Initial value of Q(2), Pa
Q(1)	Vapor pressure, Pa
Q(2)	Pressure of silane, Pa
Q(3) to Q(L+2)	Radii of characteristics, m
Q(L+3) to Q(2L+2)	Q(L+1) is the number distribution function for the radius Q(1), $\#/m^4$
Q(2L+3)	Silane lost to wall by surface reaction, Pa
RADC	Critical radius, m
REL	Relative error specification for RKF
R0	Radius of vapor molecule, m
SF	Saturation ratio, Q(1)/PSF
SM1	Material constant in expression of nucleation rate given by: SM1=(16*PI/3)*(SIG*VM$^{2/3}$/k)**3
T	Time, sec
TF	Temperature, °K

Variable	Description
TF0	Constant used to specify temp. profile, °K
TOUT	Time up to which integration is completed in RKF, sec
VM	Volume of vapor molecule, m^3
WORK(159)	Array used by RKF

Note:- SIG is the surface tension

k is the Boltzmann constant $1.38X10^{-23}$ J/ °K

R is the gas constant $8.31X10^{3}$ J/kmole °K

DESCRIPTION OF FUNCTIONS AND SUBROUTINES

INPUT

Reads input from file INPUT.DAT at start of program. N is the number of characteristics+2. LT is a flag which indicates whether output file OUTPT.DAT will be created (yes for LT>0).

OUTPT.FTN

Types output at DELT intervals. Will also record output in file OUTPT.DAT if LT>0

RESET

Reduces number of characteristics whenever they exceed a certain number (10 in the program) by eliminating some of the characteristics. K(I) is an array which maintains the original numbering of the characteristics. Also resets IFLAG for further integration.

DERIV

Computes derivatives DQ(I) of the array Q(2L+2). Subroutine is an input for RKF subroutine.

JAV

Determines total clearance volume CV and the corrected nucleation rate AJ. C(X) is the clearance volume for a single particle of radius X. Approximate expression for C(X) is used.

AV

Calculates the integral on the r.h.s. of the vapor conservation equation. This function is called only by the subroutine DERIV to determine dQ(1)/dt.

TEMP

Provides temperature profile as a function of time T. Also gives PSF and F. Input is T; outputs are TF,DTF,PSF,F.

ARV

Computes volume of aerosol (ARV). Simplified integration program is used.

RKF

Integrates a system of first order ordinary differential equations. The program, developed by Sandia Laboratories, is not included in the Fortran Codes section. It uses the Runge-Kutta-Fehlberg method described in the reference:

E. Fehlberg, "Low-order Classical Runge-Kutta Formulas With Stepsize Control," NASA TR R-315.

The parameters in RKF(F,N,Y,X,XO,REL,ABS,IFLAG,WORK,IWORK) represent

the following:

F -- subroutine of derivatives = dY(I)/dX

N -- number of equations to be integrated

Y(I) -- solution vector at the point X

X ---- independent variable

XO --- output point at which solution is desired

REL, ABS -- relative and absolute error tolerances

IFLAG --- indicator for status of integration; IFLAG=2 indicates succesful integration

WORK, IWORK --- information generated by RKF which is necessary for subsequent calls to RKF

A.2 *Fortran Code*

```
C     ------------------------------------------------------------------
C     ------------------------------------------------------------------
c     !        Program SFR.FTN   (For Silicon Flow Reactor)             !
c     !                                                                 !
c     !   This program calculates size evolution of silicon aerosol in a !
c     !   flow reactor where silane is decomposed to give silicon.      !
c     !   It requires the Runge-Kutta integrating subroutine; which is  !
C     !   RKF                                                           !
C     ------------------------------------------------------------------
C        Q(1) : Vapor Pressure     Q(2) : Silane Pressure
C        Q(3 TO L+2) : Radius of characteristics
C        Q(L+3 TO 2L+2) : Size distribution (dN/da)
C        SM1=(16*PI/3.)*(SIG*VM**.6667/K)**3          A0=VM/K
C        DT0=HVR*RMB/(P*AL)
C        EJ=ALOG((VM/(K*K))*SQRT(2.*SIG/(PI*WM)))
C        J=(P/TF)**2*EXP(EJ-SM1/(TF**3*SF**2)) defines EJ
C        PHT=2.*SIG*A0       DIM=DIF/A0        PIC=2.*PI/A0
C        F=beta*mean free path
C     ------------------------------------------------------------------
C
      EXTERNAL DERIV
C
      COMMON/DER/L,N
      COMMON/GEN/DIM,PHT,PIC,A0,beta,Q20,Q10
      COMMON/CLV/DT0,SM1,AL,EJ
      COMMON/TMP/TF0,C1,TF1
C
      DIMENSION Q(27),WORK(165),IWORK(6),K(15)
C
      DATA HVR,A0,DT0,VM/99060.,1.45E-6,14.88,2.E-29/
      DATA AL,SM1,R0,PT/0.23,1.572E12,1.683E-10,1.013E5/
      DATA B1,PIC,EJ,DIM/1.97,4.33E6,68.07,2.609E-11/
      DATA IFLAG,T,REL,ABS,PHT/1,0.0,1.E-3,1.E-10,2.52E-6/
C
C
      CALL INPUT(Q,L,N,LT,TF0,C1,TF1,DELT,Q10,Q20)
      CALL TEMP(T,TF,DTF,PSF,F)
      CALL JAV(CV,AJ,TF,PSF,F,Q)
      CALL OUTPT(Q,K,CV,TF,T,LT,N)
C
C
      M=2*L+3
      Q20=Q(2)
      DO 50 I=3,L+2
50    K(I)=I
      DO 100 I=N+1,L+2
```

```
C       ------------------------------------------------------------
C       FIND INITIAL CONDITIONS FOR THE CHARACTERISTIC
C
        Q(1)=0.0
        Q(L+1)=0.0
        IF (Q(1).LE.PSF) GO TO 38
        SF=ALOG(Q(1)/PSF)
        Q(N+1)=PHT/(SF*TF)
        IF(Q(N+1).LT.(1.5*R0)) Q(N+1)=R0*1.5
        A=DIM*(Q(1)-PSF)/(TF*(F+Q(N+1)))
        CALL JAV(CV,AJ,TF,PSF,F,Q)
        Q(N+1+L)=AJ/A
C       ------------------------------------------------------------
C
38      N=N+1
        CALL TEMP(T,TF,DTF,PSF,F)
        TYPE 40,N,Q(N),Q(N+L),Q(1),TF
40      FORMAT(/I4,'  RAD=',1PE10.3,'  N=',1PE10.3,'  P=',1PE8.1
        1 ,' TMP=',1PE9.2/)
        IF (LT.GT.0) WRITE (1,40) N,Q(N),Q(N+L),Q(1),TF
C       ------------------------------------------------------------
C       CALL RUNGA KUTTA SUBROUTINE FOR INTEGRATION UPTO T+DELT
C
56      TOUT=T+DELT
58      CALL RKF(DERIV,M,Q,T,TOUT,REL,ABS,IFLAG,WORK,IWORK)
C       ------------------------------------------------------------
        IF (IFLAG.NE.2) GO TO 200
        IF (N.GT.10) CALL OUTPT(Q,K,CV,TF,LT,N)
        IF (N.GT.10) CALL RESET(Q,K,IFLAG,LT)
        CALL TEMP (T,TF,DTF,PSF,F)
        CALL JAV(CV,AJ,TF,PSF,F,Q)
C
        CALL OUTPT(Q,K,CV,TF,T,LT,N)
C
        IF (Q(2).GT.(.001*Q20)) GO TO 90
        IF (Q(1).LT.(.01*Q20)) GO TO 150
90      IF (CV.GE.1.0) GO TO 56
100     CONTINUE
150     TYPE 160,Q(1),Q(2),TF,T
160     FORMAT('  PROG STOPS:  Q1,Q2,TF,T=',4(1PE11.3))
        STOP
200     TYPE 250,IFLAG
250     FORMAT('   PROBLEM IN RKF:    IFLAG=',I2)
        STOP
        END
C
```

```
C
C       ------------------------------------------------------------
C       ------------------------------------------------------------
C
        SUBROUTINE INPUT(Q,L,N,LT,TF0,C1,TF1,DELT,Q10,Q20)
C       Subroutine reads input data
C       ------------------------------------------------------------
C
        DIMENSION Q(26)
C
        CALL ASSIGN (1,'INPUT.DAT ')
C
        READ (1,10) DELT
        TYPE 40,DELT
        READ (1,10) TF0,C1,TF1
        TYPE 50,TF0,C1,TF1
        READ (1,30) L,N,LT
        TYPE 60,L,N,LT
        READ (1,10) Q(1),Q(2)
        TYPE 70,Q(1),Q(2)
        Q10=Q(1)
        Q20=Q(2)
        IF (N.LT.3) GO TO 6
        DO 5 I=3,N
        READ (1,10) Q(I),Q(L+I)
5       TYPE 80,Q(I),Q(L+I)
6       CALL CLOSE (1)
        TYPE 90
C
        IF (LT.LE.1) RETURN
C
        CALL ASSIGN(1,'OUTPT.DAT ')
        WRITE (1,40) DELT
        WRITE (1,50) TF0,C1,TF1
        WRITE(1,60) L,N,LT
        WRITE (1,70) Q(1),Q(2)
        IF (N.LT.3) GO TO 9
        DO 8 I=3,N
8       WRITE (1,80) Q(I),Q(L+I)
9       WRITE(1,90)
10      FORMAT(3G12.3)
30      FORMAT(4I5)
40      FORMAT (/8X,'  INITIAL TIME INTERVALS ARE :',1PE10.3/)
50      FORMAT (' TEMP PROFILE PARAMETERS:  ',3(1PE12.3))
60      FORMAT (12X,' MAX NO CHARACTERISTICS:',I3,/
     1  6X,'    INITIAL NO OF CHARACTERISTICS:',I3,'   LT:',I2/)
70      FORMAT(6X,'VAPOR PRESSURE:',1PE10.3,'  SILANE PRESSURE:',1PE10.3/)
80      FORMAT(8X,'  RADIUS (A):',1PE10.3,'   DN/DA:',1PE10.3)
90      FORMAT(/14X,' END OF INPUT FILE'//)
C
        RETURN
        END
C
```

```
C
C
C     ------------------------------------------------------------------
C     ------------------------------------------------------------------
C -
      SUBROUTINE OUTPT(Q,K,CV,TF,T,LT)
C     Subroutine to print and record output
C     ------------------------------------------------------------------
C
      COMMON/DER/L,N
      DIMENSION Q(27),K(15)
C
      AQ=ARV(Q)
C
      TYPE 40,T,TF
      TYPE 45,Q(1),Q(2)
      TYPE 48
      IF(N.LT.3) GO TO 25
      DO 20 I=3,N
20    TYPE 50,I,K(I),Q(I),Q(L+I)
      TNO=0.0
      TNR=0.0
      IF(N.EQ.3) GO TO 24
      DO 22 I=3,N-1
      TNO=TNO+(Q(L+I)+Q(L+I+1))*ABS(Q(I)-Q(I+1))
22    TNR=TNR+(Q(L+I)*Q(I)+Q(L+I+1)*Q(I+1))*ABS(Q(I)-Q(I+1))
24    TNO=0.5*(TNO+Q(L+N)*Q(N))
      TNR=0.5*(TNR+Q(L+N)*Q(N)**2)
      IF (TNO.LE.0.0) GO TO 25
      AVRDN=TNR/TNO

      AVRDM=(AQ/(TNO*4.1888))**.333333
      TYPE 80,TNO,AVRDN,AVRDM
25    TYPE 60,CV,AQ
      TYPE 90,Q(2*L+3)
C
      IF (LT.LE.0) RETURN
C
      WRITE (1,40) T,TF
      WRITE(1,45) Q(1),Q(2)
      WRITE (1,48)
      IF (N.LT.3) GO TO 35
      DO 30 I=3,N
30    WRITE (1,50) I,K(I),Q(I),Q(L+I)
      IF (TNO.LE.0.0) GO TO 35
      WRITE (1,80) TNO,AVRDN,AVRDM
35    WRITE (1,60) CV,AQ
      WRITE (1,90) Q(2*L+3)
```

```
C
40      FORMAT(/14X,'TIME=',1PE10.3,' SEC',5X,' TEMPERATURE=',1PE10.3
     1  ,' K')
45      FORMAT(8X,'VAPOR PRESSURE=',1PE10.3,3X,'SILANE PRESSURE='
     1  ,1PE10.3,'  PASCALS')
48      FORMAT(/16X,'I',4X,'K(I)',7X,'Q(I)',13X,'Q(L+I)')
50      FORMAT(12X,I5,I6,'   RAD=',1PE14.7,'  ND='1PE10.3)
60      FORMAT(14X,'TOT CL VOL=',1PE10.3,'  TOT AEROSOL VOL=',1PE10.3)
90      FORMAT (16X,' WALL LOSS BY SURFACE RXN=',1PE10.3,' PASCALS'//)
80      FORMAT(/10X,'TNO=',1PE10.3,'  NUM AV RAD=',1PE10.3
     1 ,'  MASS AV RAD=',1PE10.3)
        RETURN
        END
C
C
C       ------------------------------------------------------------------
C       ------------------------------------------------------------------
C
        SUBROUTINE RESET (Q,K,IFLAG,LT)
C       Reset resduces the number of characteristics. K(I) is an array
C       which preserves the original numbering of the characteristics.
C       ------------------------------------------------------------------
C
C
C       RESET REDUCES NUMBER OF CHARACTERISTICS
C
        COMMON/DER/L,N
        DIMENSION Q(27),K(15)
C
        IFLAG=1
        TYPE 5
        IF(LT.GT.0) WRITE(1,5)
5       FORMAT(/10X,' REDUCING NUMBER OF CHARACTERISTICS !'/)
        I=2
10      IF (N.LT.7) RETURN
        I=I+1
        IF (Q(I).GT.0.0) GO TO 50
        IF (I.EQ.N) GO TO 16
        DO 15 J=I,N-1
        Q(J)=Q(J+1)
        Q(J+L)=Q(J+L+1)
15      K(J)=K(J)+1
16      Q(N)=0.0
        Q(N+L)=0.0
        N=N-1
50      IF (I.LT.N) GO TO 10
        IF (N.LT.7) RETURN
60      RAT1=ABS(Q(4)/Q(3)-1.)
        J1=4
        DO 30 J=4,N-1
        RAT2=ABS(Q(J+1)/Q(J)-1.)
        IF (RAT2.GT.RAT1) GO TO 30
```

```
      RAT1=RAT2
      J1=J+1
30    CONTINUE
      IF (J1.EQ.N) GO TO 100
      DO 40 J=J1,N-1
      Q(J)=Q(J+1)
      Q(J+L)=Q(J+L+1)
40    K(J)=K(J)+1
100   Q(N)=0.0
      Q(N+L)=0.0
      N=N-1
      IF (N.GT.7) GO TO 60
200   RETURN
      END
C
C
C     ------------------------------------------------------------------
C     ------------------------------------------------------------------
      SUBROUTINE DERIV(T,Q,DQ)
C     Calculates derivatives DQ(I) of variables Q(I).  This subroutine
C     is an input for RKF (Runga-Kutta) integrating subroutine.
C     ------------------------------------------------------------------
      COMMON/DER/L,N
      COMMON/GEN/DIM,PHT,PIC,A0,B1,Q20,Q10
      DIMENSION Q(27),DQ(27)
C
      CALL TEMP(T,TF,DTF,PSF,F)
      DO 40 I=3,N
      IF (Q(I).LE.0.0) GO TO 40
      DQ(I)=DIM*(Q(1)-PSF)/(TF*(F+Q(I)))
      DQ2=Q(2)*EXP(-29.427+1.93E-2*(TF-833))
C     DQ2 IS INCREASE DUE TO SURFACE RXN (SOURCE: IYA ET AL)
      DQ(I)=DQ(I)+DQ2
      DQ(I+L)=Q(I+L)*(DQ(I)/(Q(I)+F)+DTF)
40    CONTINUE
C
      DO 45 I=N+1,L+2
      DQ(I)=0.0
45    DQ(I+L)=0.0
      DQ(2)=-(0.96-8.735E-4*TF)*EXP(35.71-30000./TF)*Q(2)
      DQ(1)=(Q10-Q(1)+Q20-Q(2)-Q(2*L+3))*DTF-PIC*TF*AV(Q,DQ,DTF)-DQ(2)
      DQ(2*L+3)=DQ2*TF*2.74E8
      DQ(2)=DQ(2)-DQ(2*L+3)
      IF(Q(1).LE.PSF) GO TO 60
      CALL JAV(CV,AJ,TF,PSF,F,Q)
      RADC=PHT/(ALOG(Q(1)/PSF)*TF)
      DQ(1)=DQ(1)-TF*(PIC*0.66667)*(RADC**3)*AJ
60    RETURN
      END
```

```
C
C
C     ------------------------------------------------------------------
C     ------------------------------------------------------------------
      SUBROUTINE JAV(CV,AJ,TF,PSF,F,Q)
C -     Inputs to this subroutine are: TF,PSF,F,Q.  It provides the
C     homogenous nucleation rate (AJ  #/sec m**3) and the total
C     clearance volume fraction (CV).
C     ------------------------------------------------------------------
      COMMON/CLV/DT0,SM1,AL,EJ
      COMMON/DER/L,N
      DIMENSION Q(27)
C
C     C(X) Is the clearance vol for a particle of radius X
      C(X)=5.953E6*(X**2)*(X+3.1*F)*TF/Q(1)
C
      AJ=0.0
      CV=0.0
      IF (Q(1).LE.PSF) RETURN
      IF (N.EQ.3) GO TO 200
      IF (N.LT.3) GO TO 300
      DO 100 J=3,N-1
100   CV=CV+(C(Q(J))*Q(L+J)+C(Q(J+1))*Q(L+1+J))*ABS(Q(J)-Q(J+1))
200   CV=0.5*(CV+C(Q(N))*Q(N)*Q(N+L))
      IF(CV.GE.1.0) RETURN
300   SF=ALOG(Q(1)/PSF)
      AJ=(1.-A)*(Q(1)/TF)**2*EXP(EJ-SM1/(TF**3*SF**2))
      RETURN
      END
C
C
C     ------------------------------------------------------------------
C     ------------------------------------------------------------------
      FUNCTION AV(Q,DQ,DTF)
C
C     ------------------------------------------------------------------
C     AV INTEGRATES 2*ND*A**2*(DADT+A*DTF/3)  I.E. THE INTEGRAND
C     2*Q(I+L)*Q(I)**2*(DQ(I)+Q(I)*DTF/3)
C
      COMMON/DER/L,N
      DIMENSION Q(27),DQ(27)
      AV=0.0
      IF(N.EQ.3) GO TO 70
      DO 60 J=3,N-1
      A=Q(J+L)*(DQ(J)+Q(J)*DTF/3.)*Q(J)**2
      A=A+Q(J+L+1)*(DQ(J+1)+Q(J+1)*DTF/3.)*Q(J+1)**2
60    AV=AV+A*ABS(Q(J)-Q(J+1))
70    AV=AV+Q(N+L)*(DQ(N)+Q(N)*DTF/3.)*Q(N)**3
      RETURN
      END
C
```

```
C
C
C
C     ------------------------------------------------------------------
C     ------------------------------------------------------------------
      SUBROUTINE TEMP(T,TF,DTF,PSF,F)
C =   Input is T (time). Outputs are temperature (TF), vapor
C     saturation pressure (PSF), mean free path*beta (F) and DTF.
C     DTF is -(DTF/DT)/TF
C     ASSUMING A TEMP PROFILE LINEARLY INCREASING WITH TIME
C     ------------------------------------------------------------------
C
      COMMON/TMP/TF0,C1,TF1
C
      TF=TF0+C1*T
      DTF=-C1/TF
50    F=1.97E-7*(TF/600.)**1.27
      PSF=133.4*EXP(25.23-5.59E4/TF)
      RETURN
      END
C
C
C     ------------------------------------------------------------------
C     ------------------------------------------------------------------
      FUNCTION ARV(Q)
C     ARV IS THE VOLUME OF AEROSOL
      ------------------------------------------------------------------
C
      COMMON/DER/L,N
      DIMENSION Q(27)
C
      ARV=0.0
      IF (N.EQ.3) GO TO 70
      DO 60 J=3,N-1
      A=Q(L+J)*Q(J)**3+Q(L+J+1)*Q(J+1)**3
60    ARV=ARV+A*ABS(Q(J)-Q(J+1))
70    ARV=2.094*(ARV+Q(N)*Q(N+L)*Q(N)**3)
      RETURN
      END
>
```

A.3 Sample Output

```
          INITIAL TIME INTERVALS ARE : 1.000E-01

 TEMP PROFILE PARAMETERS:     7.750E+02   4.000E+02   0.000E-01
            MAX NO CHARACTERISTICS: 12
          INITIAL NO OF CHARACTERISTICS:  7   LT: 1

     VAPOR PRESSURE: 0.000E-01  SILANE PRESSURE: 1.000E+03

         RADIUS (A): 5.000E-07   DN/DA: 1.000E+13
         RADIUS (A): 3.000E-07   DN/DA: 2.000E+17
         RADIUS (A): 1.000E-07   DN/DA: 3.000E+17
         RADIUS (A): 1.000E-08   DN/DA: 1.000E+15
         RADIUS (A): 5.000E-09   DN/DA: 0.000E-01

              END OF INPUT FILE


       TIME= 0.000E-01 SEC      TEMPERATURE= 7.750E+02 K
  VAPOR PRESSURE= 0.000E-01   SILANE PRESSURE= 1.000E+03  PASCALS

          I    K(I)       Q(I)              Q(L+I)
          3     0   RAD= 5.0000000E-07  ND= 1.000E+13
          4     0   RAD= 3.0000001E-07  ND= 2.000E+17
          5     0   RAD= 1.0000000E-07  ND= 3.000E+17
          6     0   RAD= 9.9999999E-09  ND= 1.000E+15
          7     0   RAD= 5.0000000E-09  ND= 0.000E-01

    TNO= 8.355E+10  NUM AV RAD= 1.957E-07  MASS AV RAD= 2.378E-07
        TOT CL VOL= 0.000E-01  TOT AEROSOL VOL= 4.706E-09
          WALL LOSS BY SURFACE RXN= 0.000E-01 PASCALS


8  RAD= 0.000E-01  N= 0.000E-01  P= 0.0E-01 TMP= 7.75E+02


       TIME= 1.000E-01 SEC      TEMPERATURE= 8.150E+02 K
  VAPOR PRESSURE= 3.824E+00   SILANE PRESSURE= 9.943E+02  PASCALS

          I    K(I)       Q(I)              Q(L+I)
          3     3   RAD= 5.0585078E-07  ND= 9.580E+12
          4     4   RAD= 3.0782357E-07  ND= 1.927E+17
          5     5   RAD= 1.1177767E-07  ND= 2.940E+17
          6     6   RAD= 2.5204979E-08  ND= 9.999E+14
          7     7   RAD= 2.0453324E-08  ND= 0.000E-01
          8     8   RAD= 0.0000000E-01  ND= 0.000E-01

    TNO= 7.956E+10  NUM AV RAD= 2.053E-07  MASS AV RAD= 2.447E-07
        TOT CL VOL= 6.187E+00  TOT AEROSOL VOL= 4.882E-09
          WALL LOSS BY SURFACE RXN= 1.781E+00 PASCALS
```

```
     TIME= 2.000E-01 SEC       TEMPERATURE= 8.550E+02 K
VAPOR PRESSURE= 2.186E+01    SILANE PRESSURE= 9.703E+02  PASCALS

        I    K(I)        Q(I)                Q(L+I)
        3      3    RAD= 5.4603225E-07   ND= 9.586E+12
        4      4    RAD= 3.6012420E-07   ND= 1.995E+17
        5      5    RAD= 1.8555127E-07   ND= 3.303E+17
        6      6    RAD= 1.1455893E-07   ND= 1.214E+15
        7      7    RAD= 1.1083353E-07   ND= 0.000E-01
        8      8    RAD= 0.0000000E-01   ND= 0.000E-01

  TNO= 7.655E+10  NUM AV RAD= 2.675E-07  MASS AV RAD= 2.936E-07
      TOT CL VOL= 1.802E+00  TOT AEROSOL VOL= 8.118E-09
         WALL LOSS BY SURFACE RXN= 5.771E+00 PASCALS


     TIME= 3.000E-01 SEC       TEMPERATURE= 8.950E+02 K
VAPOR PRESSURE= 8.566E+01    SILANE PRESSURE= 8.810E+02  PASCALS

        I    K(I)        Q(I)                Q(L+I)
        3      3    RAD= 6.9781123E-07   ND= 1.076E+13
        4      4    RAD= 5.4510008E-07   ND= 2.425E+17
        5      5    RAD= 4.1569328E-07   ND= 4.597E+17
        6      6    RAD= 3.6878220E-07   ND= 1.842E+15
        7      7    RAD= 3.6643470E-07   ND= 0.000E-01
        8      8    RAD= 0.0000000E-01   ND= 0.000E-01

  TNO= 7.477E+10  NUM AV RAD= 4.749E-07  MASS AV RAD= 4.835E-07
      TOT CL VOL= 1.610E+00  TOT AEROSOL VOL= 3.540E-08
         WALL LOSS BY SURFACE RXN= 1.431E+01 PASCALS


     TIME= 4.000E-01 SEC       TEMPERATURE= 9.350E+02 K
VAPOR PRESSURE= 2.082E+02    SILANE PRESSURE= 6.295E+02  PASCALS

        I    K(I)        Q(I)                Q(L+I)
        3      3    RAD= 1.0391304E-06   ND= 1.370E+13
        4      4    RAD= 9.2821688E-07   ND= 3.330E+17
        5      5    RAD= 8.4156170E-07   ND= 6.893E+17
        6      6    RAD= 8.1212511E-07   ND= 2.873E+15
        7      7    RAD= 8.1068231E-07   ND= 0.000E-01
        8      8    RAD= 0.0000000E-01   ND= 0.000E-01

  TNO= 7.295E+10  NUM AV RAD= 8.806E-07  MASS AV RAD= 8.827E-07
      TOT CL VOL= 2.968E+00  TOT AEROSOL VOL= 2.101E-07
         WALL LOSS BY SURFACE RXN= 3.005E+01 PASCALS
```

```
     TIME= 5.000E-01 SEC       TEMPERATURE= 9.750E+02 K
VAPOR PRESSURE= 2.496E+02   SILANE PRESSURE= 2.304E+02  PASCALS

        I    K(I)        Q(I)                Q(L+I)
        3     3    RAD= 1.4569168E-06   ND= 1.708E+13
        4     4    RAD= 1.3730352E-06   ND= 4.301E+17
        5     5    RAD= 1.3097053E-06   ND= 9.199E+17
        6     6    RAD= 1.2886773E-06   ND= 3.881E+15
        7     7    RAD= 1.2876533E-06   ND= 0.000E-01
        8     8    RAD= 0.0000000E-01   ND= 0.000E-01

  TNO= 7.050E+10  NUM AV RAD= 1.338E-06  MASS AV RAD= 1.339E-06
      TOT CL VOL= 7.259E+00  TOT AEROSOL VOL= 7.086E-07
         WALL LOSS BY SURFACE RXN= 4.903E+01 PASCALS


     TIME= 6.000E-01 SEC       TEMPERATURE= 1.015E+03 K
VAPOR PRESSURE= 1.089E+02   SILANE PRESSURE= 1.876E+01  PASCALS

        I    K(I)        Q(I)                Q(L+I)
        3     3    RAD= 1.7074749E-06   ND= 1.865E+13
        4     4    RAD= 1.6340931E-06   ND= 4.749E+17
        5     5    RAD= 1.5792513E-06   ND= 1.025E+18
        6     6    RAD= 1.5611563E-06   ND= 4.339E+15
        7     7    RAD= 1.5602767E-06   ND= 0.000E-01
        8     8    RAD= 0.0000000E-01   ND= 0.000E-01

  TNO= 6.788E+10  NUM AV RAD= 1.604E-06  MASS AV RAD= 1.604E-06
      TOT CL VOL= 2.709E+01  TOT AEROSOL VOL= 1.174E-06
         WALL LOSS BY SURFACE RXN= 5.800E+01 PASCALS


     TIME= 7.000E-01 SEC       TEMPERATURE= 1.055E+03 K
VAPOR PRESSURE= 1.906E+01   SILANE PRESSURE= 1.471E-01  PASCALS

        I    K(I)        Q(I)                Q(L+I)
        3     3    RAD= 1.7716562E-06   ND= 1.850E+13
        4     4    RAD= 1.7005277E-06   ND= 4.719E+17
        5     5    RAD= 1.6474739E-06   ND= 1.020E+18
        6     6    RAD= 1.6299899E-06   ND= 4.322E+15
        7     7    RAD= 1.6291403E-06   ND= 0.000E-01
        8     8    RAD= 0.0000000E-01   ND= 0.000E-01

  TNO= 6.533E+10  NUM AV RAD= 1.671E-06  MASS AV RAD= 1.672E-06
      TOT CL VOL= 1.758E+02  TOT AEROSOL VOL= 1.278E-06
         WALL LOSS BY SURFACE RXN= 5.884E+01 PASCALS
```

```
        TIME= 8.000E-01 SEC       TEMPERATURE= 1.095E+03 K
  VAPOR PRESSURE= 2.865E+00    SILANE PRESSURE= 8.657E-04  PASCALS

          I    K(I)       Q(I)              Q(L+I)
          3     3    RAD= 1.7811113E-06  ND= 1.790E+13
          4     4    RAD= 1.7103000E-06  ND= 4.568E+17
          5     5    RAD= 1.6574969E-06  ND= 9.880E+17
          6     6    RAD= 1.6400982E-06  ND= 4.185E+15
          7     7    RAD= 1.6392530E-06  ND= 0.000E-01
          8     8    RAD= 0.0000000E-01  ND= 0.000E-01

     TNO= 6.295E+10  NUM AV RAD= 1.681E-06  MASS AV RAD= 1.681E-06
        TOT CL VOL= 1.212E+03  TOT AEROSOL VOL= 1.254E-06
          WALL LOSS BY SURFACE RXN= 5.885E+01 PASCALS


 PROG STOPS:  Q1,Q2,TF,T=  2.865E+00  8.657E-04  1.095E+03  8.000E-01
TT16  --  STOP
>
```

SYMBOLS USED

a	radius of particle, m
a^*	critical radius for nucleation, m
A	dimensionless growth parameter defined by Eq. (44)
B	parameter defined by Eq. (45)
c	total molar concentration, Kmole/m^3
c_A	molar concentration of monomer vapor, Kmole/m^3
c_d	molar concentration of monomer in particles, Kmole/m^3
C_o	constant defined by Eq. (114)
C_p	specific heat of gas at constant pressure, J/Kg °K
C_v	molar specific heat of gas at constant volume, J/Kmole °K
d	diameter of reactor tube, m
d_p	diameter of particle, m
$\mathcal{D}, \mathcal{D}_{AB}$	diffusivity of monomer in gas, m^2/sec
F	function defined by Eq. (62)
g_a	acceleration due to gravity, 9.81 m/sec^2
g	cluster size of monomers
g^*	critical cluster size for nucleation
h	Planck's constant, 6.63×10^{-34} Jsec
ΔH_v	latent heat of vaporization of monomer, J/Kmole
I	mass flux of vapor, Kg/m^2sec
J	nucleation rate, #/m^3sec
k	Boltzmann constant, 1.38×10^{-23} J/°K
Kn	Knudsen number defined in section 2.
K_T	thermal conductivity of nonvolatile component, W/m°K

ℓ distance of boundary sphere from particle surface (Sec. 2), m

Le Lewis number , $K_T/(\rho_g C_p)$

m molecular mass of vapor, Kg

M molar weight, Kg/Kmole

n(a) aerosol size distribution function, $\#/m^4$

n_A monomer concentration, P_A/kT, $\#/m^3$

N_∞ total number concentration, $\#/m^3$

P total pressure, Pa

P_A vapor pressure, Pa

P_B pressure of component B, Pa

$\overline{P}$ average pressure, Pa

$\overline{\Delta P}$ change in vapor pressure from $t=0$, Pa

q function defined by Eq.(97)

Q heat flux, W/m^2

r radial coordinate from particle center, m

R gas law constant, $8.31X10^3$ J/Kmole°K

R_p rate of vapor pressure increase due to reactions, Pa/sec

S saturation ratio of vapor

t time, sec

T temperature, °K

u velocity of gases in reactor, m/sec

U volume flow rate, m^3/sec

v_m monomer volume, m^3

$\overline{V}$ mean velocity of molecules, m/sec

V radial velocity, m/sec

V^* molar averaged radial velocity, m/sec

x	molar fraction of gas
y	dimensionless radial coordinate, Eq. (22)
z	axial distance along reactor, m
Z	ratio of molar weights, M_A/M_B

Greek Symbols:

α	dimensionless variable defined by Eq. (89)
α_T	thermal diffusivity of gas, m^2/sec
α_d	thermal diffusivity of particle, m^2/sec
β	coefficient defined by Eq. (7)
γ	coefficient defined by Eq. (8)
ζ	ratio of specific heats, C_{pA}/C_{pB}
λ	mean free path of gas molecules, m
ν	symmetry number
ξ_c	condensation coefficient
Γ	dimensionless temp. defined by Eq. (71)
$\Delta_1, \Delta_2, \Delta_3$	functions defined by Eq. (90)
Δ_T	dimensionless temp. difference, Eq. (64)
Δ_x	dimensionless mole fraction difference, Eq. (65)
θ	dimensionless time scale defined by Eq. (50)
ρ	dimensionless radius of clearance volume
ρ_o	dimensionless radius of clearance volume as Kn-->0
ρ_g	bulk gas density, kg/m^3
σ	surface tension, J/m^2

σ_{yz}	collision diameter for molecules of y and z, m
τ	characteristic times, sec
ϕ	energy function, Eq. (37)
χ	scaled mole fraction, Eq.(70)
Ω	total fractional clearance volume, Eq. (24)
$\left.\begin{matrix}\Omega_{AB}^{(1,1)} \\ \Omega_{BB}^{(2,2)}\end{matrix}\right\}$	collision integrals, Equations (9), (10)

Subscripts and superscripts:

A	vapor
B	carrier gas
o	particle surface
sat	saturation point of vapor
∞	large distance from the particle
I	initial value in simulations
f	value at end point in simulations